universität wien

DISSERTATION / DOCTORAL THESIS

Titel der Dissertation /Title of the Doctoral Thesis

„Multi-chamber cardioids unravel human heart development and cardiac defects“

verfasst von / submitted by

Clara Schmidt BSc MSc

angestrebter akademischer Grad / in partial fulfilment of the requirements for the degree of

Doctor of Philosophy (PhD)

Wien, 2024/ Vienna 2024

Studienkennzahl lt. Studienblatt / degree programme code as it appears on the student record sheet:	A 794 685 490
Dissertationsgebiet lt. Studienblatt / field of study as it appears on the student record sheet:	Molekulare Biologie
Betreut von / Supervisor:	Sasha Mendjan PhD

Table of Contents

Acknowledgements

First, I would like to thank my amazing supervisor, Sasha Mendjan - thank you for infusing this project with your boundless creativity and grand visions. Your support and our collaborative energy made every interaction productive and inspiring.

I would like to thank Tobias Ilmer, who started in the lab as my master's student, and his contribution to this project and my personal growth have been incredible. You're an indispensable part of our lab's spirit.

A special thanks goes to the co-author of the paper, Alison Deyett. Her contribution and input were invaluable to the paper. Yet, our shared journey involved more than a collaboration; it encompassed early mornings spent in tissue culture, trying to realize ambitious 96-well plate layouts, and late nights working on crafting figures until frustration turned to accomplishment.

Importantly, I would also like to highlight my appreciation to the entire Mendjan lab, especially to Lavinia, Estela, Stefan, Marie, Kasia, and many former lab members, including Pablo and Nora.

Furthermore, I would like to thank Maria Novatchkova, who performed the bioinformatic analysis of RNA-seq data and the different facilities of the Vienna BioCenter, including the members of the BioOptics, Next-Generation Sequencing, Histology, Molecular Biology, Cryo-EM, and the IMBA Stem Cell Core Facility. This work would not have been possible without their support.

I would like to thank my Thesis Advisor Committee, Christa Bücker and Alex Stark, for their honest input and guidance.

Finally, I extend my deepest gratitude to the most important people in my life: my family and friends. Your unwavering support has been my rock throughout this journey.

And to Stefan, my partner, your love and support have been my anchor. Your constant encouragement sustained me through every challenge. Thank you for always believing in me.

1. Abstract

The primary cause of human fetal death are defects in heart development. Understanding the underlying causes remains challenging due to the speed of the development and the inaccessibility of the human embryonic heart. Yet, the impacts of mutations, drugs, and environmental factors on the specialized functions of different heart compartments are not captured by in vitro models. To tackle this challenge, we pioneered a human cardioid platform that recapitulates the development of all major embryonic heart compartments, including right and left ventricles, atria, outflow tract, and atrioventricular canal. Leveraging both 2D and 3D differentiation techniques, we efficiently generated distinct cardiac progenitor populations representing first, anterior, and posterior second heart field identities. This achievement allowed us to reproducible generate cardioids with compartment-specific gene expression profiles, morphologies, and functionalities similar to those found *in vivo*. We used our platform to unravel the ontogeny of signal and contraction propagation between interconnected heart chambers. Moreover, it enabled us to dissect and comprehend how mutations, teratogens, and drugs induce compartment-specific defects during the crucial stages of human heart development.

2. Zusammenfassung

Die Hauptursache für den Tod von menschlichen Föten sind Fehlbildungen in der Herzentwicklung. Aufgrund der Unzugänglichkeit und der Geschwindigkeit der frühen Herzentwicklung beim Menschen es schwierig die Ursachen von angeborenen Herzkrankheiten zu untersuchen. Zusätzlich werden die Auswirkungen von Mutationen, Medikamenten und Umweltfaktoren (Teratogene) auf die spezialisierten Funktionen verschiedener Herzkammern von bestehenden *in vitro* Modellen nicht erfasst. Um dieser Herausforderung zu begegnen, haben wir menschliche 3D-Herzorganoidmodelle entwickelt, die die Entwicklung aller wichtigen embryonalen Hauptkompartimente des sich entwickelnden Herzens, einschließlich der rechten und linken Ventrikel, Vorhöfe, Ausflusstrakt und des Atrioventrikularkanals, nachbilden. Unter Nutzung von sowohl 2D- als auch 3D-Differenzierungstechniken haben wir effizient unterschiedliche Vorläuferpopulationen herstellen können, die die Identitäten des ersten, anterior und posterior zweiten Herzfeldes repräsentieren. Dieser Fortschritt ermöglichte uns die reproduzierbare Herstellung von Kardioiden mit Kompartiment spezifischen Genexpressionsprofilen, Morphologien und Funktionalitäten, ähnlich denen, die *in vivo* gefunden werden. Wir nutzten unsere Mehrkammer-Plattform, um die Ontogenese der Signal- und Kontraktionsausbreitung zwischen verbundenen Herzkammern zu verstehen. Darüber hinaus ermöglichte sie uns, zu analysieren und zu verstehen, wie Mutationen, Teratogene und Medikamente Kompartiment spezifische Defekte während der entscheidenden Phasen der menschlichen Herzentwicklung hervorrufen.

3. Introduction

Congenital heart disease (CHD) is the major cause of infant morbidity and mortality, affecting approximately 1% of newborns worldwide (Jin et al. 2017). CHD can manifest as outflow tract malformations, atrial and ventricular septal defects, and regional ventricular diseases, such as hypoplastic left ventricle or arrhythmogenic right ventricular cardiomyopathy (Fahed et al. 2013). Despite the significant impact of CHD, current therapies for CHD remain limited. Yet, we lack a comprehensive understanding of the molecular mechanisms governing human cardiac development and the disease etiology leading to CHD (Houyel and Meilhac 2021; Rao, Kameswaran, and Bruneau 2022).

Understanding the mechanisms that lead to genetic diseases of the different compartments of the heart requires a deeper understanding of early heart development. Most of our current knowledge on cardiac development comes from studies in model organisms such as mice and zebrafish. Yet, the complexity and the rapid development of the embryonic heart limit the study of defects in model organisms. Little data is available from human embryos, mainly due to the inaccessibility of the early embryonic stages ranging from implantation to the 5th week post-fertilization. However, species-specific differences in timing and gene expression make it challenging to extrapolate findings from model organisms to humans (Cui et al. 2019; Srivastava 2021). Establishing a new physiological human *in vitro* model that follows developmental trajectories would be a great complementary system to overcome these problems. Testing and screening of new drugs can be performed on a big scale, human-specific aspects can be tested, and the number of animal models can be reduced (de Korte et al. 2020) (Table 1). Moreover, cardiac organoids give us the possibility to explore the mechanisms of cardiac defects further. In the future, *in vitro*-generated cardiac cells might even offer a cell source for regenerative therapies following myocardial infarction.

One advantage of these *in vitro* reductionist systems is that they consist only of a few cell types and are not influenced by surrounding tissues. Therefore, manipulation of specific components can be easily controlled, allowing us to understand the causes of

cardiac defects better. In fact, for 56% of cardiac defects the cause is unknown (Zaidi and Brueckner 2017). Approximately 34% of defects with known causes have been attributed to single mutations or chromosomal abnormalities, such as DiGeorge Syndrome, Holt Oram Syndrome, and Down Syndrome, and 10% are caused by environmental factors such as maternal diabetes (Zaidi and Brueckner 2017). The unknown causes could be undiscovered environmental factors, like plastic residues, or enhancer mutations. To test the impact of candidate factors, we need a cardiac *in vitro* system to test many possible causes at different conditions in high throughput (HTP).

in vivo		*in vitro*	
limitations	**advantages**	**limitations**	**advantages**
low throughput	all developmental regions	lack of control	reductionist
low accessibility	physiological maturation	limited cell types	self-organization
high complexity	data & literature	heterogeneity	high throughput
non-human	models & tools	lack of maturation	human systems
high costs			
strict regulations			

Table 1: Limitations and advantages of *in vivo* vs *in vitro* experiments to understand cardiac development and unravel cardiac defects.

In the last years, a lot of progress has been made in generating human self-organizing heart organoid models for cardiovascular disease studies (Drakhlis et al. 2021; Hofbauer et al. 2021; Lewis-Israeli, Wasserman, and Aguirre 2021). Despite the improvements in cardiac *in vitro* systems using human pluripotent stem cells in the last few years, there are still some major limitations. First, the organoid systems often include non-cardiac cells, and most protocols result in a mixed population of atrial-, ventricular-, and nodal cardiomyocytes. Second, cardiomyocytes (CM) often show an insufficient level of maturity and only mimic the fetal stage and not the adult developmental stage and physiology. Third, it is difficult to mimic and control the morphology of the heart, including the architecture of the layers of the heart, looping, chamber interactions, and integration with circulation. Fourth, current cardiac organoids fail to mimic all progenitor populations of the heart and cannot recapitulate all regions of the heart. However, most defects are compartment-specific (Figure 1),

highlighting the need for a system that mimics all compartments of the heart, including the left ventricle (LV), right ventricle (RV), Atria, outflow tract (OFT) and the atrioventricular canal (AVC).

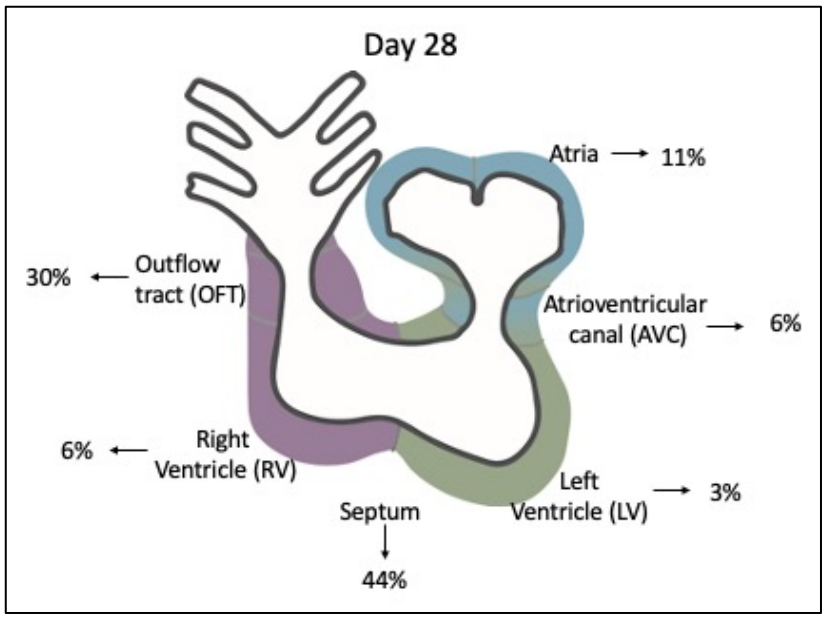

Figure 1. Compartment-specific cardiac defects. Schematic representation of the occurrence of congenital heart diseases.

Here, we established a human cardiac organoid platform, called cardioids, that recapitulates the development of all major embryonic heart compartments, including LV, RV, atria, OFT, and AVC. Our protocols precisely follow the timing and signaling of early heart development to ensure we obtain clear morphogenesis and homogenous cell populations. This platform allows us to dissect how genetic and environmental factors (teratogens) cause compartment-specific defects in the developing human heart.

3.1. Early heart development

The development of the heart is a complex process that starts during gastrulation, with the formation of the primitive streak. The heart develops from three sources of mesodermal progenitor populations: the first heart field (FHF) and the anterior and posterior secondary heart field (aSHF and pSHF) precursors recruited from the

adjacent pharyngeal mesoderm (Meilhac and Buckingham 2018; Swedlund and Lescroart 2020). While the FHF gives rise to the LV and minor parts of the atria, the aSHF gives rise to the RV and OFT, and the pSHF gives rise to most of the atria and the AVC (Figure 2).

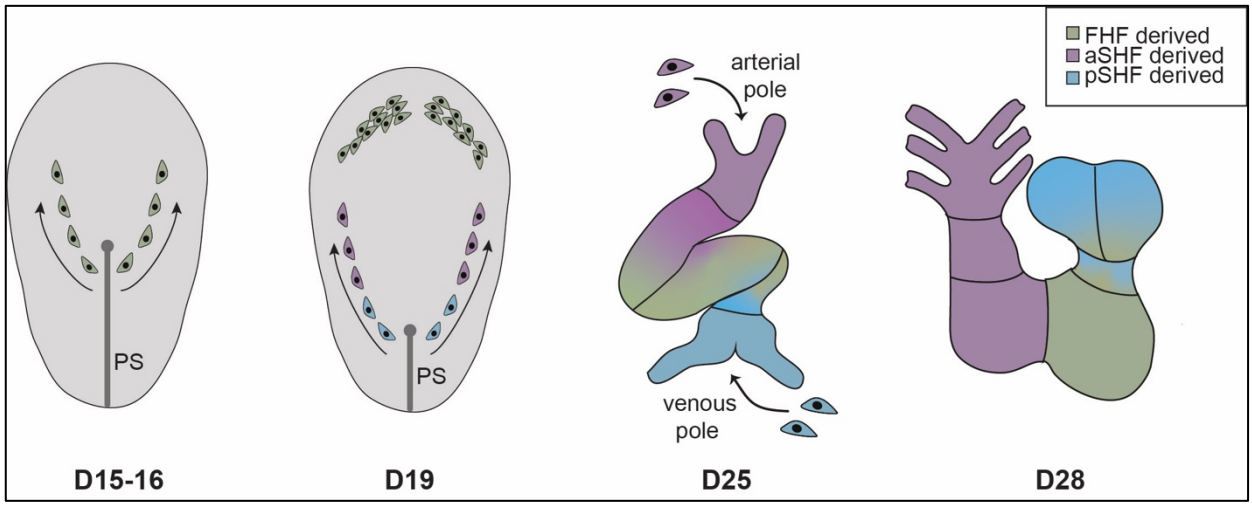

Figure 2. Early human heart development. Schematic representation of early stages of human heart development from the onset of gastrulation to the initial formation of the four-chambered heart. The green color indicates the first heart field (FHF) population of the heart, purple indicates the anterior second heart field (aSHF) population, and blue the posterior second heart field (pSHF) population.

Fate mapping and single-cell sequencing experiments have shown that distinct cell populations arise sequentially at gastrulation and independently activate the expression of Mesp1, which is considered to be the earliest cardiac specification marker and controls the epithelial to mesenchymal (EMT) process in the primitive streak (PS) (Devine et al. 2014; Lescroart et al. 2014; 2018). These cell populations are the FHF and SHF, which undergo EMT and migrate away from the PS sequentially. Ivanovitch et al. identified the FHF progenitors as the first to arise, located at the distal primitive streak and characterized by high expression levels of EOMES and FOXA2 and lower levels of T. RV progenitors (EOMES high / T low / FOXA2+) migrate away from the distal PS, followed by OFT progenitors (EOMES low / T high / FOXA2 upregulated). Finally, atrial progenitors (EOMES low / T high / FOXA2-) exit from the proximal area of the PS (Ivanovitch et al. 2021). The FHF progenitors form the primitive heart tube, which is the first area of the heart that starts to beat (R. C. V. Tyser and

Srinivas 2020). The aSHF and pSHF progenitors migrate into the arterial (anterior) and venous (posterior) poles of the heart tube, respectively (Figure 3). Cells At the tube stage, FHF progenitors express HAND1, TBX5, and NKX2-5. aSHF proliferation is promoted by TBX1, which directly interferes with intracellular components of the BMP signaling cascade and negatively regulates the Mef2c transcript and SRF protein levels, leading to delayed differentiation. TBX1 is highly expressed in mice between E8.5 and E9.5, while the levels decrease with the progression of differentiation (Greulich, Rudat, and Kispert 2011). FOXC1/2, FGF8/10, SIX1 are downstream of TBX1 and are other important transcription factors of the aSHF at this stage, whereas TBX5 is not expressed. pSHF is characterized by the expression of OSR1, TBX5, FOXF1 and HOXB1 (Kelly, Buckingham, and Moorman 2014; Meilhac and Buckingham 2018; Kelly 2023).

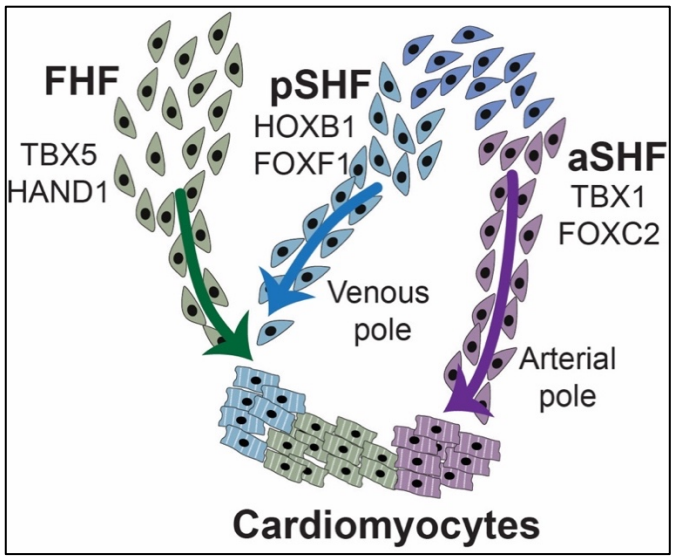

Figure 3. Cardiac progenitors and tube formation. Graphical representation of scRNA-seq data showing the migration of the cardiac progenitors into the heart tube (adopted from (Kelly 2023)).

During this early stage of heart development, Retinoic acid (RA) plays a critical role. It is necessary to prepattern the SHF progenitors and to set the anterior and posterior boundaries (De Bono et al. 2018). RA is released from the presomitic mesoderm and liver endoderm and diffuses anteriorly to influence the cardiogenic regions (Sirbu et al. 2005). Strong RA signaling inhibits Tbx1 and thereby defines the posterior boundary of the SHF, while relatively weak RA signaling is required to express Tbx1 in the

anterior SHF (Niederreither and Dollé 2008; Nakajima 2019). RA-induced Tbx5 in the pSHF is required to suppress the Tbx1-dependent aSHF program (Figure 4). In Aldh1a2-null mutant mice with defective RA synthesis, the expression of SHF genes expands posteriorly (Ryckebusch et al. 2008), indicating the crucial role of RA in setting the boundaries of the heart progenitor compartments during development.

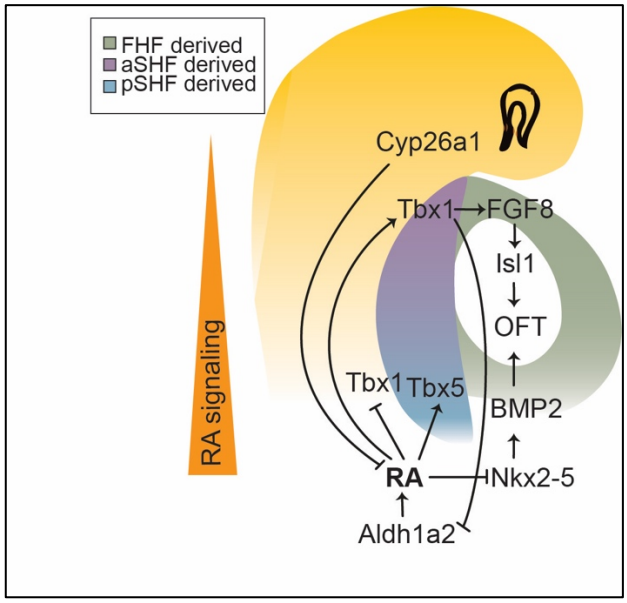

Figure 4. The role of RA in the development of the SHF. Schematic representation of a mouse embryo and the RA gradient, which is influencing the expression of transcription factors and formation of different compartments in the heart, adopted from (Nakajima 2019)

The proliferation and migration of the two SHF populations into the heart tube lead to rightward looping, a massive increase in the number of cardiac cells, and thereby rapid growth. During this stage, the progenitors are further patterned by BMP, FGF, WNT inhibition, and RA signaling (Abu-Issa and Kirby 2007). All three progenitors, FHF, aSHF, and pSHF, can give rise to two layers of the heart: the innermost layer, the endocardium, and the middle layer, the myocardium, which are the contracting cells of the heart. At a later stage of development, the outer layer of the heart, the epicardium, envelopes the whole organ. The epicardium is the source of multiple progenitor cell types, including smooth muscle cells, fibroblasts, and mesenchymal (interstitial) valve cell (Fc and Pr 2018).

During this stage, CMs either upregulate chamber-specific programs, such as LV, RV, and atrial genes, or express regulators promoting the non-chamber specific program, as seen in the AVC and OFT. The upregulation of the chamber program is characterized by the expression of NPPA/NPPB in all chambers, NF2F1/2 in the atria, IRX4, HEY2, and HAND1 in the LV, and IRX1/2 and HAND2 in the RV. In contrast, the CMs located in the AVC or OFT express various BMPs, which inhibits the upregulation of the chamber program (Wang, Greene, and Martin 2011). The AVC is characterized by the expression of the BMP targets TBX2 and MSX2, while the OFT expresses WNT11, WNT5A, and RSPO3. The OFT and AVC are also the regions where valve development is initiated, where BMP and TGFb signaling lead to the invasion of endocardium-derived mesenchymal cells into the cardiac jelly, which is the extracellular matrix located between the myocardium and the endocardium (Haack and Abdelilah-Seyfried 2016). This process initiates the formation of valves to ensure the proper development and flow direction of the systemic and pulmonary mammalian circulatory systems.

3.2. Modeling SHF development *in vitro*

Modeling the SHF lineages *in vitro* has been challenging due to the lack of a clear understanding of the drivers of SHF lineage specification and the underlying molecular mechanisms. In recent years, most *in vitro* systems have focused on developing FHF-derived CMs and ECs, whereas only a few research groups have aimed to establish specific protocols for SHF-derived CMs. In this section, we will examine several approaches used to model SHF lineages *in vitro*, highlighting the advantages and limitations of each approach (Table 2).

Nandkishore and colleagues used dual WNT and TGF-beta signaling inhibition in attempting to recapitulate the development of mouse and human ESCs into the cardiopharyngeal mesoderm (Nandkishore et al. 2018), which gives rise to head mesoderm as well as the aSHF. Using their protocol, they upregulated main aSHF markers, including TBX1, FGF8/10, and ISL1. In addition, they were able to further differentiate these progenitors into 2D CM beating clusters; however, the identity of these CMs was not analyzed in their study. In a more recent study, Pezhouman et al.

used a dual reporter line for TBX5 and NKX2.5 to distinguish TBX5+NKX2.5+ FHF cells from the TBX5-NKX2.5+ SHF cells and TBX5+NKX2-5- nodal cells (Pezhouman et al. 2022). After FACS sorting, they reported the expression of main FHF, aSHF, and nodal markers in their obtained progenitor populations. However, FHF and SHF progenitor populations mainly gave rise to atrial CMs and not as expected from mouse literature to LV, RV, and OFT.

In another recent work, Yang and colleagues aimed at recapitulating the development of all three cardiac progenitors, FHF, aSHF and pSHF, using human iPSCs in an embryoid body protocol (Yang et al. 2022). They obtained a mixture of all three lineages by using different levels of Activin and BMP during mesoderm induction. Thus, the protocol contains a sorting step to further homogenize progenitor populations. They claimed that the sorted aSHF populations could give rise to RV and OFT derivatives, the sorted pSHF to the atria and sinus venosus, and the FHF progenitors to LV and AVC derivatives. They generated a comprehensive scRNA-seq dataset at the mesoderm, progenitor, and specification stage and compared it to hPSC-derived, human fetal-, and mouse fetal cardiac populations. In addition, they were able to show distinct molecular and electrophysiological characteristics of the CM subtypes; however, functional validation using KO lines showing compartment-specific defects is missing. Moreover, the sorting step to obtain a homogenous progenitor population and the subsequent re-aggregation limits the self-organization in the organoid.

Zawada et al. recently developed a (epi)cardioid protocol based on Hofbauer at al., 2021, where they observed FHF, SHF, and juxta-cardiac field progenitors, giving rise to CMs as well as epicardial cells (Zawada et al. 2023). They separated the progenitors by modulating retinoic acid signaling and reported that the FHF and SHF cells could differentiate into ventricular, OFT, AVC, and MYOZ2-high CMs. In addition, they tried to mimic compartment-specific defects using a hypoplastic left heart Syndrome patient iPSC line. However, in their study, the morphogenesis of the organoids remains unclear, and again, a sorting step is required at the progenitor stage.

Recent studies reported several self-organizing embryoids that include SHF-like cells. Anderson et al., were among the first to generate 3D spheroids derived from mouse as well as human PSCs, containing FHF and SHF progenitors (Andersen et al. 2018). They showed that Wnt/β-catenin and BMP signaling controls the specification of the progenitors. Additionally, they tried to isolate the progenitor populations based on the expression of the cell surface protein CXCR4 and showed that SHF cells are CXCR4 positive, whereas FHF cells are CXCR4 negative. Further, they reported the differentiation of these progenitors into CMs; however, as in many other studies, the characterization of these CMs is missing. Lewis-Israeli and colleagues generated cardiac organoids claiming to represent cells from both progenitor populations, FHF and SHF (Lewis-Israeli et al. 2021). They further reported that these progenitors developed into left and right ventricular CMs, respectively, based on the expression of HAND1 and HAND2. However, the SHF progenitors within the organoid were not labeled, making it difficult to confirm the origin of the HAND2+ CMs. In addition, HAND1 and HAND2 have been reported to not be exclusively expressed in either FHF or SHF.

Finally, Rossi and colleagues developed a protocol for mouse ESC-derived self-organizing gastruloids (G et al. 2021). These axially patterned gastruloids co-developed FHF and SHF progenitor cells, which appear in a temporal sequence, recapitulating the early steps of heart development. They reported that the progenitors formed a cardiac crescent-like structure and developed into an early cardiac tube-like system. Moreover, the gastruloid co-developed a primitive gut-like structure, and vascularization was initiated. Yet, further developmental stages, including looping and four-chambered heart formation, are not achieved in the system.

paper	species	system	progenitor identities	CM identities	mixed progenitors	sorting step required	morphogenesis	quantifiable morphogenesis	disease aspect
Nandhishore et al., 2018	mouse, human	embryoid body/ 2D	cardiopharyngeal/ head mesoderm	not analysed	no	no	no	no	no
Pezhouman et al., 2022	human	2D	SHF, FHF and nodal progenitors	mainly atria (SHF and FHF-derived) and nodal-like CMs	yes	yes (NKX2-5 TBX5 reporter at progenitor stage)	no	no	no
Anderson et al., 2018	mouse, human	precardiac spheroid	SHF and FHF	not analysed	yes	no	no	no	no
Lewis-Israeli et al., 2021	human	organoids	SHF and FHF	FHF-derived (HAND1+) and SHF-derived (HAND2+)	yes	no	ECM composition, vascularization	no (number of SHF and FHF derived CMs)	diabetes
Rossi et al., 2021	mouse	embryonic organoids/ gastruloids	SHF and FHF	not analysed	yes	no	cardiac crescent-like, vascularization (endocardial layer), axially patterned	yes	no
Yang et al., 2022	human	organoids	aSHF, pSHF and FHF	LV and AVC (FHF-derived), RV and OFT (aSHF-derived), Atria and SV (pSHF-derived)	yes	yes (mesoderm stage)	no	no	no
Zawada et al., 2023	human	organoids	SHF, FHF and juxta-cardiac field progenitors	Ventricular, OFT, AVC, MYOZ2-high CMs	yes	yes (progenitor stage)	Epicardial cells	no	HPLH syndrome

Table 2: *In vitro* SHF protocols. Advantages and limitations of recently published *in vitro* cardiac differentiation protocols of the SHF lineage.

In summary, most approaches to modeling the SHF population fail to separate the aSHF and pSHF, except for Yang et al. Mostly, SHF and FHF populations were obtained within the same organoid, requiring sorting to obtain a homogenous progenitor population. Crucially, most studies did not investigate the identity of FHF and SHF-derived CMs. Since many cardiac defects are compartment-specific, functional validation of the CMs derived from the different lineages using KO lines or drug testing is a powerful tool to verify the different identities of the CMs. However, in most studies, this functional validation is missing.

4. Aims and outline of the thesis

The project of my Ph.D. had four main aims:

1. Contribute to the development of the LV-like cardioid system
2. Incorporation of the SHF lineage into the cardioid system
3. Development and characterization of the multi-chambered cardioid platform
4. Genetic and teratogenic validation of the multi-chambered cardioids by modeling compartment-specific cardiac defects

Our group recently developed a self-organizing cardiac organoid system (called cardioids) that is recapitulating the early development of the LV derived from FHF progenitors. I contributed to that work by developing a protocol leading to the emergence of the inner endothelial lining cardioids, resembling *in vivo* tissue architecture. In addition, I contributed to the general optimization of the cardioid differentiation approach, generated an H9 HAND2 knockout line, and used it to validate the cardioid system.

The main goal of my Ph.D. was to expand the cardioid approach and integrate the SHF lineage. Thus, I developed a protocol for the aSHF using dual WNT and TGFb inhibition. Since the original 3D cardioid protocol led to a heterogenous TBX1+

population, I optimized the protocol and developed a so-called 2D->3D approach, where we induce mesoderm of the cells in 2D, and 36-40 hours later, dissociate, and let the progenitors aggregate in a 96 well low attachment plate. In the next step, I established a robust and highly efficient differentiation protocol to differentiate these aSHF progenitors into RV and OFT CMs. In addition, I studied the potential of SHF progenitors to differentiate into endothelial cells and smooth muscle cells. In a collaborative effort, my lab Ph.D. student colleague Alison Deyett established a protocol for pSHF progenitors and a robust differentiation into cardioids with atrial and AVC-like identities. I optimized all these cardioid protocols for various cell lines, including hPSC H9 line, iPSC WTC line, and the 178/5 iPSC lines. Together with Alison and our colleague, Tobias Ilmer, we characterized the morphology and the gene expression of the cardioids derived from different progenitors using RNAseq, various histology techniques, and flow cytometry. Moreover, I generated a comprehensive scRNA-seq dataset, confirming the identities of the different CM subpopulations and comparing them to available published datasets. Finally, Alison focused on the functional analysis of the cardioids, including contraction rate, contraction movement, and signal propagation speed.

The next goal of the Ph.D. was to study the interaction of cardioids by generating multi-chambered cardioids. Tobias Ilmer established the fusion approach (under my supervision) and analyzed the morphology of the multi-chambered cardioids. Together with Alison Deyett, we analyzed the signal propagation of the multi-chambered cardioids using a GCaMP line. Moreover, I studied the sorting potential of the progenitors by dissociating, mixing, and aggregating different progenitors.

The final goal of my Ph.D. project was to use the multi-chambered cardioid system to recapitulate and study heart defects. Particularly, we were interested in compartment-specific defects to validate our system. With the help of the IMBA Stem Cell Facility, we generated KO lines of genes known that, when mutated, lead to developmental defects (TBX5 and ISL1 KO) and genes whose functions are less studied (FOXF1). I mainly focused on the morphological, gene expression, and beating behavior changes of the TBX5 KO line, whereas Tobias Ilmer and Aranxa Torres analyzed the TBX1 KO

and FOXF1 KO, respectively. Moreover, we analyzed compartment-specific effects of teratogens, including Acitretin, All-trans Retinol, Thalidomide, and Aspirin (control), in our cardioids. Taken together, we developed a validated multi-chamber cardioid platform representing all the major compartments of the human embryonic heart.

5. Multi-chamber cardioids unravel human heart development and cardiac defects

Schmidt Clara, Alison Deyett, Tobias Ilmer, Simon Haendeler, Aranxa Torres Caballero, Maria Novatchkova, Michael A. Netzer, Lavinia Ceci Ginistrelli, Estela Mancheno Juncosa, Tanishta Bhattacharya, Amra Mujadzic, Lokesh Pimpale, Stefan M. Jahnel, Martina Cirigliano, Daniel Reumann, Katherina Tavernini, Nora Papai, Steffen Hering, Pablo Hofbauer, and Sasha Mendjan, 2023. 'Multi-Chamber Cardioids Unravel Human Heart Development and Cardiac Defects'. Cell 186 (25): 5587-5605.e27. https://doi.org/10.1016/j.cell.2023.10.030.

5.1. Contribution

C.S., A.D., and S.M. co-designed experiments and co-wrote the paper. C.S. developed RV and OFT differentiations, established cell sorting assay, and performed the scRNA-seq experiment. A.D. developed atrial and AVC differentiations and designed and set up contraction, Ca2+, and MEA analysis. T.I. established multi-chamber cardioid generation. C.S., A.D., T.I., and A.T.C. characterized cardioids and performed teratogenic, mutant, and drug screens. M.A.N. did the patch clamp. S. Haendeler., L.P., and M.N. performed the image/movie-based and scRNA-seq bioinformatic analysis, respectively. N.P., S. Hering., and P.H. helped with training and advice. All other authors performed experiments. S.M. designed and supervised the study.

Cell

Resource

Multi-chamber cardioids unravel human heart development and cardiac defects

Graphical abstract

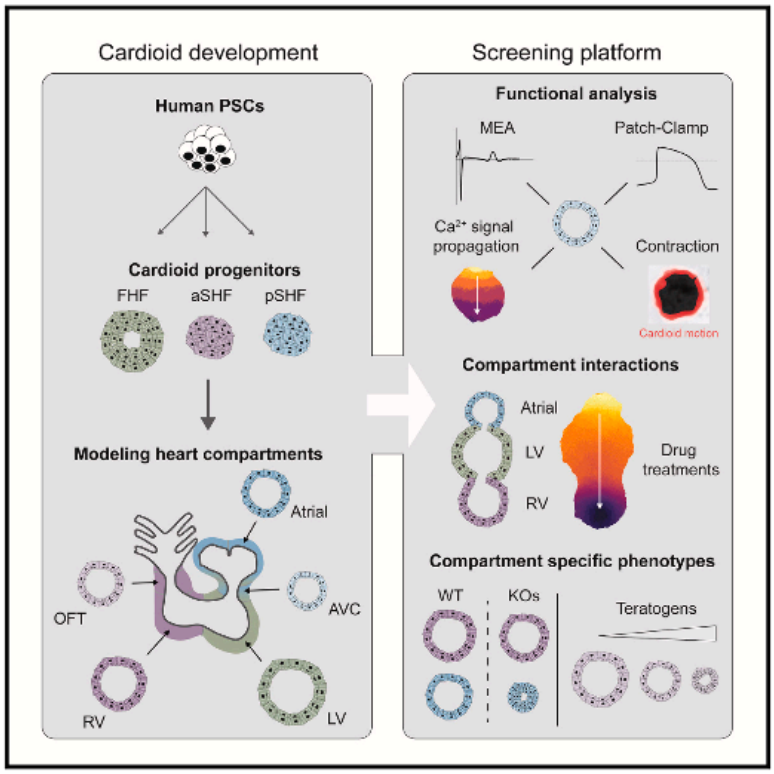

Authors

Clara Schmidt, Alison Deyett, Tobias Ilmer, ..., Steffen Hering, Pablo Hofbauer, Sasha Mendjan

Correspondence

sasha.mendjan@imba.oeaw.ac.at

In brief

Multi-chamber cardioids representing all major compartments of the human embryonic heart are developed and used to investigate electrophysiological signal propagation between chambers as well as dissect genetic and teratogenic causes of human cardiac defects.

Highlights

- Mesoderm induction and patterning signals specify aSHF, pSHF, and FHF progenitors
- Progenitors sort, co-develop, and functionally connect in multi-chamber cardioids
- Multi-chamber cardioids coordinate contraction propagation and share a lumen
- Multi-chamber platform dissects genetic, teratogenic, and physiological defects

Schmidt et al., 2023, Cell *186*, 5587–5605
December 7, 2023
Published by Elsevier Inc.
https://doi.org/10.1016/j.cell.2023.10.030

CellPress

Cell

CellPress
OPEN ACCESS

Resource

Multi-chamber cardioids unravel human heart development and cardiac defects

Clara Schmidt,[1,7,8] Alison Deyett,[1,7,8] Tobias Ilmer,[1,5] Simon Haendeler,[2,7] Aranxa Torres Caballero,[1] Maria Novatchkova,[6] Michael A. Netzer,[3] Lavinia Ceci Ginistrelli,[1,7] Estela Mancheno Juncosa,[1,7] Tanishta Bhattacharya,[1] Amra Mujadzic,[1] Lokesh Pimpale,[4] Stefan M. Jahnel,[1] Martina Cirigliano,[1] Daniel Reumann,[1,7] Katherina Tavernini,[1,7] Nora Papai,[1,7] Steffen Hering,[3] Pablo Hofbauer,[4] and Sasha Mendjan[1,9,*]

[1]Institute of Molecular Biotechnology of the Austrian Academy of Sciences (IMBA), Dr. Bohr Gasse 3, 1030 Vienna, Austria
[2]Center for Integrative Bioinformatics Vienna, Max Perutz Laboratories, University of Vienna, Medical University of Vienna, 1030 Vienna, Austria
[3]Division of Pharmacology and Toxicology, University of Vienna, Josef-Holaubek-Platz 2, 1090 Vienna, Austria
[4]HeartBeat.bio AG, Dr. Bohr Gasse 7, 1030 Vienna, Austria
[5]FH Campus Wien, Favoritenstraße 226, 1100 Vienna, Austria
[6]Institute of Molecular Pathology (IMP), Campus-Vienna-Biocenter, 1030 Vienna, Austria
[7]Vienna BioCenter PhD Program, Doctoral School of the University of Vienna, and Medical University of Vienna, 1030 Vienna, Austria
[8]These authors contributed equally
[9]Lead contact
*Correspondence: sasha.mendjan@imba.oeaw.ac.at
https://doi.org/10.1016/j.cell.2023.10.030

SUMMARY

The number one cause of human fetal death are defects in heart development. Because the human embryonic heart is inaccessible and the impacts of mutations, drugs, and environmental factors on the specialized functions of different heart compartments are not captured by *in vitro* models, determining the underlying causes is difficult. Here, we established a human cardioid platform that recapitulates the development of all major embryonic heart compartments, including right and left ventricles, atria, outflow tract, and atrioventricular canal. By leveraging 2D and 3D differentiation, we efficiently generated progenitor subsets with distinct first, anterior, and posterior second heart field identities. This advance enabled the reproducible generation of cardioids with compartment-specific *in vivo*-like gene expression profiles, morphologies, and functions. We used this platform to unravel the ontogeny of signal and contraction propagation between interacting heart chambers and dissect how mutations, teratogens, and drugs cause compartment-specific defects in the developing human heart.

INTRODUCTION

Congenital heart disease (CHD) is the most common human developmental birth defect and the most prevalent cause of embryonic and fetal mortality.[1,2] CHDs most often affect specific compartments of the embryonic heart, such as the outflow tract (OFT), the atria, the atrioventricular canal (AVC), and the right ventricle (RV).[3] For about 56% of diagnosed CHD cases, the underlying cause is unknown but is assumed to originate from undiscovered genetic mutations, environmental factors, or a combination of both.[4] To identify possible causes and preventive measures, we need models encompassing all compartments of the developing human heart.

CHDs occur early in embryonic development, making the characterization of disease etiology particularly challenging.[5,6] These difficulties are compounded by the lack of control over the interactions between genetic background and environmental factors during human embryonic development.[4] Understanding the etiology of CHD solely through animal models is not feasible, given tissue complexity, developmental speed, inaccessibility, and species-specific differences.[7] These differences include the disc-like shape of the human embryo, divergence in extraembryonic tissues and implantation, the gestational timing and proliferation rates, and the distinct expression of some cardiac transcription factors (TFs), structural proteins, and ion channels, resulting in specific electrophysiological characteristics and disease suspensibility. We do not have human *in vivo* references for some of these disparities, as there are no molecular and physiological data for the crucial cardiac developmental period between 19 and 28 days post-fertilization (dpf). Nevertheless, the general principles of heart development, such as the role of signaling, cell types, lineage architecture, and function, are conserved. Inspired and guided by *in vivo* cardiogenesis, recently reported human self-organizing cardiac organoids are important and complementary, as these represent experimental models of human cardiac development and thereby allow reductionist dissection of mechanisms in high throughput, obtaining results with high statistical significance.[8,9] However, these

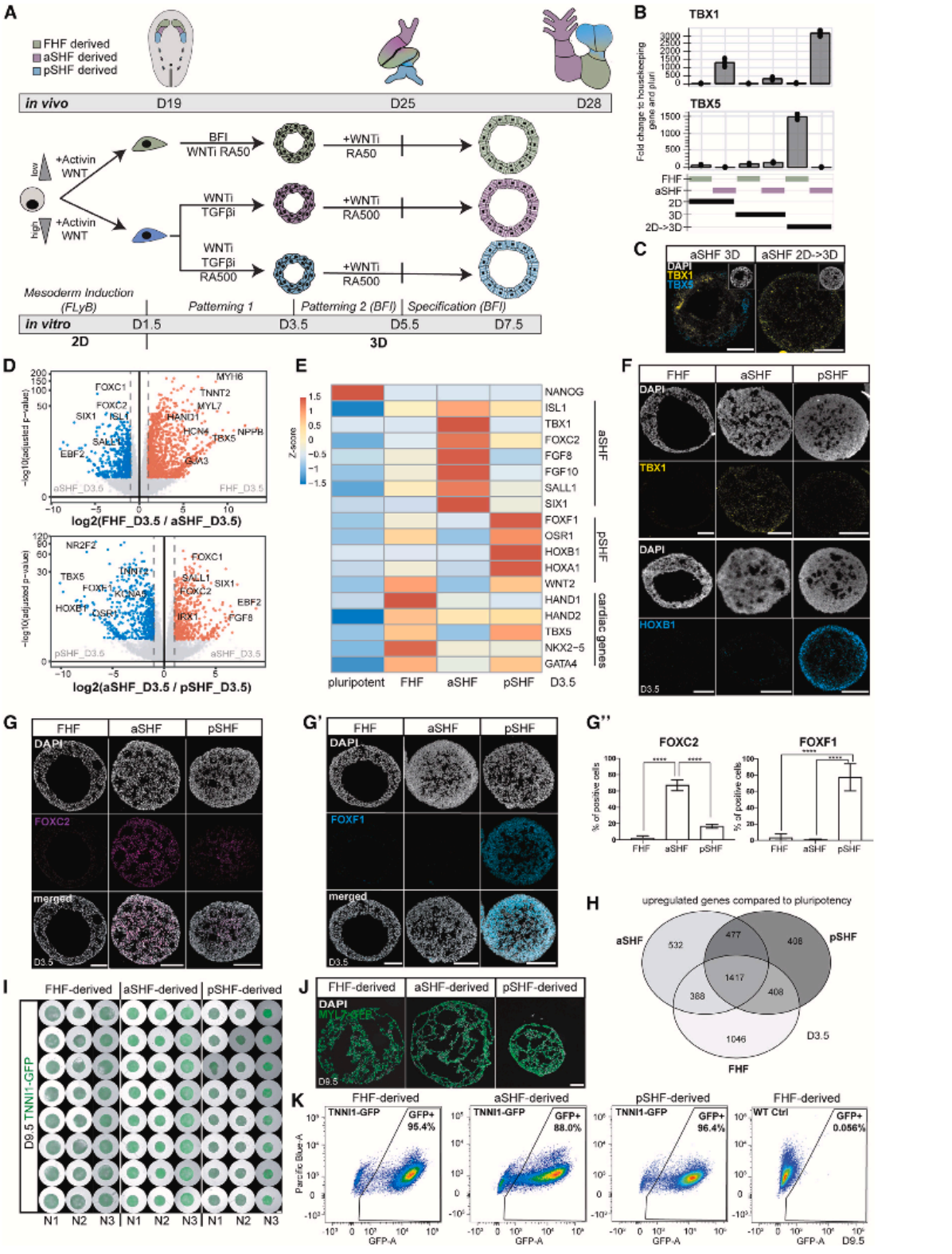

(legend on next page)

systems do not yet allow the mechanistic interrogation of defects representing all interacting compartments (OFT, AVC, atria, RV, and left ventricle [LV]) of the human embryonic heart.

For a controlled *in vitro* system to mimic human heart development, it is essential to deploy the *in vivo* principles that govern the coalescence of all lineages in building a heart.[10,11] Heart structures are predominantly derived from three progenitor populations that give rise to specific cardiomyocyte (CM) lineages. The first heart field (FHF) primarily gives rise to the developing LV, the anterior second heart field (aSHF) to the developing RV and most of the OFT, and the posterior second heart field (pSHF) gives rise to most of the atria and a portion of the AVC. The development of these structures is carefully timed such that the FHF-derived CMs form the heart tube and the LV, while the aSHF and pSHF differentiate to form the remaining compartments in a delayed and gradual fashion. This complex and dynamic process is orchestrated by developmental signaling pathways (WNT, Nodal/Activin, BMP, etc.) at specific stages.[12] The signaling pathways control key downstream compartment-specific TFs (e.g., TBX1, TBX5, and IRX4), instructing progenitor specification, morphogenesis, and physiology.[13] Although much is known about these core network components, we lack a human model enabling mechanistic dissection of how mutations or environmental factors lead to CHD or fetal death.

Here, we established a multi-chamber cardioid platform that unravels how interacting chambers coordinate contractions and how mutations, drugs, and environmental factors impact specific regions of the developing human heart.

RESULTS

Generation of cardioids from aSHF and pSHF progenitors

To derive SHF progenitors, we first hypothesized that the aSHF is exposed to WNT and Nodal signaling inhibition, a similar signaling environment as other anterior and dorsal embryonic regions (neuroectoderm and head mesoderm).[14,15] Thus, we derived cardioids[16] from the aSHF lineage by inducing mesoderm first, followed by the aSHF-patterning-1 stage using dual WNT and Nodal/Activin signaling inhibition (Figure 1A). Synergistic WNT and Nodal/Activin inhibition were necessary for early aSHF lineage marker (TBX1 and FOXC2) upregulation, while any Nodal/Activin signaling modulation interfered with FHF differentiation (Figures S1D and S1F). As *in vivo*, BMP signaling at the patterning-1 stage hampered aSHF specification (Figure S1E).[10] After 3.5 days of 3D differentiation, we observed aSHF and FHF/pSHF (TBX5+) progenitor heterogeneity and traced its origin to the earlier induction stage (day 1.5) with the mesoderm marker EOMES expressed only at the surface and the pluripotency and neuroectoderm marker SOX2 in the cardioid core (Figures 1B, 1C, S1A, and S1B). Thus, we hypothesized that cells in 2D receive more equally distributed induction signals, resulting in a homogeneous exit from pluripotency and differentiation, whereas mesoderm is not induced homogeneously in 3D. When we induced mesoderm in 2D and initiated differentiation in 3D only at patterning-1 (day 1.5), cells exited pluripotency efficiently (Figure S1B), expressed high levels of TBX1 and FOXC2 (67%, protein level), and only a few cells expressed TBX5 (Figures 1B, 1C, S1A, S1D, S1G, and S1H). In contrast, the expression of head mesoderm markers was absent (Figure S1C),[17] indicating that the staged 2D-3D differentiation produces more homogeneous progenitor populations.

In contrast to the aSHF, the pSHF is exposed to retinoic acid (RA) signaling *in vivo*,[18] which activates pSHF regulators (HOXB1, HOXA1, and TBX5) and inhibits the aSHF expression signature. Consistently, we observed that adding RA during aSHF-patterning-1 promoted pSHF identity (Figures 1A, 1E–1G′, and S1E), while manipulation of other signaling pathways (SHH, WNT, and FGF) had little to no effect (Figure S1E).[19] As *in vivo*,[20] different Nodal/Activin and WNT signaling levels during mesoderm induction stimulated the aSHF and pSHF over the FHF lineage (Figure S1G). When we analyzed the three progenitor subtypes by RNA sequencing (RNA-seq), we found that the FHF, aSHF, and pSHF markers were among the most differentially expressed genes (Figures 1D and 1E). The specificity and homogeneity of the progenitor populations were further underscored by the mutually exclusive expression of lineage-specific markers (Figures 1D–1H and S1H). Still, all populations were positive for the cardiac progenitor marker NKX2-5 and mostly negative for SOX2 (Figure S1I). Overall, these data suggest that in the cardioid system, we can efficiently and homogeneously generate all three major cardiac progenitors.

The FHF, aSHF, and pSHF give rise to several different cardiac cell types in the embryo, including CMs and endothelial cells (ECs). We showed previously that FHF progenitors generate LV

Figure 1. aSHF and pSHF progenitors express specific markers and form functional cardioids

(A) Differentiation protocol into three main cardiac lineages: first heart field (FHF), anterior second heart field (aSHF), and posterior second heart field (pSHF). WNT, CHIR99021; LY, LY 294002; B, BMP4; F, FGF2; I, insulin; WNTi, C59 or XAV-939; TFGBi, SB 431542; RA, retinoic acid (numbers represent μM).

(B) Marker RT-qPCR in FHF/aSHF progenitors in 2D, 3D, and 2D→3D protocols.

(C) RNA-scope marker staining of aSHF-cardioid cryosections in 2D→3D vs. 3D differentiation. For subsequent figures, the 2D-3D protocol is used.

(D) RNA-seq volcano plot of differentially expressed genes in indicated conditions.

(E) RNA-seq expression heatmap for lineage-specific cardiac mesoderm TFs.

(F) RNA-scope marker staining as specified.

(G) (G and G′) Marker immunostaining in cardioids with (G″) quantification (N = 3, n = 3–9).

(H) RNA-seq Venn diagram of shared upregulated genes in different cardiac progenitors.

(I) Biological and technical replicates of representative whole-mount cardioid images derived from TNNI1-GFP-hPSCs. Scale bars, 500 μm.

(J) MYL7-GFP-hPSC-derived cardioid subtype cryosections.

(K) Representative CM flow cytometry plot derived from TNNI1-GFP/WT-hPSCs. Indicated day of analysis (D). Scale bars, 200 μm, except where specified. hPSC lines: H9 and WTC11. Bar graphs show mean ± SD. Statistics: one-way ANOVA. *$p < 0.05$, **$p < 0.01$, ***$p < 0.001$, ****$p < 0.0001$. ns: not significant.

N, biological replicate number; n: technical replicate number.

See also Figure S1.

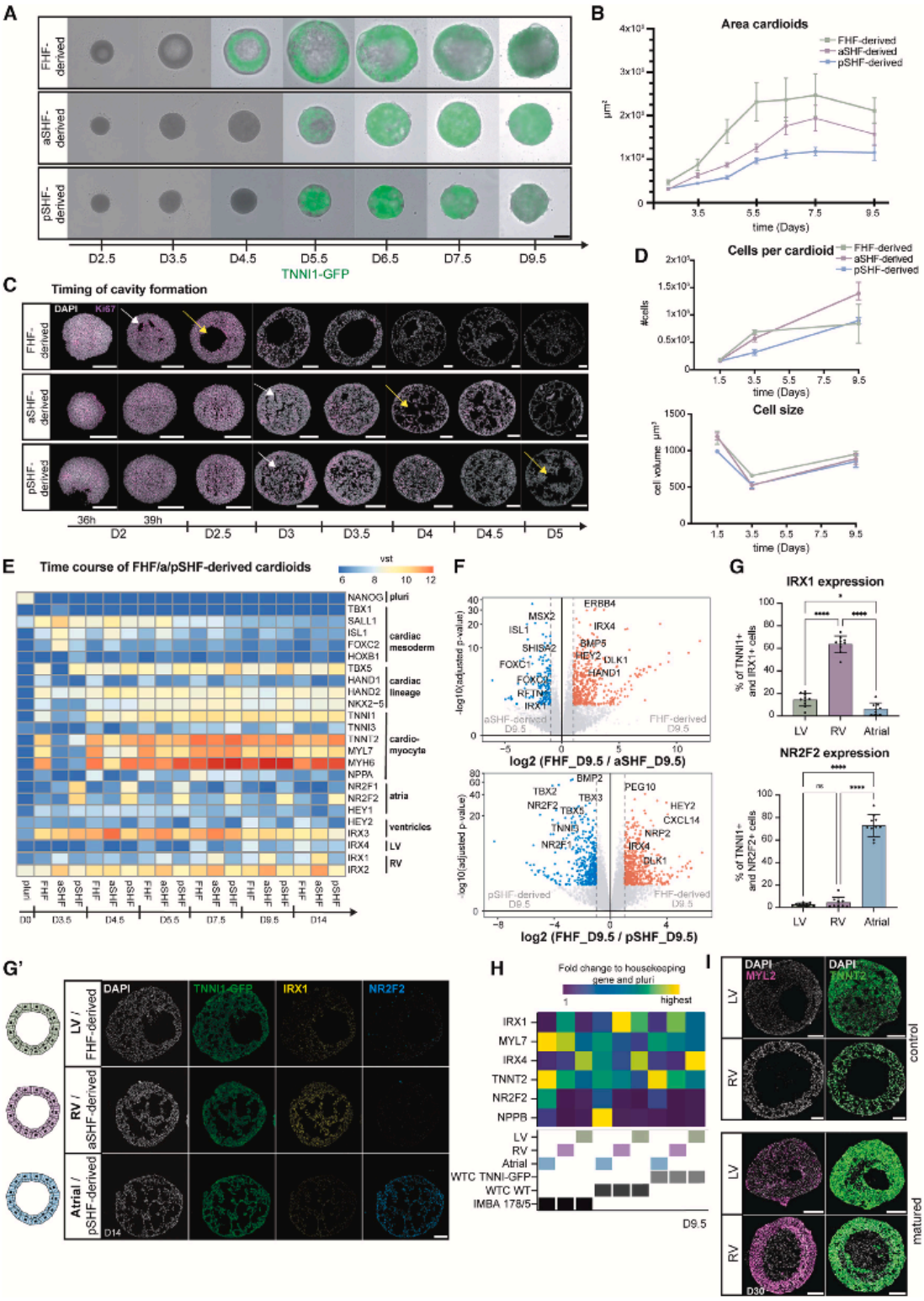

Figure 2. aSHF/pSHF-derived cardioids exhibit *in vivo*-like morphogenesis delay and gene expression

(A) Representative whole-mount images of a time course for TNNI1-GFP-hPSC-derived cardioid subtypes. Scale bars, 500 µm.

(B) Quantification of cardioid area change during differentiation in (A) (N = 3, n = 75–96) per time point.

(legend continued on next page)

chamber-like contracting cardioids (LV cardioids) containing CMs and ECs.[16] Following this method, we continued to inhibit WNT signaling while treating the aSHF/pSHF progenitors with BMP, FGF, insulin, and RA (patterning-2) (Figure 1A), resulting in the reproducible formation of contracting cavity-containing cardioids in high throughput (Figures 1I and 1J). In contrast to FHF-derived cardioids, aSHF/pSHF-derived cardioids require higher RA dosage at this stage. Efficient aSHF differentiation also necessitated a lower seeding density (Figures S1K and S1L) during mesoderm induction, as a high density led to inefficient CM differentiation and expression of neural markers within the organoid core (Figures S1K and S1K′). Precise cell counting before patterning-1 aggregation was essential for robust cardioid formation (Figure S1L). As a result, more than 85% of the cardioid cells expressed the CM marker TNNI1 (Figures 1K and S1M) and low levels of SOX2, endoderm (FOXA2), and fibroblast (COL1A1) markers (Figure S1J). Finally, aSHF and pSHF progenitors differentiated efficiently into PECAM1+ ECs in 2D when exposed to VEGF and forskolin after aSHF/pSHF-patterning-1 (Figures S1N and S1O). In summary, by applying *in vivo*-like signaling and cell number optimizations, aSHF/pSHF progenitors can be differentiated efficiently into CM and endothelial lineages within the cardioid system.

Formation of RV and atrial cardioids

During development, FHF progenitors differentiate into CMs that form the heart tube, while aSHF progenitors first proliferate and then differentiate together with pSHF progenitors at a later developmental stage.[10] Consistently, a detailed time course analysis revealed a CM specification and morphogenesis delay in SHF cardioids (Figures 2A–2C and S2A), while proliferation rate and Ki67 expression were elevated in aSHF progenitors until day 4.5 (Figures 2C, 2D, and S2B). In addition, aSHF progenitors appeared more epithelial-like, as seen by higher CDH1 and lower CDH2 expression, reminiscent of *in vivo*.[19,21] The aSHF/pSHF cardioids were also smaller than FHF cardioids and showed delayed TNNI1 expression (Figures 2A, 2B, and S2A). The FHF cardioids were larger despite containing fewer cells than aSHF cardioids and similarly sized individual cells, indicating that the intercellular space accounts for the observed differences (Figures 2D and S2A). Global gene expression confirmed that structural CM gene expression was delayed in SHF cardioids (Figures 2E and S2C), and we observed a delay in cavity formation (Figure 2C). Thus, the staggered differentiation of SHF and FHF cardioids *in vitro* is consistent with the *in vivo* developmental timing and morphogenesis.

Next, we asked whether the acquisition of chamber identity also followed the developmental trajectory in aSHF/pSHF-derived cardioids. *In vivo*, the FHF gives rise to the LV and a minor portion of atrial CMs, whereas the aSHF and pSHF give rise to the RV and atria, respectively.[11] To answer that question, we compared the specification potential of aSHF/pSHF/FHF progenitors by adjusting the concentration of RA. We observed that aSHF progenitors gave rise to early RV-like identity (IRX1+, IRX2+, IRX3+, and NPPA+), while the pSHF progenitors differentiated into early atrial CMs (HEY1+, NR2F1+, and NR2F2+) (Figures 2E–2G′). In a global gene expression comparison at day 9.5, we found that the top upregulated genes in aSHF cardioids included ISL1, IRX1, HEY2, and RFTN1 (Figures 2F and S2D), which have been implicated in ventricular identity and physiology. In contrast, in pSHF cardioids, TBX5, NR2F2, and NR2F1 were upregulated, consistent with early atrial identity (Figures 2F and S2D). These findings were confirmed on a protein level for IRX1, NR2F2, and HEY2 (Figures 2G, 2G′, and S2E). The specification of the CM subtypes was also achieved using H9 human embryonic stem cells (hESCs), different WTC human-induced PSC (hiPSC) sublines, and another independent hiPSC line (Figures 2H and S2F–S2H). In summary, aSHF progenitors specify into RV-like cardioids (RV cardioids), and pSHF progenitors form atrial cardioids (A cardioids), showing that the early priming of progenitors is crucial to obtaining different chamber identities in the developing heart.

To achieve further chamber specification and maturation, we tested several recently published ventricular CM signaling and metabolic treatments (Figure S2I).[22–24] In an adapted combination of these conditions, LV/RV cardioids upregulated the key ventricular structural protein MYL2, chamber markers NPPA and NPPB, and showed a typical maturation shift in MYH7 and MYH6 expression ratio (Figures 2I and S2J–S2M), resulting in well-defined sarcomere structures and higher contraction amplitude (Figures S2L and S2N). However, as this approach interfered with atrial differentiation, we sought to identify the combination of factors promoting further atrial chamber maturation (Figure S2I). We found that the FGF and RA pathway activation and NOTCH and BMP signaling inhibition combined with metabolic maturation promoted the atrial chamber program (NPPA+, NPPB+, NR2F2+, IRX4−, and MYL2−) while strongly downregulating the heart tube and AVC-specific transcripts TBX2 and TBX3 (Figure S2O). Cumulatively, we demonstrated that we could specify and differentiate cardioids into the three chamber identities found in the embryonic heart.

Specification of OFT and AVC cardioids

Besides the RV, aSHF progenitors differentiate into the OFT, which gives rise to the aortic and pulmonary valve and vessel structures.[10] Abnormalities in OFT derivatives are the most

(C) Ki67 immunostaining of cardioid cryosections, showing delayed cavity initiation (white arrow) and cavity expansion (yellow arrow).
(D) Representative quantification of cell number per cardioid and cell size change during differentiation; N = 3, n = 8 per time point.
(E) RNA-seq expression heatmap of lineage- and compartment-specific genes.
(F) RNA-seq volcano plot showing differentially expressed genes in indicated conditions.
(G) (G′) Lineage-specific immunostaining and (G) quantification (N = 3, n = 8–11), as specified.
(H) RT-qPCR expression heatmap of chamber-specific marker cardioids derived from different cell lines.
(I) MYL2 immunostaining in matured LV/RV cardioids. Indicated day of analysis (D). Scale bars, 200 μm, except where specified. Bar and dot plot graphs show mean ± SD. Statistics: one-way ANOVA. vst, variance-stabilized transformed counts. *p < 0.05, **p < 0.01, ***p < 0.001, ****p < 0.0001. ns: not significant.
N, biological replicate number; n: technical replicate number.
See also Figure S2.

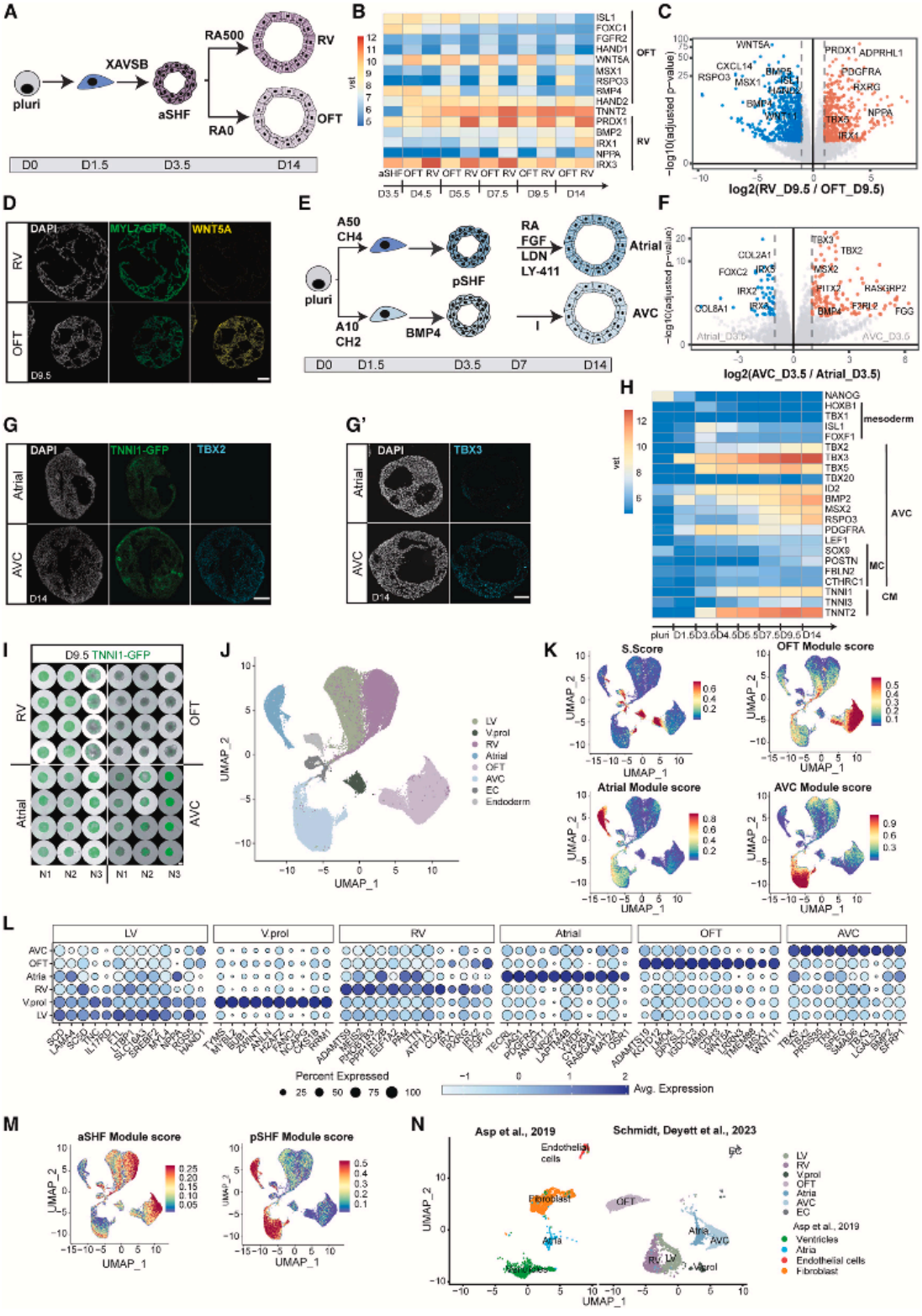

(legend on next page)

frequent congenital heart defects.[3] We observed that higher RA dosages promoted aSHF specification toward the RV identity (Figures 3A and S3A), while the absence of exogenous RA promoted the expression of OFT (WNT5A, ISL1, HAND2, and RSPO3) but not chamber markers (Figures 3B–3D, S3B, and S3C).[19] OFT cardioids were more mesenchymal (MC)-like (Figure S3E), delayed in differentiation (Figure 3B), and smaller compared with RV cardioids (Figure 3I). Further optimization revealed that C59 (inhibits canonical and non-canonical WNT) led to higher expression of chamber markers in the RV cardioid, whereas XAV-939 (inhibits only canonical WNT) promoted upregulation of OFT genes (Figure S3D). OFT cardioids contained mostly TNNI1+ CMs, and few showed fibroblast or endothelial marker expression (Figure S3G). As a functional validation, OFT cardioids displayed more efficient smooth muscle cell (SMC) differentiation propensity (ACTA2+ and TNNT2−), compared with the FHF that typically does not give rise to SMCs *in vivo* (Figures S3F and S3F′).[25] They could also be stimulated by VEGF to form an inner EC layer and show MC SOX9+ cells upon treatment with EMT-promoting factors transforming growth factor β (TGF-β) and FGF2 (Figure S3E). Thus, aSHF progenitors can be directed into OFT cardioids with SMC and endothelial EMT differentiation potential reminiscent of early valve and great vessel development.

In vivo, pSHF-derived CMs comprise most of the atria and contribute to the AVC, a crucial region where valves and pacemaker elements develop. Studies in mice showed that pSHF precursors are located in different primitive streak areas and will migrate out at different time points (AVC earlier, atrial later).[20,27,28] Thus, we hypothesized that mesoderm induction conditions for the two pSHF populations will differ. Indeed, we found that intermediate Activin and low WNT activation levels during mesoderm induction resulted in higher expression of primitive streak markers at day 1.5 (Figures 3E and S3H), leading subsequently to the upregulation of AVC-specific genes (TBX2 and TBX3) and downregulation of atrial genes at day 9.5 (Figure S3I). The pSHF signature at day 3.5 remained in both pSHF populations (Figure S3I). Another difference between AVC and atrial development *in vivo* is the high exposure of the AVC region to BMP ligands. As hypothesized, the addition of BMP4 at the patterning stage upregulated early AVC markers (Figure S3I), and optimized induction and patterning (Figure 3E) drove pSHF specification toward AVC identity (Figures 3F–3H). AVC cardioids were smaller than atrial (Figure 3I), and only a few cells were PECAM1+ or COL1A1+ (Figure S3G). Overall, the subspecification of pSHF progenitors into atrial or AVC cardioids started as early as the mesoderm induction stage, reflecting the developmental plasticity of the pSHF.

scRNA-seq analysis of cardioids and *in vivo* comparison

Human embryonic cardiogenesis between 19 and 28 dpf is inaccessible and poorly characterized, and current single-cell RNA-seq (scRNA-seq) datasets typically correspond to later developmental stages. Thus, we aimed to compare all five cardioid subtypes by scRNA-seq analysis and explore the specification differences of early human heart compartments beyond well-established animal markers. We performed scRNA-seq on LV (day 7.5), RV, AVC, OFT, and A cardioids (day 9.5) matched for their structural CM differentiation stage (see Figures 2A–2C). Quality control filtering required the removal of only 5%–10% of cells, and uniform manifold approximation and projection (UMAP) cluster analysis separated different cell types and compartment-specific CMs (Figure 3J). The clustering revealed small non-CM (ECs and endoderm) populations, efficient CM differentiation, and a reproducible cluster arrangement of biological replicates (Figures S4A and S4B). As in development, many early ventricular CMs had a proliferative transcriptomic signature and a high S. score (Figures 3J–3L). Compartment-specific CM clusters diverged, including the RV and LV (Figures S3J–3L and S4C), and expressed literature-curated gene modules (Figures 3L, 3M, and S3J–S3L). Many of the differentially expressed genes are well-known markers. Still, others have not been highlighted before, such as PDGFRA (atrial), CD24 (RV), TMEM88 (OFT), and TRH (AVC) (Figures 3L and S3J), revealing a valuable resource window into a hidden human developmental stage. We then compared these data corresponding approximately to 25–28 dpf of human cardiogenesis with two scRNA-seq datasets, derived from dissected human embryonic ventricles, atria,[26] and OFT (30–50 dpf),[29] using the same parameters. Randomized downsampling to facilitate integration with the *in vivo* cell numbers revealed a remarkable overlap in the clustering of ventricular and atrial CMs (Figures 3N and S3N). Since the *in vivo* samples represented a later developmental stage, there was an expected larger population of fibroblasts and a

Figure 3. Specification of OFT/AVC cardioids and scRNA-seq *in vivo* comparison

(A) RV/OFT cardioid differentiation protocols, emphasizing treatment differences.
(B) RNA-seq expression heatmap time course of markers in developing RV/OFT cardioids.
(C) RNA-seq volcano plot showing gene expression differences between RV and OFT cardioids.
(D) *In situ* hybridization chain reaction cryosections of MYL7-GFP-hPSC-derived RV/OFT cardioids.
(E) A/AVC cardioid differentiation protocol, emphasizing treatment differences.
(F) RNA-seq volcano plot showing differentially expressed genes at indicated conditions.
(G) (G) TBX2 and (G′) TBX3 immunostaining on cryosections of A/AVC cardioids.
(H) RNA-seq expression heatmap time course of developing AVC cardioids. MC, mesenchymal.
(I) Whole-mount images of TNNI1-GFP-hPSC-derived RV/OFT/A/AVC cardioids (N = 3). Scale bars, 500 μm.
(J–N) scRNA-seq analysis comparing all protocols (N = 2, atrial: N = 1, n = 16–72). (J) scRNA-seq UMAP showing different clusters; V.prol, ventricular proliferating. (K) Expression of S. score (cycling cells), OFT, AVC, and atrial gene modules. (L) Dot plot showing the most expressed genes of each CM cluster. (M) Expression of aSHF and pSHF gene modules. (N) UMAP showing integration with the scRNA-seq *ex vivo* dataset of Asp et al.[26] Samples were randomly downscaled to 3,000 cells. Indicated day of analysis (D). vst, variance-stabilized transformed counts. Scale bars, 200 μm. Module gene lists are in Table S2.
N, biological replicate number; n: technical replicate number.
See also Figure S3.

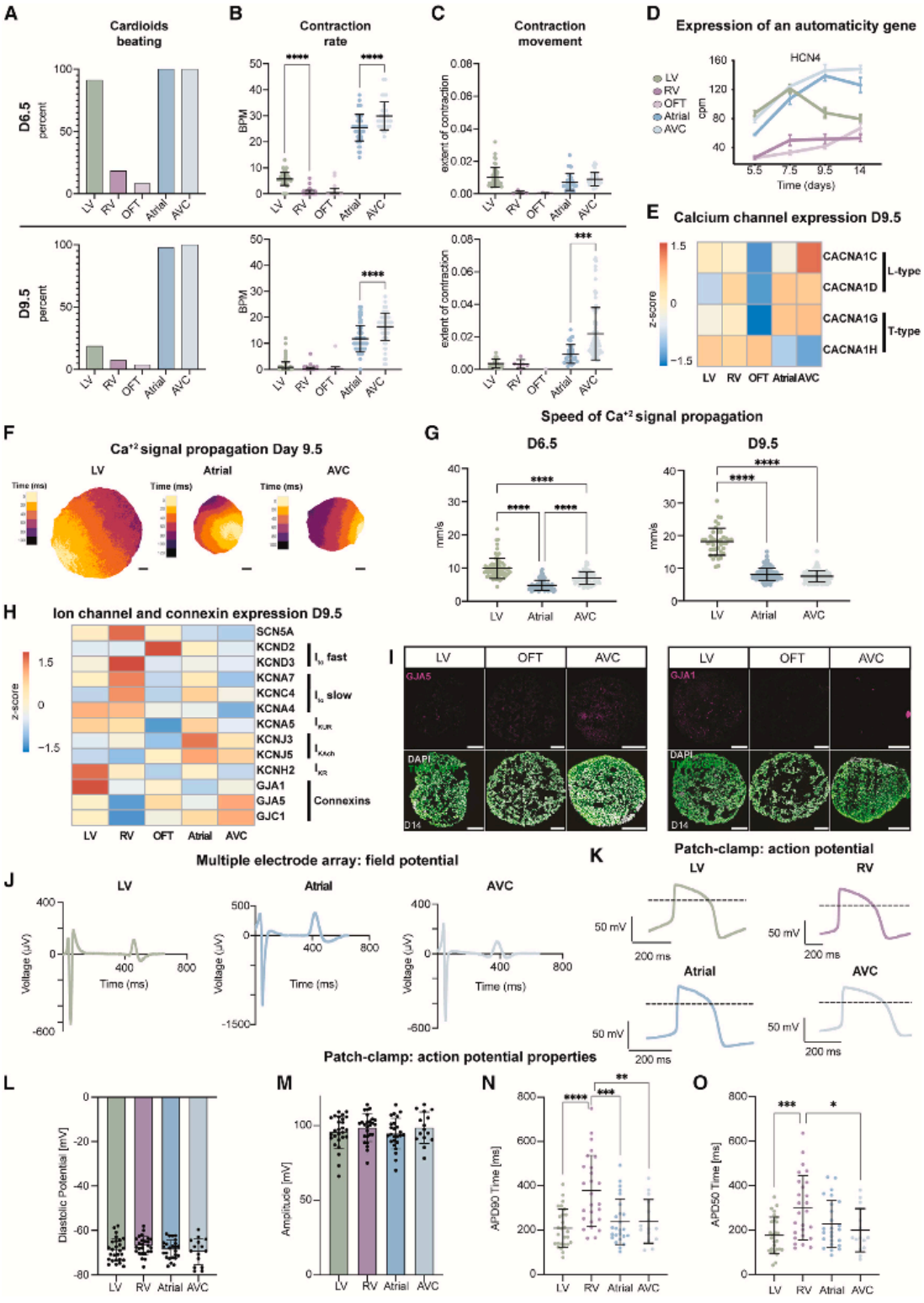

(legend on next page)

more mature but similar OFT signature. Overall, the cardioid subtype scRNA-seq analysis confirmed the compartment-specific CM identities, providing an invaluable resource to reveal early specification mechanisms at an obscure stage of human development.

Functional characterization of the five cardioid subtypes

The heart must function while developing; thus, understanding early cardiac activity during embryonic heart compartment formation is imperative. We hypothesized that the cardioid platform could investigate functional developmental differences between compartments in the absence of human *in vivo* data. Contraction behavior of day 6.5 cardioid subtypes showed spontaneous contraction (automaticity) in 90%–100% of LV, atrial, and AVC, and a greater extent of contraction. In contrast, only 18% of RV cardioids contracted spontaneously, and 8% of OFT cardioids showed a lower contraction extent (Figures 4A, 4C, and S4B; Video S1). On day 9.5, A/AVC cardioids automaticity was maintained, while the contraction rate decreased in LV, RV, and OFT cardioids (Figures 4A–4C; Video S1). Similar to *in vivo*,[30] the loss of automaticity correlated with the expression downregulation of the HCN4 potassium/sodium channel found in pacemakers (Figure 4D). These observations were reproducible across both technical and biological replicates and cell lines (Figures 4A–4C and S4A). To gain further insights into signal propagation in cardioids, we generated GCaMP6f reporter lines to trace Ca^{2+} transients (Figure S4C) and found that each cardioid subtype has its distinct Ca^{2+} wave pattern; the A, AVC, and LV cardioids beat very regularly (100% beating), while RV cardioids tended not to contract but exhibited Ca^{2+} waves that constantly signaled in one long burst ("re-entry," 80%) (Figure S4C; Video S2).

When we investigated how Ca^{2+} transits across the whole cardioid, LV cardioids showed a prolonged transient, compared with atrial and AVC,[19] as reported *in vivo*.[31] The signal propagation speed across cardioids differed between subtypes and differentiation stages, where LV cardioid's Ca^{2+} transients further increased from day 6.5 to propagate faster than A/AVC cardioids at day 9.5 (Figures 4F and 4G). This is consistent with the upregulation of GJA1 (CX43), specifically in LV cardioids, which have high conductance, and the upregulation of GJC1 (CX45), in AVC cardioids, which have low conductance properties (Figure 4H and 4I).[32] Within one cardioid, the origin of signal propagation varied between beats (Video S2). We also observed differences between cardioid subtypes, as reflected by expression differences in T- and L-type Ca^{2+} channels (Figure 4E). Overall, compartment-specific cardioids have distinct contraction and signal propagation profiles at these early embryonic stages, which are not accessible in humans.

During early heart development, ion channel expression is relatively uniform, but in later stages, chamber-specific gene expression profiles and species-specific action potential (AP) shapes emerge, often measured by field potential (FP) or AP duration (APD).[33] The cardioid subtypes also develop distinct ion channel expressions by day 9.5 (Figure 4H). As it is crucial to characterize how FPs and APs of early human CM subtypes differ within 3D cardioids, 2D monolayers derived from cardioids, and in single 2D CMs, we used multiple electrode arrays (MEAs), voltage-sensitive dye (FluoVolt) imaging, and manual patch clamp. Whole cardioids were placed on a 64 × 64 electrode grid to measure the FP at a high spatial resolution. We observed FP diversity across cardioid subtypes (Figures 4J and S4H–S4L), where a single LV cardioid showed a more homogeneous signal propagation FP spread than A/AVC cardioids (Figures S4I–S4L). In 2D monolayers, using FluoVolt, we found that the LV/RV CMs had longer APDs than atrial (Figures S4M–S4P). Patch-clamp analysis on single CMs revealed that the APD in atrial/AVC was shorter than in RV CMs, confirming the trends in monolayers, and similar to human primary CMs (Figures 4K, 4N, 4O, and S4Q–S4U). The diastolic potential was around −70 mV (Figure 4L), upstroke velocity (Figure S4S) and amplitude (Figure 4M) of the APs resembled the most advanced *in vitro* models,[34] and importantly, specific CMs were electrophysiologically homogeneous. Taken together, the electrochemical signaling of cardioid subtypes is diverse and fetal-like, enabling the functional investigation of early human cardiogenesis.

Multi-chamber integration of cardioid subtypes

Embryonic cardiac progenitors become specified in neighboring areas and self-sort to form separate compartments,[11] but studying the molecular basis of sorting mechanisms in embryos is

Figure 4. Functional characterization of cardioid subtypes

(A–C) Experiments were performed in N = 2–7, n = 80, 65, 48, 48, and 33 cardioids for LV, RV, OFT, atrial, and AVC, respectively. All experiments in the WTC11 hPSCs. (A) Quantification of the percentage of cardioids that spontaneously contract within 1 min of recording. (B) Quantification of beats per minute (BPM). (C) Quantification of contraction extent. Non-beating cardioids were excluded.

(D) RNA-seq quantification of HCN4 expression over time. Each dot represents the mean ± SD. cpm, counts per million.

(E) RNA-seq expression heatmap with indications.

(F) Representative calcium signal propagation image of TNNT2-GCaMP6f-hPSC-derived LV/A/AVC cardioids for one beat. Underneath, distance scale bars, 200 μm.

(G) Quantification of signal propagation speed across TNNT2-GCaMP6f-hPSC-derived cardioid subtypes. Each point represents the mean speed for all beats of a single cardioid. LV: N = 3, (n = 71, day 6.5; n = 40, day 9.5); atrial: N = 3, n = 159; AVC: N = 3, n = 85.

(H) RNA-seq expression heatmap with indications.

(I) Immunostained LV/OFT/AVC cardioid cryosections.

(J) Representative MEA FP curves of LV/A/AVC cardioids.

(K–O) Patch-clamp analysis of single CMs dissociated from WTC11-hPSC-derived cardioids. Each point represents the mean from one cell for 15–20 consecutive APs. N = 1, n: LV: 27, RV: 26, Atrial: 25, AVC: 15. (K) Representative AP curves. (L) Diastolic potential. (M) AP amplitude. (N) AP duration (APD90). (O) APD50. Indicated day of analysis (D). Scale bars, 200 μm. All graphs show mean ± SD. Statistics: one-way ANOVA. *p < 0.05, **p < 0.01, ***p < 0.001, ****p < 0.0001. N, biological replicate number; n: technical replicate number.

See also Figure S4.

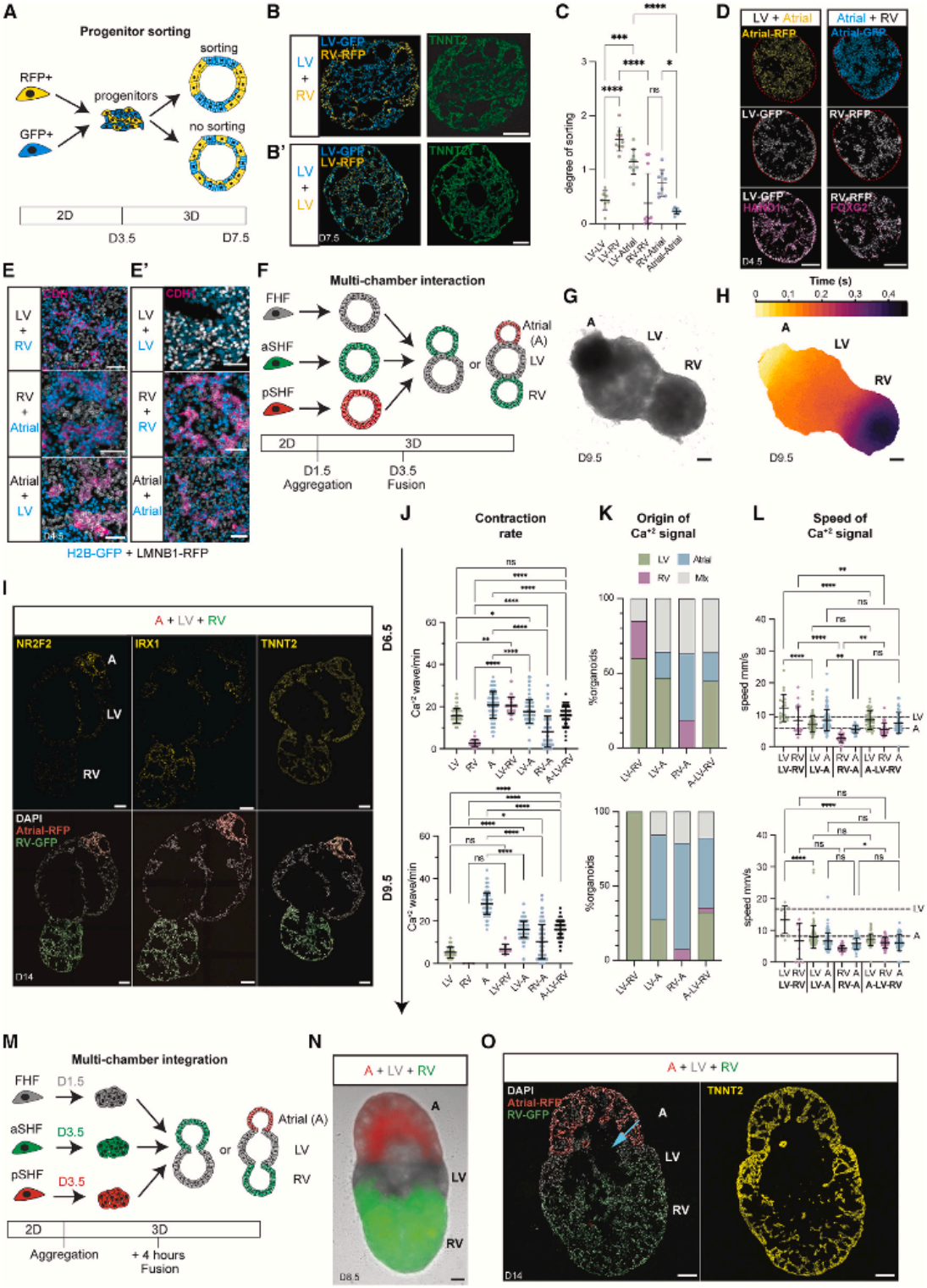

Figure 5. Multi-chamber integration of cardioid subtypes

(A) Sorting experiments schematic.

(B and B′) Representative cryosections of hPSC-H2B-EGFP/hPSC-LMNB1-RFP-derived cardioids from (B) different or (B′) the same progenitors.

(C) Sorting quantification of H2B-GFP+ and LMNB1-RFP+ progenitors; N = 2–3, n = 7–11.

(legend continued on next page)

challenging. To test whether aSHF/pSHF/FHF progenitors have the same self-sorting potential as their *in vivo* counterparts, we dissociated day 3.5 cardioid subtypes derived from either H2B-GFP- or LMNB1-RFP-hPSCs, mixed them (Figure 5A), and observed self-sorting within 24 h while keeping their CM identity until day 7.5 (Figures 5B–5D, S5A, and S5B). In contrast, progenitors of the same subtype tended not to sort upon mixing (Figures 5B′, 5C, and S5A′). The sorting was consistent with the specific cadherin and TF expression signatures in the different progenitors, reminiscent of *in vivo* (Figures 5D, 5E, 5E′, and S5C).[21] Compartments retained the appropriate chamber fate (Figure S5D), confirming that the first two stages of differentiation determine lineage identity and that co-differentiation was possible from day 3.5 onward.

In vivo, cardiac chambers co-develop seamlessly; however, we lack a multi-chamber model to study this crucial stage and the complex process of cardiac morphogenesis. As progenitors are specified and sorted already at day 3.5, we hypothesized that co-developing cardioids would also remain separate at this stage but undergo morphogenesis together. When we placed different cardioid subtypes together on day 3.5 (Figure 5F), they co-developed to form a structural connection after 24 h (Figure S5E and S5F). Still, they maintained their distinct identities and compartments (Figures 5G and 5I). In contrast, when we placed cardioid subtypes together on day 5.5, they failed to connect by day 9.5 (Figure S5E). Cardioids only co-developed when combined on day 3.5, electrochemically connected, and contracted in a coordinated manner by day 6.5 (Figures 5H and S5G; Video S3), demonstrating functional interaction. When we combined the progenitors just before cavity formation (Figure 5M) (day 1.5 FHF/LV; day 3.5 aSHF/RV and pSHF/A), we found that they also shared a lumen while retaining CM identity (Figures 5M–5O, S5Q, and S5R). Hereafter, we refer to these structures as multi-chambered cardioids. Multi-chambered cardioids co-developed in all combinations, allowing us to study the interactions of two-chambered cardioids or three-chambered cardioids (atrial, LV, and RV fusions; Figures 5G–5I and S5G; Video S3) in the same order as within the developing embryonic heart or in alternative experimental arrangements (Figure S5J and S5K; Video S3).

The directionality of the electrochemical signal propagation in early cardiogenesis is established gradually, initially without pacemakers, valves, and septa. Yet, this process has not been tracked in human embryos.[35] In mice and chicken, the FHF-derived heart tube and early LV region start to contract first but lose automaticity as they mature.[36,37] In contrast, the developing atria and AVC start to beat later and maintain automaticity until the cardiac pacemakers have formed, ensuring unidirectional signal motion and flow from the atria over the LV to the RV and OFT.[32] To investigate whether the multi-chambered cardioid system recapitulates this process, we measured its Ca^{2+} signal propagation and FP in a whole organoid and its compartments. We found that each beat originated typically from one compartment and then propagated through the entire multi-chambered cardioid (Figures 5H and S5K; Video S3), generating unidirectional signal and FP propagation in A-LV-RV cardioids. On day 6.5, most Ca^{2+} signals originate from the LV region (Figure 5K) and propagate through the RV area, which does not beat independently (Figures 4A, S5G, and S5H). We validated these observations by showing that multi-chambered cardioids paced by the LV region on day 6.5 maintained a similar beat frequency as LV cardioids (Figure 5J). From days 6.5 to 9.5, the contraction rate of A cardioids increased while that of LV cardioids decreased, which was consistent with the atrial region becoming gradually dominant in pacing the two- and three-chamber cardioids (Figure 5J). Consistently, as the multi-chambered cardioids developed to day 9.5, the Ca^{2+} signal and FP originated predominantly from the atrial region in all combinations, and the signal propagation speed became atrial dictated with a homogeneous FP profile in all subcompartments (Figures 5H, 5J, 5K, and S5K–S5P; Video S3). Interestingly, compartment interactions decreased signal propagation speed in the LV region specifically and in the whole multi-chamber cardioid (Figures 5L and S5I). Thus, our comprehensive analysis platform deciphers the ontogeny of electrochemical signal propagation in multi-chamber cardioids and their subcompartments and how their interactions affect co-developing individual chambers.

Mutations cause compartment-specific defects in cardioids

Mutations in genes encoding cardiac TFs cause compartment-specific congenital defects, where autonomous and non-autonomous effects are difficult to disentangle. Moreover, species-

(D) Immunostaining post-mixing; red lines indicate the cardioid edge.
(E and E′) Zoomed immunostaining images of different (E) mixed progenitors and (E′) control in cardioids post-mixing (day 4.5).
(F) Multi-chambered cardioid protocol schematic with H2B-EGFP/LMNB1-RFP-labeled compartments.
(G) A representative bright-field image from an A-LV-RA multi-chamber cardioid.
(H) Representative Ca^{2+} signal propagation through a triple-chambered cardioid for one beat. Each pixel at 50% of peak intensity.
(I) Immunostained cryosection of multi-chambered cardioid. Atrial section (A, RFP+), LV unmarked, and RV (EGFP+).
(J) Ca^{2+} waves per minute for different multi-chamber subtypes.
(K) Origin of Ca^{2+} signal for multi-chamber cardioids. The color indicates the beat initiation subcompartment. Mix: >10% of beats initiated by different subcompartments.
(L) Speed of Ca^{2+} signal propagation for multi-chambered cardioid subcompartments. Dotted lines: mean of LV/A cardioid speed.
(I–K) N = 2–5, n = 41–160 per subtype; exclusions: Table S3.
(M) Multi-chambered cardioids with shared lumen protocol schematic.
(N) Representative bright-field multi-chamber cardioid image using protocol depicted in (M).
(O) Immunostained cryosection of a triple-chambered cardioid using protocol depicted in (M). Arrow indicates a shared cavity. Indicated day of analysis (D). Scale bars, 200 μm. Graphs show mean ± SD. Statistics: one-way ANOVA. *p < 0.05, **p < 0.01, ***p < 0.001, ****p < 0.0001. ns: not significant.
N, biological replicate number; n: technical replicate number.
See also Figure S5.

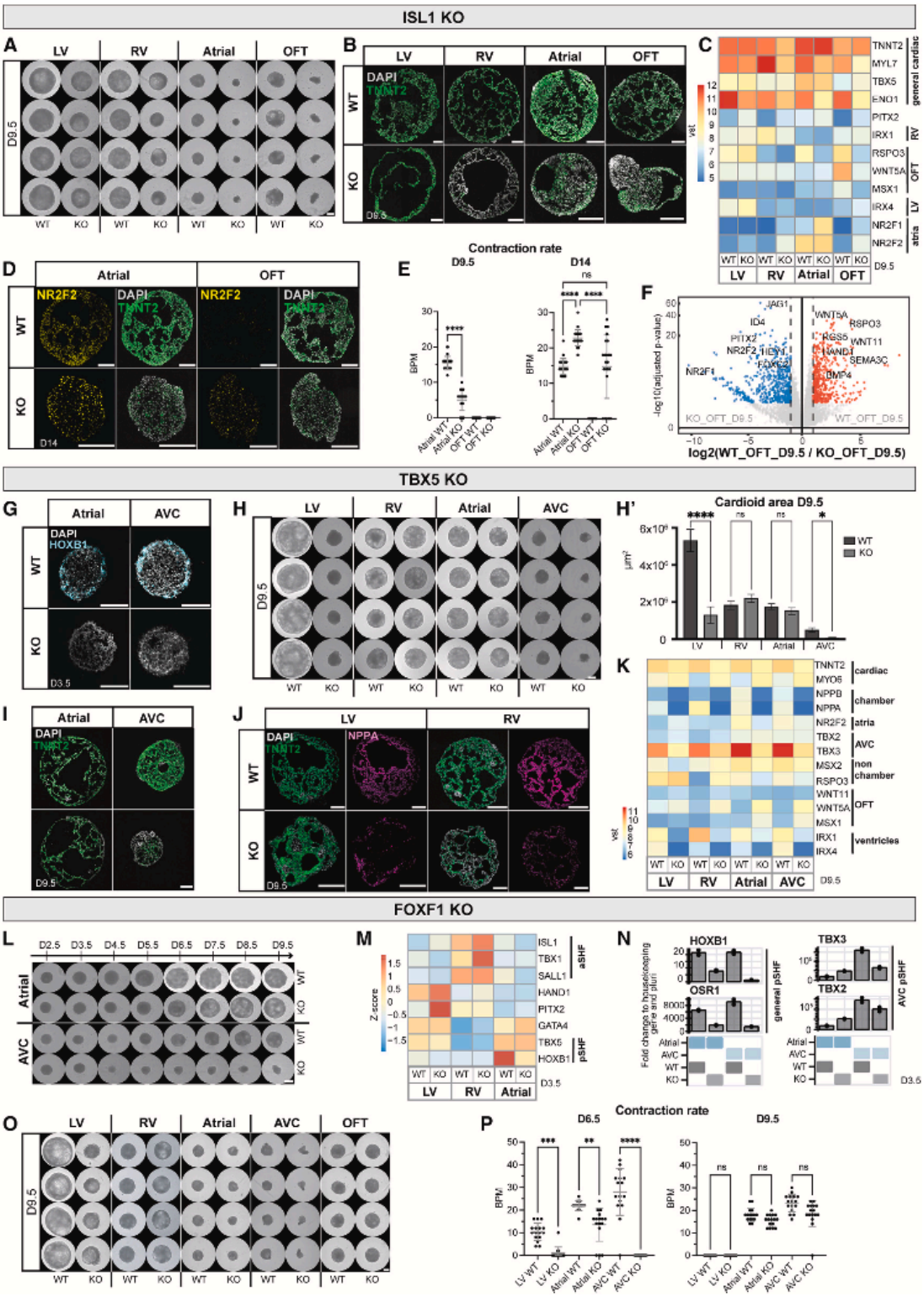

Figure 6. Mutations cause compartment-specific defects in cardioids

(A) Whole-mount images of WT and ISL1-KO cardioids using indicated protocols; scale bars, 500 μm.

(B) Immunostained cryosections in indicated conditions.

(legend continued on next page)

specific TF expression and functional variations are becoming increasingly prominent.[38] To genetically validate the specificity of the human cardioid compartment platform, we generated knockout (KO)-hPSCs for the prominent TFs ISL1 and TBX5 and the less-characterized FOXF1 (Figures S6A, S6G, and S6J).

Mutations in ISL1 are known to cause severe cardiac malformations in the OFT and RV, partial defects in the atria, and lethality in mice at embryonic day (E)10.5.[39] In a time course analysis of ISL1-KO cardioids from days 2.5 to 9.5, we noted severe impairment of cavity morphogenesis and size at day 5.5 in the OFT/A cardioids, while the impact on RV cardioids was more subtle (Figure S6D). On day 9.5, KO and wild type (WT) showed a significant size difference in all cardioid subtypes (Figures 6A and S6E). We found that gene expression was affected already at day 3.5, as evidenced by lower levels of MEF2C and MYOCD, indicative of aberrant differentiation progression (Figure S6B).[40] OFT cardioids showed the most drastic gene expression changes, with HAND2 and BMP4 being downregulated and TBX5 being upregulated (Figure S6B).[39] In A cardioids, the pSHF marker HOXB1 was downregulated (Figure S6B), while NR2F2, RSPO3, WNT5A, and MYL7 were misregulated in all subtypes at day 9.5 (Figure 6C). The CM differentiation efficiency was severely affected in the KO-RV cardioids, noticeably lower in A/OFT cardioids, while the LV was less affected (Figure 6B). Although A cardioids still maintained their identity, albeit with delayed differentiation and onset of contraction (Figures 6B–6D and S6C), OFT cardioids exhibited a global gene expression shift to atrial (NR2F2+, HEY1+, and WNT5A−) identity (Figures 6D, 6F, and S6F).[41,42] Consistent with the gene expression analysis, most ISL1-KO OFT cardioids started beating at a similar rate as A cardioids on day 14 (Figure 6E). Thus, the cardioid platform mimics aspects of *in vivo* ISL1-KO compartment-specific defects, allowing human-specific and autonomous dissection of specific effects at high resolution.

TBX5, another prominent cardiac TF, is a critical regulator in FHF and pSHF progenitors responsible for driving the chamber gene expression program.[43,44] Mutations in TBX5 lead to atrial and ventricular septal defects and conduction disorders and are associated with Holt-Oram syndrome patients.[43] When we differentiated TBX5-KO cardioids, global gene expression analysis on day 3.5 revealed that aSHF markers got upregulated in TBX5-KO A/AVC cardioids while the pSHF-specific gene HOXB1 was downregulated, consistent with *in vivo* findings (Figures 6G and S6H).[44] TBX5-KO-LV cardioids upregulated HAND2 and FGF10 and downregulated NKX2-5 and GATA4 (Figure S6H). In contrast, KO-RV cardioids showed no major defects except for FOXC2 upregulation on day 3.5 (Figure S6H). On day 9.5, we observed severe morphogenetic phenotypes in LV/AVC cardioids (Figures 6H, 6H′, and S6H), where AVC CMs failed to differentiate (Figure 6I). KO-LV/RV/A cardioids mainly featured inefficient CM differentiation, with downregulation of TNNT2 and the chamber-specific marker NPPA (Figures 6I–6K). All TBX5-KO cardioid subtypes showed a prominent defect in ventricular chamber markers expression and upregulation of non-chamber markers TBX2 and WNT5A in KO-RV/LV cardioids (Figure 6K), similar to *in vivo*.[45] TBX5-KO cardioids also lost the ability to spontaneously contract across all subtypes and time points (Figure S6I). Overall, the TBX5-KO showed specific phenotypes at different stages; while LV/A/AVC cardioids were affected already as progenitors, RV cardioids featured a mild phenotype at the CM specification stage.

Finally, FOXF1 is a specific regulator of the pSHF lineage; mutations lead to atrial septation defects, and KO mice die early at E8.0 due to defects in extraembryonic mesoderm, precluding further analysis of cardiac phenotypes.[46,47] When we analyzed FOXF1-KO cardioid subtypes, we observed at day 3.5 an earlier onset of cavity morphogenesis in A cardioids (Figure S6J, yellow arrow). In contrast, the KO-AVC cardioids failed to form full cavities (Figures 6L and S6L). The main pSHF (HOXB1 and OSR1) and AVC markers (TBX2 and TBX3) were downregulated in FOXF1-KO cardioids (Figures 6M and 6N), consistent with pSHF specification failure. Only a few genes were misregulated at day 3.5 in KO-LV/RV cardioids, including upregulation of PITX2 and TBX1, respectively (Figure 6M). On day 9.5, the KO-LV/AVC cardioids were smaller (Figures 6O and S6K). Interestingly, KO-A cardioids acquired a more ventricular identity and developed more extensive cavities, while KO-AVC cardioids failed to differentiate efficiently (Figures S6L–S6N). As expected, we did not observe a severe phenotype in KO-RV/OFT cardioids, except for the downregulation of NPPA in all subtypes (Figures 6O, S6L, and S6M). A less severe phenotype appeared in the KO-LV cardioids, where genes involved in cardiac contraction (ENO1) were downregulated (Figure S6M), leading to a lower beating rate (Figure 6P). KO-A cardioids also showed a lower beating rate, while KO-AVC cardioids did not

(C) RNA-seq expression heatmap shows misregulated genes in ISL1-KO cardioids, compared with WT.
(D) Immunostained WT and ISL1-KO A/OFT cardioids.
(E) Contraction analysis of A/OFT WT and ISL1-KO cardioids (N = 1, n = 24).
(F) RNA-seq volcano plot showing global gene expression differences in indicated conditions.
(G) RNA-scope staining as specified.
(H and H′) (H) Representative whole-mount images of TBX5-KO and WT cardioids and (H′) area quantification (N = 3, n = 24). Scale bars, 500 μL.
(I and J) Immunostained cryosections of cardioids as indicated.
(K) RNA-seq expression heatmap showing differentially expressed developmental genes as specified.
(L and O) Whole-mount images of a time course in indicated conditions. Scale bars, 500 μm.
(M) RNA-seq expression heatmap showing misregulated marker genes as indicated.
(N) Representative RT-qPCR in indicated conditions.
(P) Contraction analysis as specified (N = 1, n = 24). Indicated day of analysis (D). vst, variance-stabilized transformed counts. Scale bars, 200 μm, unless otherwise specified. Bar graphs show mean ± SD. Statistics: one-way ANOVA. *p < 0.05, **p < 0.01, ***p < 0.001, ****p < 0.0001. ns: not significant.
N, biological replicate number; n: technical replicate number.
See also Figure S6.

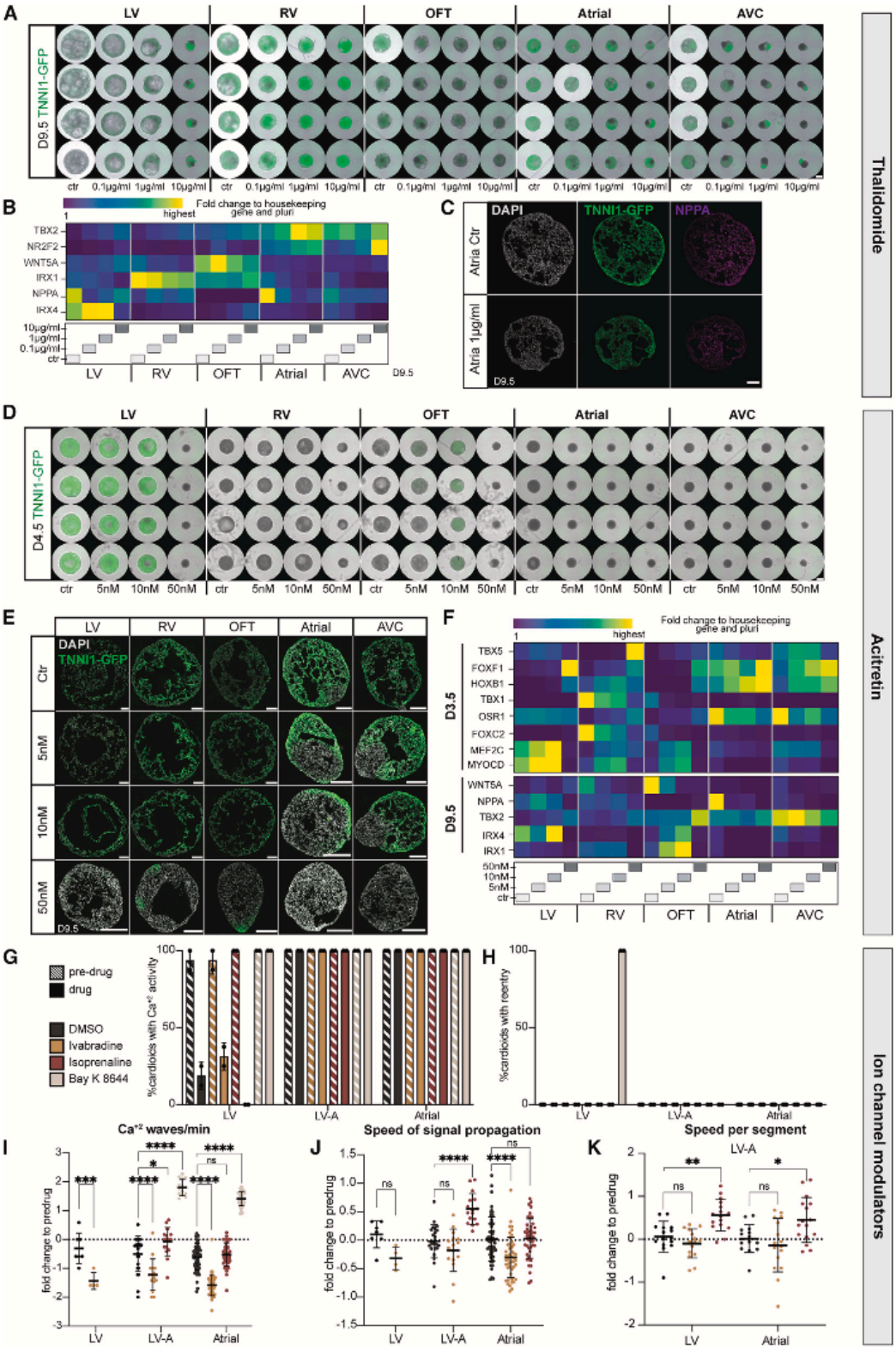

(legend on next page)

contract at day 6.5 (Figure 6P). These results suggest that FOXF1 has compartment-specific roles, particularly in the pSHF lineage, showing differential effects in A vs. AVC cardioids. In summary, the cardioid platform can be employed to dissect human stage- and compartment-specific genetic cardiac defects of specification, morphogenesis, and function without compensatory mechanisms present in the embryo.

A comprehensive screening platform for teratogen and drug effects

Beyond genetic origins, congenital heart defects can also be caused by teratogens (e.g., drugs, toxins, metabolites).[48] Currently, we still miss human systems to investigate, in a high-throughput and easily quantifiable manner, whether teratogens cause compartment-specific cardiac defects.[49] We first confirmed that a non-teratogenic factor, Aspirin, did not cause any morphological or significant gene expression differences (Figures S7A and S7B).[49,50] Next, we tested thalidomide, a well-known teratogen in humans but not rodents, that interferes with TBX5 function, causing severe cardiac and limb defects.[51,52] We used the cardioid platform to dissect the effects of thalidomide at concentration ranges found in the human plasma[53] and detected previously unseen striking effects on the AVC compartment, intermediate phenotypes in LV/RV cardioids, and more subtle effects on A/OFT cardioids (Figures 7A and S7G). Gene expression profiles and immunostaining of treated samples revealed the downregulation of the TBX5 target NPPA for all lineages except for the RV and OFT and a dosage-specific misregulation of compartment identity markers NR2F2, IRX1, and IRX4 (Figures 7B and 7C).

Next, we considered retinoid derivatives, used in treatments against leukemia, psoriasis, and acne, as another class of compounds known to induce congenital defects, particularly malformations of the AVC and OFT derivatives. Since RA plays a crucial role during heart development, we expected the cardioid platform to allow us to dissect the underlying stage-specific mechanisms. When we tested acitretin and isotretinoin (data not shown), we found that strikingly low dosages caused severe compartment-specific and stage-specific effects. OFT/A/AVC cardioids had defects in specification, patterning, and morphogenesis when treated with acitretin (Figures 7D, 7E, S7C, and S7C′). Surprisingly, when using *trans*-retinol, we only saw a severe morphological effect in OFT cardioids, while all the other subtypes were unaffected (Figures S7E and S7E′). In OFT cardioids, retinoids caused the downregulation of OFT genes and upregulation of ventricular but not atrial genes (Figures 7F and S7F). Moreover, OFT cardioids treated with retinoids differentiated earlier into CMs (Figures 7D and S7D). These data suggest that the cardioid system is surprisingly sensitive to different retinoid compounds exhibiting drug- and compartment-specific effects.

Finally, we considered that the multi-chamber platform could be used to test for the effects of drugs on single or interacting cardioids, as such approaches are currently limited, despite the urgent need to prevent drug-induced electrochemical perturbations in developing fetuses. At first, we confirmed that MEA three-chamber cardioid analysis could be used in principle to detect elongated FPs upon treatment with the potassium channel modulator 4AP (Figures S7H and S7I). To increase throughput, we focused on measuring Ca^{2+} signal propagation in A, LV, and two-chambered LV-A cardioids treated with different electrophysiological modulators, such as ivabradine (HCN4 channel blocker), isoprenaline (stimulates beta-adrenoreceptors), and Bay K 8644 (stimulates L-type calcium channels). Although the Ca^{2+} activity of LV cardioids was affected by the drug-solvent DMSO and showed aberrant Ca^{2+} signal re-entry in the presence of Bay K 8644, A/LV-A cardioids were not affected in this manner (Figures 7G and 7H). Instead, Bay K 8644 stimulated both A and LV-A cardioid beating, while ivabradine decreased it in all subtypes (Figure 7I). Interestingly, isoprenaline increased the Ca^{2+} signal speed propagation in both subcompartments of LV-A cardioids but not in the single cardioids (Figures 7J and 7K). The reverse effect was observed with ivabradine, where the individual A cardioid was affected but not the LV-A cardioid. Thus, the platform allows us to screen for specific drug effects in single cardioids, within interacting subcompartments, and in a whole multi-chamber cardioid.

Together, these results validate that we can discern early developmental effects of mutations, known teratogenic and arrhythmogenic drugs and therapeutic agents in a human multi-compartment cardiac platform and relate these to cardiac defects observed in patients. Thus, our work has broad implications for studying the effects on human cardiac biology in contexts ranging from therapeutic development to environmental studies.

DISCUSSION

Recently, several self-organizing human heart models have been reported, including cardiac and cardio-endodermal

Figure 7. A multi-chamber cardioid platform for screening teratogen/drug-induced cardiac defects

(A–F) All cardioids were induced with teratogens starting from day 0 until day 9.5. Ctr, control. (A) Representative whole-mount images of hPSC-TNNI1-GFP-derived cardioids in indicated conditions. Scale bars, 500 μm.(B) Representative RT-qPCR of thalidomide-treated cardioids showing lineage-specific genes. (C) Immunostained cryosections of A cardioids treated with thalidomide. (D) Representative whole-mount images of hPSC-TNNI1-GFP-derived cardioid subtypes treated with acitretin as indicated. Scale bars, 500 μm. (E) Cryosections of hPSC-TNNI1-GFP-derived cardioid subtypes treated with acitretin as specified. (F) Representative RT-qPCR of acitretin-treated cardioids.

(G–K) Ca^{2+} signal analysis for indicated cardioid subtypes. At day 9.5, before drug treatment (pre-drug) and after drug treatment (drug) of DMSO (control), ivabradine, isoprenaline, and Bay K 8644. N = 2, n = 16. Check Table S3 for speed analysis exclusions. (G) Percentage of cardioids with calcium activity. Dots: N. (H) Percentage of cardioids with calcium re-entry. Dots: N. (I) Fold change of Ca^{2+} waves/min normalized to pre-drug. Dots: n. (J) Fold change of signal propagation speed normalized to pre-drug. Dots: n. (K) Fold change of speed per segment normalized to pre-drug. Dots: n. hPSCs: WTC11. Indicated day of analysis (D). Scale bars, 200 μm, except where specified. All bar graphs show mean ± SD. Statistics: one-way ANOVA. *$p < 0.05$, **$p < 0.01$, ***$p < 0.001$, ****$p < 0.0001$. ns: not significant.

N, biological replicate number; n: technical replicate number.

See also Figure S7.

organoids.[54–58] Because this earlier work did not delineate relationships with aSHF, pSHF, and FHF lineages, the resulting identities and physiology of the cardiac cell types have remained unclear. As a result, ratios of different CM subtypes, heterogeneity, and the structures they form *in vitro* are challenging to control and relate to the *in vivo* heart. To complement the embryo gold standard model, we demonstrated that our platform is versatile, highly efficient, reproducible, compatible with multiple cell lines, and screenable in high throughput using multiple readouts (Ca^{2+} transients, contraction movies, FluoVolt, MEAs, morphology, and gene expression) on single-compartment or multi-chamber cardioids.

Several reports describe atrial and ventricular CMs differentiated from hPSCs, but whether these originate from the FHF, aSHF, or pSHF lineage has not been determined.[41,59] *In vivo*, the dosage and timing of signaling are coordinated to drive lineage specification during mesoderm induction, and as mesodermal cells migrate at different times, taking defined positions within the heart fields. We found that stage-specific levels of Activin/Nodal, WNT, BMP, and RA signaling instruct specification into distinct SHF, AVC, and FHF progenitors consistent with the signaling environment in the anterior region of the embryo and recent *in vitro* findings.[14,15,60] Specifically, Activin/Nodal signaling inhibition is crucial to determining SHF lineage fate choice, which was not highlighted before *in vivo* or *in vitro*. We also showed that the role of RA signaling was more complex in terms of dosage and timing than previously thought.[41,59] The absence of exogenous RA signaling is essential for initial aSHF specification and later OFT differentiation, low RA levels for LV specification, high RA levels for early atrial, and later RV specification. Thus, only highly specific combinations of mesoderm induction and patterning signals allow for mimicking the identities, (morphogenetic) dynamics, and later functionality of the developing cardiac lineages, enabling the control and dissection of progenitor sorting and chamber interaction mechanisms.

Interactions between cardiac lineages during the earliest stages of heart development, including cardiac mesoderm specification, morphogenesis, and functional differentiation, are notoriously difficult to analyze and inaccessible in human embryos. In addition, studies of human embryo development reveal a growing list of differences between species in expression patterns of critical developmental and functionality genes.[38,61,62] Such aspects are key to understanding the human-specific impact of mutations and teratogens on early human heart development and how this causes embryo failure. A significant advance of our work is the deep and comprehensive phenotyping that we used to explore the ontology of contraction signal propagation, differentiation speed, specification direction, efficiency, and morphogenesis through the early stages of cardiogenesis. This is particularly important to understand cases of embryonic cardiac failure that have been attributed to faulty specification and morphogenesis but where defects in early contraction signal propagation between chambers might have been the culprit.

In conclusion, despite decades of experimental and clinical research, the underlying causes of most cardiac defects remain unknown. Potential culprits include still unidentified mutations in regulatory elements such as enhancers; environmental factors such as pollutants; and more complex interactions between genetic and environmental factors, including drugs and diet. Previously, we lacked a system to test all these options in a human context with high throughput, encompassing all cardiac compartments, and the multi-chamber cardioid platform will allow us to close this gap.

Limitations of the study

Despite its usefulness, the cardioid system has several limitations at this stage of development. This work focuses on the comprehensive modeling of early specification, morphogenesis, and signal contraction propagation of the human embryonic heart. However, we have not modeled processes such as aSHF/pSHF progenitor migration and heart looping, nor interaction with the endoderm where other complementary *in vitro* systems might be more suitable to compare with the embryo.[54,57,63] Later stages and processes during heart development have not been represented yet in cardioids, including forming valves, septation, pacemakers, chamber trabeculation and ballooning, coronary vasculature and circulation, and the general growth and maturation[24] of the heart. Thus, the multi-chamber platform has been validated mainly using mutations and teratogens affecting the earliest stages while providing, at the same time, a solid basis for further developments.

STAR★METHODS

Detailed methods are provided in the online version of this paper and include the following:

- KEY RESOURCES TABLE
- RESOURCE AVAILABILITY
  - Lead contact
  - Materials availability
  - Data and code availability
- EXPERIMENTAL MODEL AND STUDY PARTICIPANT DETAILS
  - Human pluripotent stem cell (hPSC) lines
- METHOD DETAILS
  - hPSC culture
  - Generation of ISL1, TBX5, and FOXF1 knockout hPSCs
  - Cardioid generation
  - Cardioid Subtype Differentiation
  - Atria Chamber specification protocol
  - Ventricular Maturation Protocol
  - 2D Endothelial cell differentiation
  - OFT cardioids treatment with EMT-promoting factors
  - Smooth Muscle Cell Differentiation
  - Mixing of progenitors
  - Generation of multi-chambered cardioids
  - Molds for multi-chamber cardioids
  - Cardioid total cell number and cell size analysis
  - Cryosectioning
  - Immunostaining
  - RNAscope and In Situ Hybridization Chain reaction (HCR)

- Image acquisition and analysis
- Flow cytometry
- RNA extraction and bulk RNA-seq preparation
- Real-time quantitative polymerase chain reaction
- Sample preparation for scRNA-seq
- Contraction Analysis
- Calcium Transients – Cell Line Generation and Imaging
- Patch clamp recordings of single cardiomyocytes
- Optical action potentials
- Multiple Electrode Array (MEA)

● QUANTIFICATION AND STATISTICAL ANALYSIS

- Degree of sorting quantification
- Bulk RNA-seq analysis
- Single-cell RNA-seq analysis
- scRNA-seq integration with *in vivo* cardiac embryonic chambers datasets
- scRNA-seq integration with an *in vivo* OFT dataset
- Ca2+ Transients Quantification
- MEA Data Analysis
- Statistics

SUPPLEMENTAL INFORMATION

Supplemental information can be found online at https://doi.org/10.1016/j.cell.2023.10.030.

ACKNOWLEDGMENTS

We thank all laboratory members for their help and discussions and Katarzyna Warczok for lab management. We are grateful to the VBC Histology & NGS, IMP/Institute for Molecular Biotechnology (IMBA) Core, and IMBA SCC facilities for their services and to the Allen Institute for cell lines. We thank Life Science Editors for scientific editing. This work was funded by the Austrian Academy of Sciences (OEAW) and the Austrian Research Promotion Agency (FFG) (to the Mendjan lab), by the EU Horizon 2020 R&D Innovation Program under grant agreement no. 964518, and the Austrian Science Fund (FWF) under grant agreement no. W1232 (to S. Hering. and M.A.N.), and by the FWF Special Research Program SFB-F78, F 7811-B (to Prof. Dr. Arndt von Haeseler and S. Haendeler).

AUTHOR CONTRIBUTIONS

C.S., A.D., and S.M. co-designed experiments and co-wrote the paper. C.S. developed RV and OFT differentiations, established cell sorting assay, and performed the scRNA-seq experiment. A.D. developed atrial and AVC differentiations and designed and set up contraction, Ca^{2+}, and MEA analysis. T.I. established multi-chamber cardioid generation. C.S., A.D., T.I., and A.T.C. characterized cardioids and performed teratogenic, mutant, and drug screens. M.A.N. did the patch clamp. S. Haendeler., L.P., and M.N. performed the image/movie-based and scRNA-seq bioinformatic analysis, respectively. N.P., S. Hering., and P.H. helped with training and advice. All other authors performed experiments. S.M. designed and supervised the study.

DECLARATION OF INTERESTS

The IMBA filed a patent application (Nr.21712188.8) on multi-chamber cardioids with C.S., A.D., T.I., and S.M. named as inventors. P.H. and S.M. are co-founders, and S.M. is a SAB member of HeartBeat.bio AG, the IMBA cardioid drug discovery platform spin-off.

INCLUSION AND DIVERSITY

We worked to ensure diversity in experimental samples through the selection of the cell lines. While citing references scientifically relevant to this work, we also actively worked to promote gender balance in our reference list.

Received: July 12, 2022
Revised: July 31, 2023
Accepted: October 30, 2023
Published: November 28, 2023

REFERENCES

1. van der Linde, D., Konings, E.E.M., Slager, M.A., Witsenburg, M., Helbing, W.A., Takkenberg, J.J.M., and Roos-Hesselink, J.W. (2011). Birth prevalence of congenital heart disease worldwide: a systematic review and meta-analysis. J. Am. Coll. Cardiol. *58*, 2241–2247. https://doi.org/10.1016/j.jacc.2011.08.025.
2. Jin, S.C., Homsy, J., Zaidi, S., Lu, Q., Morton, S., DePalma, S.R., Zeng, X., Qi, H., Chang, W., Sierant, M.C., et al. (2017). Contribution of rare inherited and de novo variants in 2,871 congenital heart disease probands. Nat. Genet. *18*, 25. https://doi.org/10.1038/ng.3970.
3. Fahed, A.C., Gelb, B.D., Seidman, J.G., and Seidman, C.E. (2013). Genetics of congenital heart disease: the glass half empty. Circ. Res. *112*, 707–720. https://doi.org/10.1161/CIRCRESAHA.112.300853.
4. Zaidi, S., and Brueckner, M. (2017). Genetics and genomics of congenital heart disease. Circ. Res. *120*, 923–940. https://doi.org/10.1161/CIRCRESAHA.116.309140.
5. Gonzalez-Teran, B., Pittman, M., Felix, F., Thomas, R., Richmond-Buccola, D., Hüttenhain, R., Choudhary, K., Moroni, E., Costa, M.W., Huang, Y., et al. (2022). Transcription factor protein interactomes reveal genetic determinants in heart disease. Cell *185*, 794–814.e30. https://doi.org/10.1016/j.cell.2022.01.021.
6. Kathiresan, S., and Srivastava, D. (2012). Genetics of human cardiovascular disease. Cell *148*, 1242–1257. https://doi.org/10.1016/j.cell.2012.03.001.
7. Srivastava, D. (2021). Modeling human cardiac chambers with organoids. N. Engl. J. Med. *385*, 847–849. https://doi.org/10.1056/NEJMcibr2108627.
8. Hofbauer, P., Jahnel, S.M., and Mendjan, S. (2021). In vitro models of the human heart. Development *148*, dev199672. https://doi.org/10.1242/dev.199672.
9. Kim, H., Kamm, R.D., Vunjak-Novakovic, G., and Wu, J.C. (2022). Progress in multicellular human cardiac organoids for clinical applications. Cell Stem Cell *29*, 503–514. https://doi.org/10.1016/j.stem.2022.03.012.
10. Kelly, R.G., Buckingham, M.E., and Moorman, A.F. (2014). Heart fields and cardiac morphogenesis. Cold Spring Harb. Perspect. Med. *4*, a015750. https://doi.org/10.1101/cshperspect.a015750.
11. Meilhac, S.M., and Buckingham, M.E. (2018). The deployment of cell lineages that form the mammalian heart. Nat. Rev. Cardiol. *15*, 705–724. https://doi.org/10.1038/s41569-018-0086-9.
12. Bruneau, B.G. (2013). Signaling and transcriptional networks in heart development and regeneration. Cold Spring Harb. Perspect. Biol. *5*, a008292. https://doi.org/10.1101/cshperspect.a008292.
13. Christoffels, V., and Jensen, B. (2020). Cardiac morphogenesis: specification of the four-chambered heart. Cold Spring Harb. Perspect. Biol. *12*, a037143. https://doi.org/10.1101/cshperspect.a037143.
14. Arkell, R.M., and Tam, P.P.L. (2012). Initiating head development in mouse embryos: integrating signalling and transcriptional activity. Open Biol. *2*, 120030. https://doi.org/10.1098/rsob.120030.
15. Nandkishore, N., Vyas, B., Javali, A., Ghosh, S., and Sambasivan, R. (2018). Divergent early mesoderm specification underlies distinct head and trunk muscle programmes in vertebrates. Development *145*. dev160945-dev160925. https://doi.org/10.1242/dev.160945.

16. Hofbauer, P., Jahnel, S.M., Papai, N., Giesshammer, M., Deyett, A., Schmidt, C., Penc, M., Tavernini, K., Grdseloff, N., Meledeth, C., et al. (2021). Cardioids reveal self-organizing principles of human cardiogenesis. Cell *184*, 3299–3317.e22. https://doi.org/10.1016/j.cell.2021.04.034.

17. Bothe, I., Tenin, G., Oseni, A., and Dietrich, S. (2011). Dynamic control of head mesoderm patterning. Development *138*, 2807–2821. https://doi.org/10.1242/dev.062737.

18. Ghyselinck, N.B., and Duester, G. (2019). Retinoic acid signaling pathways. Development *146*, dev167502. https://doi.org/10.1242/dev.167502.

19. Schmidt, C., Deyett, A., Ilmer, T., Caballero, A.T., Haendeler, S., Pimpale, L., Netzer, M.A., Ginistrelli, L.C., Cirigliano, M., Mancheno, E.J., et al. (2022). Multi-chamber cardioids unravel human heart development and cardiac defects. https://doi.org/10.1101/2022.07.14.499699.

20. Ivanovitch, K., Soro-Barrio, P., Chakravarty, P., Jones, R.A., Bell, D.M., Gharavy, S.N.M., Stamataki, D., Delile, J., Smith, J.C., and Briscoe, J. (2021). Ventricular, atrial and outflow tract heart progenitors arise from spatially and molecularly distinct regions of the primitive streak3. 497-489. https://doi.org/10.1101/2020.07.12.198994.

21. Cortes, C., Francou, A., De Bono, C., and Kelly, R.G. (2018). Epithelial properties of the second heart field. Circ. Res. *122*, 142–154. https://doi.org/10.1161/CIRCRESAHA.117.310838.

22. Feyen, D.A.M., McKeithan, W.L., Bruyneel, A.A.N., Spiering, S., Hörmann, L., Ulmer, B., Zhang, H., Briganti, F., Schweizer, M., Hegyi, B., et al. (2020). Metabolic maturation media improve physiological function of human iPSC-derived cardiomyocytes. Cell Rep. *32*, 107925. https://doi.org/10.1016/j.celrep.2020.107925.

23. Garay, B.I., Givens, S., Abreu, P., Liu, M., Yücel, D., Baik, J., Stanis, N., Rothermel, T.M., Magli, A., Abrahante, J.E., et al. (2022). Dual inhibition of MAPK and PI3K/AKT pathways enhances maturation of human iPSC-derived cardiomyocytes. Stem Cell Rep. *17*, 2005–2022. https://doi.org/10.1016/j.stemcr.2022.07.003.

24. Karbassi, E., Fenix, A., Marchiano, S., Muraoka, N., Nakamura, K., Yang, X., and Murry, C.E. (2020). Cardiomyocyte maturation: advances in knowledge and implications for regenerative medicine. Nat. Rev. Cardiol. *36*, 1–19. https://doi.org/10.1038/s41569-019-0331-x.

25. Majesky, M.W. (2007). Developmental basis of vascular smooth muscle diversity. Arterioscler. Thromb. Vasc. Biol. *27*, 1248–1258. https://doi.org/10.1161/ATVBAHA.107.141069.

26. Asp, M., Giacomello, S., Larsson, L., Wu, C., Fürth, D., Qian, X., Wärdell, E., Custodio, J., Reimegård, J., Salmén, F., et al. (2019). A spatiotemporal organ-wide gene expression and cell atlas of the developing human heart. Cell *179*, 1647–1660.e19. https://doi.org/10.1016/j.cell.2019.11.025.

27. Lawson, K.A., Meneses, J.J., and Pedersen, R.A. (1991). Clonal analysis of epiblast fate during germ layer formation in the mouse embryo. Development *113*, 891–911.

28. Tam, P.P., Parameswaran, M., Kinder, S.J., and Weinberger, R.P. (1997). The allocation of epiblast cells to the embryonic heart and other mesodermal lineages: the role of ingression and tissue movement during gastrulation. Development *124*, 1631–1642. https://doi.org/10.1242/dev.124.9.1631.

29. Sahara, M., Santoro, F., Sohlmér, J., Zhou, C., Witman, N., Leung, C.Y., Mononen, M., Bylund, K., Gruber, P., and Chien, K.R. (2019). Population and single-cell analysis of human cardiogenesis reveals unique LGR5 ventricular progenitors in embryonic outflow tract. Dev. Cell *48*, 475–490.e7. https://doi.org/10.1016/j.devcel.2019.01.005.

30. van Weerd, J.H., and Christoffels, V.M. (2016). The formation and function of the cardiac conduction system. Development *143*, 197–210. https://doi.org/10.1242/dev.124883.

31. Koopman, C.D., De Angelis, J., Iyer, S.P., Verkerk, A.O., Da Silva, J., Berecki, G., Jeanes, A., Baillie, G.J., Paterson, S., Uribe, V., et al. (2021). The zebrafish grime mutant uncovers an evolutionarily conserved role for Tmem161b in the control of cardiac rhythm. Proc. Natl. Acad. Sci. USA *118*, e2018220118. https://doi.org/10.1073/pnas.2018220118.

32. Christoffels, V.M., Smits, G.J., Kispert, A., and Moorman, A.F.M. (2010). Development of the pacemaker tissues of the heart. Circ. Res. *106*, 240–254. https://doi.org/10.1161/CIRCRESAHA.109.205419.

33. Christoffels, V.M., and Moorman, A.F.M. (2009). Development of the cardiac conduction system: why are some regions of the heart more arrhythmogenic than others? Circ. Arrhythm. Electrophysiol. *2*, 195–207. https://doi.org/10.1161/CIRCEP.108.829341.

34. Verkerk, A.O., Marchal, G.A., Zegers, J.G., Kawasaki, M., Driessen, A.H.G., Remme, C.A., de Groot, J.R., and Wilders, R. (2021). Patch-clamp recordings of action potentials from human atrial myocytes: optimization through dynamic clamp. Front. Pharmacol. *12*, 649414. https://doi.org/10.3389/fphar.2021.649414.

35. Watanabe, M., Rollins, A.M., Polo-Parada, L., Ma, P., Gu, S., and Jenkins, M.W. (2016). Probing the electrophysiology of the developing heart. J. Cardiovasc. Dev. Dis. *3*, 10. https://doi.org/10.3390/jcdd3010010.

36. Tyser, R.C.V., and Srinivas, S. (2020). The first heartbeat-origin of cardiac contractile activity. Cold Spring Harb. Perspect. Biol. *12*, a037135. https://doi.org/10.1101/cshperspect.a037135.

37. Tyser, R.C., Miranda, A.M., Chen, C.-M., Davidson, S.M., Srinivas, S., and Riley, P.R. (2016). Calcium handling precedes cardiac differentiation to initiate the first heartbeat. eLife *5*, 454. https://doi.org/10.7554/eLife.17113.

38. Rossant, J., and Tam, P.P.L. (2022). Early human embryonic development: blastocyst formation to gastrulation. Dev. Cell *57*, 152–165. https://doi.org/10.1016/j.devcel.2021.12.022.

39. Cai, C.-L., Liang, X., Shi, Y., Chu, P.-H., Pfaff, S.L., Chen, J., and Evans, S. (2003). Isl1 identifies a cardiac progenitor population that proliferates prior to differentiation and contributes a majority of cells to the heart. Dev. Cell *5*, 877–889.

40. Gao, R., Liang, X., Cheedipudi, S., Cordero, J., Jiang, X., Zhang, Q., Caputo, L., Günther, S., Kuenne, C., Ren, Y., et al. (2019). Pioneering function of Isl1 in the epigenetic control of cardiomyocyte cell fate. Cell Res. *29*, 486–501. https://doi.org/10.1038/s41422-019-0168-1.

41. Devalla, H.D., Schwach, V., Ford, J.W., Milnes, J.T., El-Haou, S., Jackson, C., Gkatzis, K., Elliott, D.A., Chuva de Sousa Lopes, S.M., Mummery, C.L., et al. (2015). Atrial-like cardiomyocytes from human pluripotent stem cells are a robust preclinical model for assessing atrial-selective pharmacology. EMBO Mol. Med. *7*, 394–410. https://doi.org/10.15252/emmm.201404757.

42. Quaranta, R., Fell, J., Rühle, F., Rao, J., Piccini, I., Araúzo-Bravo, M.J., Verkerk, A.O., Stoll, M., and Greber, B. (2018). Revised roles of ISL1 in a hES cell-based model of human heart chamber specification. eLife *7*, 12209. https://doi.org/10.7554/eLife.31706.

43. Bruneau, B.G., Nemer, G., Schmitt, J.P., Charron, F., Robitaille, L., Caron, S., Conner, D.A., Gessler, M., Nemer, M., Seidman, C.E., et al. (2001). A murine model of Holt-Oram syndrome defines roles of the T-box transcription factor Tbx5 in cardiogenesis and disease. Cell *106*, 709–721.

44. Xie, L., Burnicka-Turek, O., Friedland-Little, J.M., Zhang, K., and Moskowitz, I.P. (2012). Tbx5-hedgehog molecular networks are essential in the second heart field for atrial septation. Dev. Cell *23*, 280–291. https://doi.org/10.1016/j.devcel.2012.06.006.

45. Bruneau, B.G., Logan, M., Davis, N., Levi, T., Tabin, C.J., Seidman, J.G., and Seidman, C.E. (1999). Chamber-specific cardiac expression of Tbx5 and heart defects in Holt-Oram syndrome. Dev. Biol. *211*, 100–108. https://doi.org/10.1006/dbio.1999.9298.

46. Hoffmann, A.D., Yang, X.H., Burnicka-Turek, O., Bosman, J.D., Ren, X., Steimle, J.D., Vokes, S.A., McMahon, A.P., Kalinichenko, V.V., and Moskowitz, I.P. (2014). Foxf genes integrate Tbx5 and hedgehog pathways in the second heart field for cardiac septation. PLOS Genet. *10*, e1004604. https://doi.org/10.1371/journal.pgen.1004604.

47. Kang, J., Nathan, E., Xu, S.M., Tzahor, E., and Black, B.L. (2009). Isl1 is a direct transcriptional target of Forkhead transcription factors in second-heart-field-derived mesoderm. Dev. Biol. *334*, 513–522. https://doi.org/10.1016/j.ydbio.2009.06.041.

48. Kalisch-Smith, J.I., Ved, N., and Sparrow, D.B. (2020). Environmental risk factors for congenital heart disease. Cold Spring Harb. Perspect. Biol. *12*, a037234. https://doi.org/10.1101/cshperspect.a037234.

49. Mantziou, V., Baillie-Benson, P., Jaklin, M., Kustermann, S., Arias, A.M., and Moris, N. (2021). In vitro teratogenicity testing using a 3D, embryo-like gastruloid system. Reprod. Toxicol. *105*, 72–90. https://doi.org/10.1016/j.reprotox.2021.08.003.

50. van Meer, B.J., Krotenberg, A., Sala, L., Davis, R.P., Eschenhagen, T., Denning, C., Tertoolen, L.G.J., and Mummery, C.L. (2019). Simultaneous measurement of excitation-contraction coupling parameters identifies mechanisms underlying contractile responses of hiPSC-derived cardiomyocytes. Nat. Commun. *10*, 4325. https://doi.org/10.1038/s41467-019-12354-8.

51. Yamanaka, S., Murai, H., Saito, D., Abe, G., Tokunaga, E., Iwasaki, T., Takahashi, H., Takeda, H., Suzuki, T., Shibata, N., et al. (2021). Thalidomide and its metabolite 5-hydroxythalidomide induce teratogenicity via the cereblon neosubstrate PLZF. EMBO J. *40*, e105375. https://doi.org/10.15252/embj.2020105375.

52. Khalil, A., Tanos, R., El-Hachem, N., Kurban, M., Bouvagnet, P., Bitar, F., and Nemer, G. (2017). A HAND to TBX5 explains the link between thalidomide and cardiac diseases. Sci. Rep. *7*, 1416. https://doi.org/10.1038/s41598-017-01641-3.

53. Bai, N., Cui, X.-Y., Wang, J., Sun, C.-G., Mei, H.-K., Liang, B.-B., Cai, Y., Song, X.-J., Gu, J.-K., and Wang, R. (2013). Determination of thalidomide concentration in human plasma by liquid chromatography-tandem mass spectrometry. Exp. Ther. Med. *5*, 626–630. https://doi.org/10.3892/etm.2012.847.

54. Drakhlis, L., Biswanath, S., Farr, C.-M., Lupanow, V., Teske, J., Ritzenhoff, K., Franke, A., Manstein, F., Bolesani, E., Kempf, H., et al. (2021). Human heart-forming organoids recapitulate early heart and foregut development. Nat. Biotechnol. *18*. 246-210. https://doi.org/10.1038/s41587-021-00815-9.

55. Feng, W., Schriever, H., Jiang, S., Bais, A., Wu, H., Kostka, D., and Li, G. (2022). Computational profiling of hiPSC-derived heart organoids reveals chamber defects associated with NKX2-5 deficiency. Commun. Biol. *5*, 399. https://doi.org/10.1038/s42003-022-03346-4.

56. Lewis-Israeli, Y.R., Wasserman, A.H., Gabalski, M.A., Volmert, B.D., Ming, Y., Ball, K.A., Yang, W., Zou, J., Ni, G., Pajares, N., et al. (2021). Self-assembling human heart organoids for the modeling of cardiac development and congenital heart disease. Nat. Commun. *12*, 5142. https://doi.org/10.1038/s41467-021-25329-5.

57. Silva, A.C., Matthys, O.B., Joy, D.A., Kauss, M.A., Natarajan, V., Lai, M.H., Turaga, D., Alexanian, M., Bruneau, B.G., and McDevitt, T.C. (2020). Developmental co-emergence of cardiac and gut tissues modeled by human iPSC-derived organoids*34*, pp. 405–423. https://doi.org/10.1101/2020.04.30.071472.

58. Meier, A.B., Zawada, D., De Angelis, M.T., Martens, L.D., Santamaria, G., Zengerle, S., Nowak-Imialek, M., Kornherr, J., Zhang, F., Tian, Q., et al. (2023). Epicardioid single-cell genomics uncovers principles of human epicardium biology in heart development and disease. Nat. Biotechnol., 1–14. https://doi.org/10.1038/s41587-023-01718-7.

59. Lee, J.H., Protze, S.I., Laksman, Z., Backx, P.H., and Keller, G.M. (2017). Human pluripotent stem cell-derived atrial and ventricular cardiomyocytes develop from distinct mesoderm populations. Stem Cells *21*, 179–194.e4. https://doi.org/10.1016/j.stem.2017.07.003.

60. Yang, D., Gomez-Garcia, J., Funakoshi, S., Tran, T., Fernandes, I., Bader, G.D., Laflamme, M.A., and Keller, G.M. (2022). Modeling human multi-lineage heart field development with pluripotent stem cells. Cell Stem Cell *29*, 1382–1401.e8. https://doi.org/10.1016/j.stem.2022.08.007.

61. Cui, Y., Zheng, Y., Liu, X., Yan, L., Fan, X., Yong, J., Hu, Y., Dong, J., Li, Q., Wu, X., et al. (2019). Single-cell transcriptome analysis maps the developmental track of the human heart. Cell Rep. *26*, 1934–1950.e5. https://doi.org/10.1016/j.celrep.2019.01.079.

62. Verheule, S., and Kaese, S. (2013). Connexin diversity in the heart: insights from transgenic mouse models. Front. Pharmacol. *4*, 81. https://doi.org/10.3389/fphar.2013.00081.

63. Rossi, G., Boni, A., Guiet, R., Girgin, M., Kelly, R.G., and Lutolf, M.P. (2019). Embryonic organoids recapitulate early heart organogenesis*141*. 4231-4226. https://doi.org/10.1101/802181.

64. Schindelin, J., Arganda-Carreras, I., Frise, E., Kaynig, V., Longair, M., Pietzsch, T., Preibisch, S., Rueden, C., Saalfeld, S., Schmid, B., et al. (2012). Fiji: an open-source platform for biological-image analysis. Nat. Methods *9*, 676–682. https://doi.org/10.1038/nmeth.2019.

65. Chen, G., Gulbranson, D.R., Hou, Z., Bolin, J.M., Ruotti, V., Probasco, M.D., Smuga-Otto, K., Howden, S.E., Diol, N.R., Propson, N.E., et al. (2011). Chemically defined conditions for human iPSC derivation and culture. Nat. Methods *8*, 424–429. https://doi.org/10.1038/nmeth.1593.

66. Patsch, C., Challet-Meylan, L., Thoma, E.C., Urich, E., Heckel, T., O'Sullivan, J.F., Grainger, S.J., Kapp, F.G., Sun, L., Christensen, K., et al. (2015). Generation of vascular endothelial and smooth muscle cells from human pluripotent stem cells. Nat. Cell Biol. *17*, 994–1003. https://doi.org/10.1038/ncb3205.

67. Fridericia, L.S. (2003). The duration of systole in an electrocardiogram in normal humans and in patients with heart disease. 1920. Ann. Noninvasive Electrocardiol. *8*, 343–351. https://doi.org/10.1046/j.1542-474x.2003.08413.x.

68. de Soysa, T.Y., Ranade, S.S., Okawa, S., Ravichandran, S., Huang, Y., Salunga, H.T., Schricker, A., Del Sol, A., Gifford, C.A., and Srivastava, D. (2019). Single-cell analysis of cardiogenesis reveals basis for organ-level developmental defects. Nature *572*, 120–124. https://doi.org/10.1038/s41586-019-1414-x.

6. Cardioids reveal self-organizing principles of human cardiogenesis

Hofbauer Pablo, Stefan M. Jahnel, Nora Papai, Magdalena Giesshammer, Alison Deyett, Clara Schmidt, Mirjam Penc, Katherina Tavernini, Nastasja Grdseloff, Christy Meledeth, Lavinia Ceci Ginistrelli, Claudia Ctortecka, Sejla Salic, Maria Novatchkova, and Sasha Mendjan, 2021. 'Cardioids Reveal Self-Organizing Principles of Human Cardiogenesis'. Cell, May. https://doi.org/10.1016/j.cell.2021.04.034

6.1. Contribution

P.H., S.M.J., N.P., and S.M. co-designed experiments and co-wrote the paper. P.H. developed CM and EC differentiations in 2D and co-differentiations in 3D aggregates and in cardioids and also set up the high-throughput analysis pipeline and the cardioid injury model. S.M.J. established, optimized, and characterized cardioid generation. N.P. developed and characterized epicar- dial differentiations in 2D, 3D, and cardioids, characterized cardioids, and set up the cardioid injury model. M.N. helped with the bioinformatic analysis. All other authors performed experiments. S.M. performed experiments and supervised the study.

Cell

Resource

Cardioids reveal self-organizing principles of human cardiogenesis

Graphical abstract

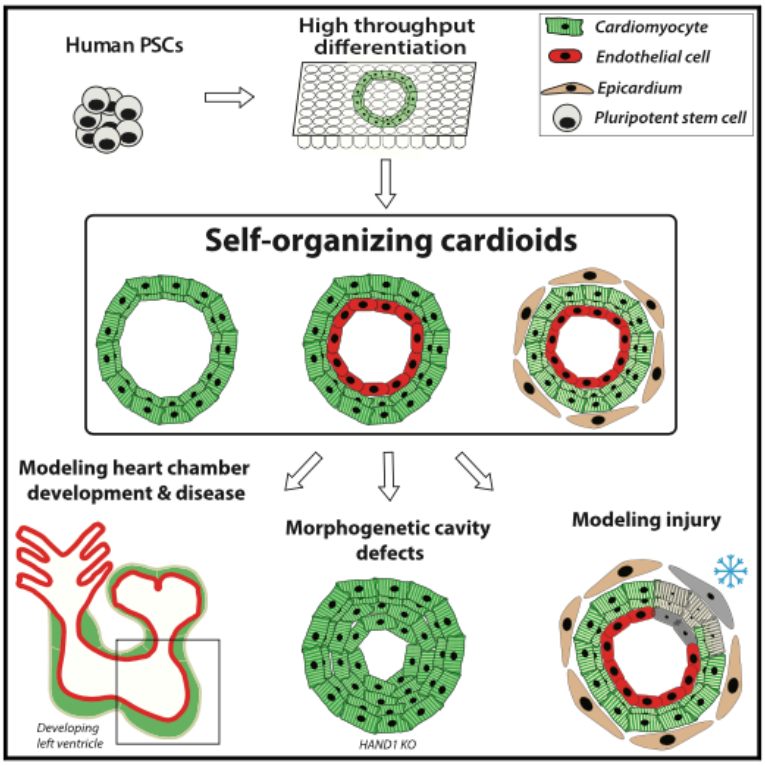

Highlights

- Chamber-like cardioids form a cavity and recapitulate heart lineage architecture
- Cardioid self-organization and lineage identity is instructed by signaling
- WNT-BMP signaling directs cavity formation via HAND1
- Cryoinjury initiates an *in vivo*-like fibronectin and collagen accumulation

Authors

Pablo Hofbauer, Stefan M. Jahnel, Nora Papai, ..., Šejla Šalic, Maria Novatchkova, Sasha Mendjan

Correspondence

sasha.mendjan@imba.oeaw.ac.at

In brief

Cardioids that pattern and morph into chamber-like structures are established from human pluripotent stem cells.

Hofbauer et al., 2021, Cell *184*, 3299–3317
June 10, 2021
https://doi.org/10.1016/j.cell.2021.04.034

CellPress

Cell

CellPress

Resource

Cardioids reveal self-organizing principles of human cardiogenesis

Pablo Hofbauer,[1,3] Stefan M. Jahnel,[1,3] Nora Papai,[1,3] Magdalena Giesshammer,[1] Alison Deyett,[1] Clara Schmidt,[1] Mirjam Penc,[1] Katherina Tavernini,[1] Nastasja Grdseloff,[1] Christy Meledeth,[1] Lavinia Ceci Ginistrelli,[1] Claudia Ctortecka,[1] Šejla Šalic,[1] Maria Novatchkova,[2] and Sasha Mendjan[1,4,*]

[1]Institute of Molecular Biotechnology of the Austrian Academy of Sciences (IMBA), Vienna BioCenter, Dr. Bohr Gasse 3, 1030 Vienna, Austria
[2]Institute of Molecular Pathology (IMP), Vienna Biocenter 1, 1030 Vienna, Austria
[3]These authors contributed equally
[4]Lead contact
*Correspondence: sasha.mendjan@imba.oeaw.ac.at
https://doi.org/10.1016/j.cell.2021.04.034

SUMMARY

Organoids capable of forming tissue-like structures have transformed our ability to model human development and disease. With the notable exception of the human heart, lineage-specific self-organizing organoids have been reported for all major organs. Here, we established self-organizing cardioids from human pluripotent stem cells that intrinsically specify, pattern, and morph into chamber-like structures containing a cavity. Cardioid complexity can be controlled by signaling that instructs the separation of cardiomyocyte and endothelial layers and by directing epicardial spreading, inward migration, and differentiation. We find that cavity morphogenesis is governed by a mesodermal WNT-BMP signaling axis and requires its target HAND1, a transcription factor linked to developmental heart chamber defects. Upon cryoinjury, cardioids initiated a cell-type-dependent accumulation of extracellular matrix, an early hallmark of both regeneration and heart disease. Thus, human cardioids represent a powerful platform to mechanistically dissect self-organization, congenital heart defects and serve as a foundation for future translational research.

INTRODUCTION

The human heart, the first functional organ to form in development, is one of the most difficult organs to model *in vitro* (Lancaster and Huch, 2019; Schutgens and Clevers, 2020). Malformations of the heart are by far the most common human birth defects (Majumdar et al., 2021) but their developmental etiology is poorly understood (Nees and Chung, 2020). These often-dramatic morphogenetic disorders can be caused by mutations that affect the activity of cardiogenic signaling pathways and transcription factors during early embryogenesis (Kelly et al., 2014; Meilhac and Buckingham, 2018; Zaidi and Brueckner, 2017). From work in animal and cellular models, we know how the cardiac lineage is specified in a stage-specific manner from embryonic mesoderm (Birket et al., 2015; Costello et al., 2011; Lee et al., 2017; Lian et al., 2012; (Marvin et al., 2001); Mendjan et al., 2014) to produce cardiomyocytes (CMs), endocardial cells (ECs), and epicardial cells (Guadix et al., 2017; Iyer et al., 2015; [illegible] et al., 2017; Witty et al., 2014). How [illegible]s these cell types to self-organize into layers and shape a heart chamber, or fail in cardiac defects, remains unclear. These questions are challenging to tackle in complex systems, because manipulating signaling pathways at the spatial and temporal resolution required to dissect rapid and complex developmental processes is not yet feasible. Thus, we need *in vitro* models that mimic aspects of development but are simple enough to resolve the intricate dynamics of cardiogenesis and its malformations in humans.

Human organoids have been used to dissect mechanisms of patterning and morphogenesis in multiple tissues and organs. These structures emerge in culture from human pluripotent stem cells (hPSCs) or adult stem cells and are coaxed by signaling to form a tissue-like architecture, organ-specific cell types, and exert organ-specific functions (Clevers, 2016; Lancaster and Knoblich, 2014) for use in numerous applications (Lancaster and Huch, 2019; Schutgens and Clevers, 2020). Their hallmark feature is the capability of self-organization that is driven by intrinsically coordinated specification, patterning, and morphogenesis (Sasai, 2013), in the absence of spatial constraints and interactions with other embryonic tissues. These properties allow the dissection of complex developmental processes in an organ-specific context as embryonic redundancies and compensation mechanisms are removed (Little and Combes, 2019; Sasai, 2013). For instance, pioneering work using optic cup organoids elucidated the morphogenesis of the eye (Eiraku et al., 2011; Nakano et al., 2012), gut organoids have been used to tease apart the initiation of intestinal crypt morphogenesis (Serra et al., 2019), and cerebral organoids allow the study of the etiology of human brain malformations (Lancaster et al., 2013). By harnessing developmental mechanisms, self-organization allows not only the study of organogenesis and its defects but results in more physiological models

Go to page 19

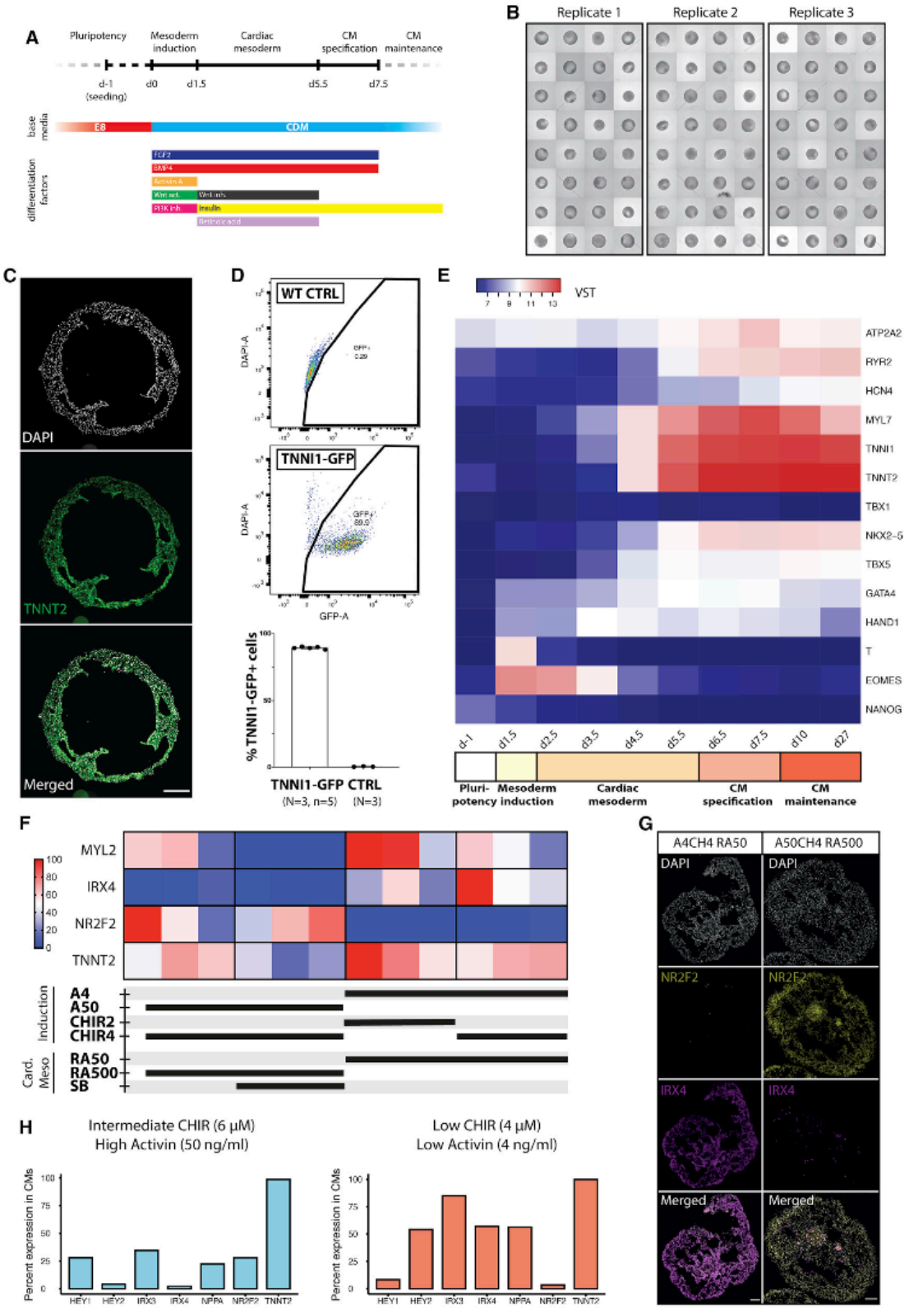

(legend on next page)

for a much wider range of diseases and applications (Lancaster and Huch, 2019; Tuveson and Clevers, 2019). Although self-organizing organoids have been reported for almost all major organs, there are currently no cardiac-specific self-organizing human cardiac organoids that autonomously pattern and morph into an *in vivo*-like structure (Lancaster and Huch, 2019; Schutgens and Clevers, 2020).

Bioengineering approaches have successfully been applied to create artificially engineered heart tissues (often termed heart/cardiac organoids, microchambers, etc.) using scaffolds, molds, geometric confinement, and protein matrices (Ma et al., 2015; Mills et al., 2017; Ronaldson-Bouchard et al., 2018; Tiburcy et al., 2017; Zhao et al., 2019). These have proven immensely useful to measure contraction force, perform compound screens, and model structural muscle and arrhythmogenic disorders. Similarly, mouse and human PSC-derived 3D cardiac models including spherical aggregates (microtissues) of CMs and other (cardiac) cell types (Giacomelli et al., 2017, 2020; Richards et al., 2020) have been established as promising high throughput tools for drug discovery. Moreover, recent embryoid models (Drakhlis et al., 2021; Rossi et al., 2021; Silva et al., 2020) rely on complex self-organization of non-cardiac (e.g., foregut endoderm) and cardiac lineages and thus provide further insights into germ layer interactions during early organogenesis. However, existing models do not recapitulate cardiac-specific self-organization to acquire *in vivo*-like architecture such as a CM chamber with inner endocardial cavity lining and are therefore limited as models of human cardiogenesis and heart disease.

Here, we established hPSC-derived self-organizing "cardioids" that recapitulate chamber-like morphogenesis in the absence of non-cardiac tissues and use them to study mechanisms of human cardiogenesis and heart disease.

RESULTS

Formation of cardiac chamber-like structures *in vitro*

To investigate whether an *in vitro* 3D chamber-like structure can be created intrinsically, we developed a differentiation approach based on temporal control of the key cardiogenic signaling pathways—ACTIVIN, bone morphogenic protein (BMP), fibroblast growth factor (FGF), retinoic acid (RA), and WNT. By recapitulating *in vivo* developmental staging, we sequentially specified hPSCs into mesoderm, cardiac mesoderm, and beating CM progenitors at above 90% efficiency in 2D culture (Mendjan et al., 2014) (Figure 1A). To screen for factors that are sufficient to stimulate intrinsic 3D cardiac structure formation in 2D culture, we supplemented the media with selected extracellular matrix (ECM) proteins that are involved in mesoderm development (Yap et al., 2019). Addition of laminins 521/511 before mesoderm induction resulted in intrinsic self-assembly of cells and the striking formation of hollow, beating 3D structures expressing the CM marker TNNT2 after 7 days of differentiation (Figure S1A; Video S1). When we performed cardiac differentiation entirely in 3D non-adherent high-throughput culture, we found that exogenous ECM was not required for rapid and reproducible self-assembly into beating cavity-containing structures positive for CM markers ACTN2, TNNT2, TNNI1, MYL7, TTN, NPPA, and ATP2A2 (Figures 1B, 1C, S1B, and S1C; Videos S2, S3, and S4). On an ultrastructural level, these CMs contained organized sarcomeres and are interconnected via intercalated discs (Figures S1C′ and S1D). The self-assembly was robust in the WTC hiPSC line, including its vast live fluorescent reporter resource collection (Roberts et al., 2019), the widely used hESC lines H9 and H7, as well as in three hiPSC lines routinely used to generate cerebral organoids (Figures S1E and S1E′). The CM differentiation efficiency measured by flow cytometry (N = 3, n = 5) and 3D z stack image analysis (N = 3, n = 8) averaged at ~90% (Figures 1D and S1F). We hereafter refer to these cavity-containing cardiac structures as cardioids.

We next sought to characterize cardioids at the molecular level. An RNA sequencing (RNA-seq) time course analysis of cardioids revealed an expression signature most similar to the first heart field (FHF) lineage of cardiac mesoderm (HAND1$^+$, TBX5$^+$, NKX2-5$^+$, and TBX1$^-$) (Figure 1E), which *in vivo* gives rise to the heart tube—the primary precursor of the left ventricular chamber and, to a smaller extent, the atria (Meilhac and Buckingham, 2018). During cardioid specification and maturation, structural and ion channel gene expression, as well as β-adrenergic receptors 1 and 2 expression, increased (Figure S2A). When we compared expression profiles of cardioids relative to CMs differentiated in 2D, we noted that genes encoding ion channels (e.g., the HERG channel KCNH2), structural proteins (TNNI1, TTN, and MYH6), cardiac transcription factors (TBX5 and MEF2C), and sarcoplasmic reticulum proteins (RYR2 and ATP2A2) showed higher expression levels in 3D cavity-forming structures,

Figure 1. Formation of cardiac chamber-like structures *in vitro*

(A) Cardiac differentiation protocol.

(B) Representative whole mount image (day 5.5) of a high-throughput differentiation approach showing robust generation of cavity-containing, beating structures in three biological replicates (iPSC WTC line).

(C) Cryosection of a cardioid at day 7.5 showing the cavity and expression of the CM-specific marker TNNT2. Scale bar, 200 μm.

(D) Quantification of TNNI1-GFP$^+$ cells in cardioids at day 7.5 via flow cytometry. Mean +/− SD.

(E) Expression of key genes during CM differentiation. VST, variance-stabilized transformed counts.

(F) Real-time qPCR from day 14 organoids with varying activin (in ng/mL) and CHIR99021 (in μM) concentrations at induction stage, and varying retinoid acid concentration (in nM) at the cardiac mesoderm stage with either the presence or absence of SB43154. Scale bar shows the fold change from housekeeping gene, PBGD, and pluripotent stem cells normalized with min-max normalization.

(G) Immunostaining for ventricular (IRX4) and atrial (NR2F2) CMs of a cardioid (day 10) showing the optimized left ventricular conditions (A4CH4 RA50) versus the non-optimized condition (A50CH4 RA500). A, activin; CH, CHIR99021; RA, retinoic acid; SB, SB43154. Scale bar, 100 μm.

(H) scRNA-seq analysis of percentage of CMs in intermediate WNT(CH6)/high activin (A50)/RA500 (N = 2, n = 1,717) versus low WNT(CH4)/low activin(A4)/RA50 (N = 2, n = 5,097) conditions expressing more atrial versus more ventricular markers. TNNT2 is expressed in all CM. Used cell lines in this figure: WTC.

See also Figures S1 and S2 and Videos S1, S2, S3, S4, and S5.

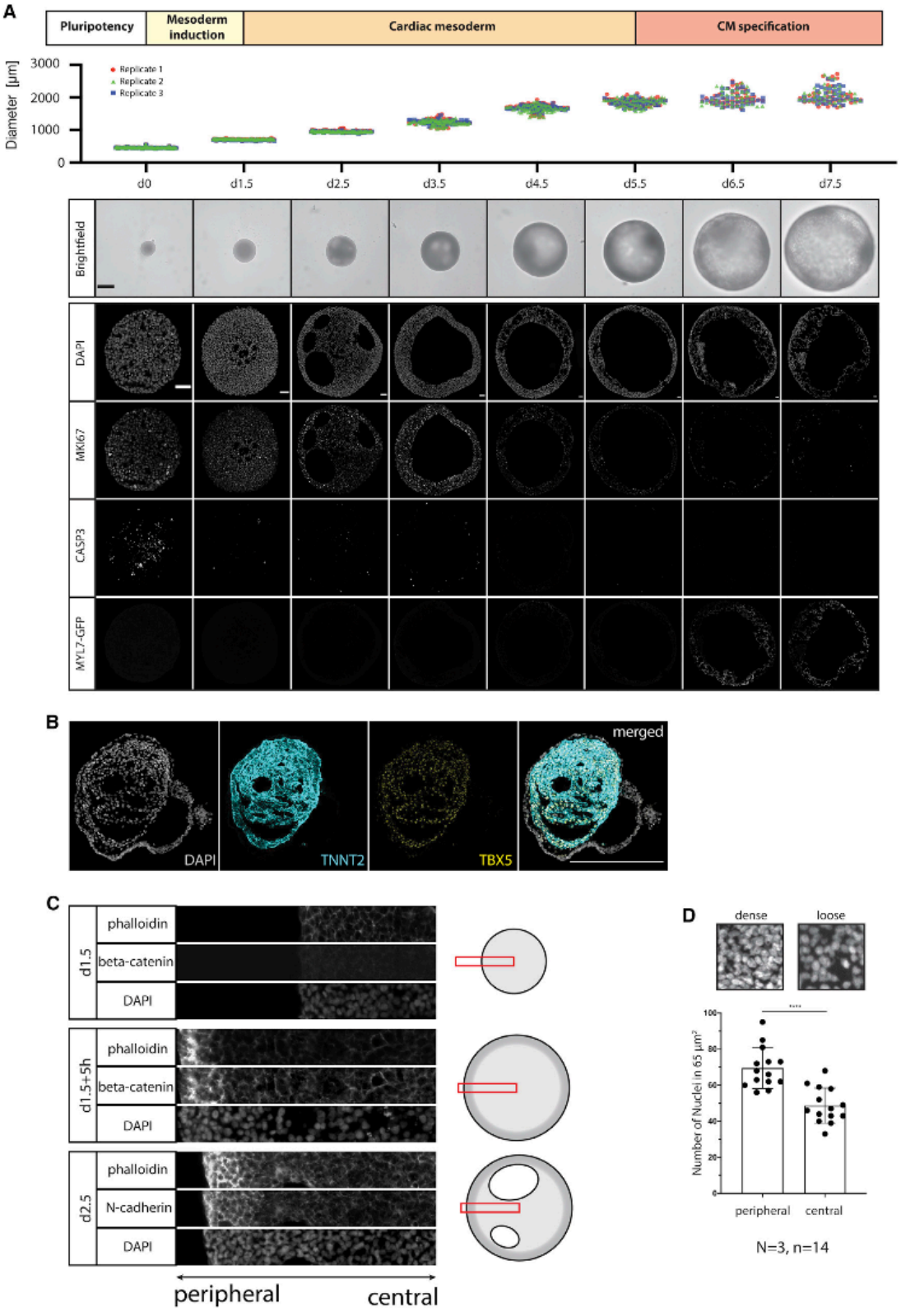

(legend on next page)

suggesting improved functionality (Figure S2B). Gene Ontology (GO)-term analysis showed that cardioids exhibited gene expression patterns of heart morphogenesis and development, which were significantly upregulated over 2D CMs (Figure S2C) and aggregated 3D CM microtissues (Figure S2D). In both models, beating started between day 5 and 7 of differentiation, continued at a similar rate and frequency (Ca^{2+} transients, beating frequency) (Figures S1G and S1H; Videos S4 and S5), and cardioids could be maintained in culture for at least 3 months. Overall, we successfully generated functional hPSC-derived cardioids that reproducibly self-assembled and maintained their molecular CM identity.

We further aimed to explore the CM subtype potential of cardioids. The initial RNA-seq analysis of cardioids indicated a mixed ventricular ($IRX4^+$ and $MYL2^+$) and atrial ($NR2F2^+$and $KCNJ3^+$) profile (Figures S2A and S2B) consistent with its FHF origin. Drawing from recent *in vivo* and *in vitro* findings (Devalla et al., 2015; Ivanovitch et al., 2021; Lee et al., 2017; Lescroart et al., 2018) that implicate mesoderm induction and low RA signaling dosage as critical for posterior heart tube and left ventricular chamber specification, we optimized WNT and ACTIVIN dosage during mesoderm induction and reduced RA dosage during the cardiac mesoderm stage. These optimizations resulted in increased expression of ventricular-specific markers (IRX3, IRX4, HEY2, and MYL2) and near absence of atrial-specific marker expression (NR2F2 and HEY1) as seen by real-time qPCR, immunocytochemistry, and single-cell RNA-seq (scRNA-seq) analysis of CMs (Figures 1F–1H). Consistent with these data, action potential measurements using a FluoVolt dye assay indicated a primarily ventricular-like profile (Figure S1I). In conclusion, cardioids can be directed toward an early left ventricular chamber-like identity.

Cardiac mesoderm self-organizes to form a cavity *in vitro* and *ex vivo*

We next employed this system to ask whether the cavity within cardioids is formed by an intrinsic morphogenesis process (Sasai, 2013). By analyzing the developmental time course capturing cavity formation, we found that cavities were initiated and expanded robustly during the cardiac mesoderm ($HAND1^+$) stage preceding expression of key cardiac structural markers, such as MYL7 (Figures 1E and 2A; Videos S2 and S3). Cardioids expanded rapidly and reproducibly due to proliferation and formation of multiple cavities (Videos S2, S3, and S4). Most smaller cavities eventually coalesced into one major cavity. Cavity expansion was neither driven by apoptosis nor regional proliferation differences, as evidenced by cleaved CASP3 and MKI67 staining (Figure 2A). Importantly, $SOX17^+$/$EOMES^+$ endoderm was absent during differentiation, indicating that cardiac mesoderm cavities were not generated as a result of endoderm instruction (Figure S2E). This is consistent with findings *in vivo*, because bilateral hearts can still form when foregut endoderm morphogenesis is disrupted (Kuo et al., 1997; Li et al., 2004). Lumen formation also occurred when vascular endothelial growth factor (VEGF)-driven EC differentiation was inhibited using the potent vascular endothelial growth factor receptor (VEGFR) inhibitor sunitinib (Figure S2F) suggesting an endothelium-independent mechanism. We concluded that cardiac mesoderm has an intrinsic capacity for self-assembly into a CM-made chamber-like structure.

In vivo, cardiac mesoderm does not require foregut endoderm for basic morphogenesis of the heart in the mouse (Li et al., 2004) and in the chick (DeHaan, 1959). We therefore asked whether *ex vivo* dissected mesoderm from developing chick embryos can also form chamber-like structures in conditions we developed for human cardiac self-organization. Strikingly, in the absence of $SOX2^+$ foregut, chick mesodermal explants developed into beating chamber-like structures *in vitro* similar to human cardiac mesoderm, demonstrating robust conservation of *in vitro* cardiogenic self-morphogenesis under permissive conditions (Figures 2B, S2G, and S2H).

Besides self-morphogenesis during specification, intrinsic self-patterning of a homogeneous starting cell population is a key hallmark of self-organization (Sasai, 2013). To this end, we performed a closer analysis of cardiac mesoderm to determine when the first self-patterning event occurs. Although mesoderm at the induction stage appeared homogeneous, we observed a higher peripheral signal of F-actin and membrane bound beta-catenin at the onset of the cardiac mesoderm stage. Subsequent cavitation coincided with increased mesoderm density at the periphery, reflected by accumulation of F-actin, N-cadherin, and higher nuclear density (Figures 2C and 2D). It is likely that this denser cardiac mesoderm layer acts as a permeability barrier, because the cavity structures were impermeable to low-molecular-weight (4 kDa) dextran (data not shown). In contrast, the central part of the developing structures, where cavities first appeared, had a looser appearance with decreased N-cadherin and beta-catenin signal (Figure 2C). These observations are consistent with the *in vivo* pattern of N-cadherin and beta-catenin in the denser dorsal region of cardiac mesoderm and the less compact region facing endocardial tubes and foregut endoderm (Linask, 2003). We concluded that human cardioids feature the key hallmarks of self-organization (Sasai, 2013)—ongoing specification, intrinsic self-patterning into mesoderm layers, and self-morphogenesis to shape a cavity.

Figure 2. Cardiac mesoderm self-organizes forming a cavity *in vitro* and *ex vivo*

(A) Time course of cardioid formation. Top: quantification of size-change in the course of differentiation. Bottom: whole mount bright-field images and immunostaining of cryosections showing the size increase and cavity formation over time. Scale bars, 500 μm (bright-field images), 50 μm (sections).

(B) Cardiac mesoderm explants from chick embryos in human cardiac mesoderm conditions form chamber-like CM structures with cavities. Scale bar, 200 μm.

(C) Detailed images of cardioids (ranging from the periphery to the center) between day 1.5 and day 2.5 showing formation of loose and dense mesodermal compartments by differential expression of F-actin (phalloidin), membrane-bound beta-catenin (PY-654-beta-catenin), and N-cadherin.

(D) Representative image and quantification of number of nuclei in a 65 μm^2 square in loose (central) versus dense (peripheral) layer of cardiac mesoderm (N = 3, n = 14). Used cell lines in this figure: WTC. Mean +/− SD. ****$p < 0.0001$.

See also Figure S2 and Video S2.

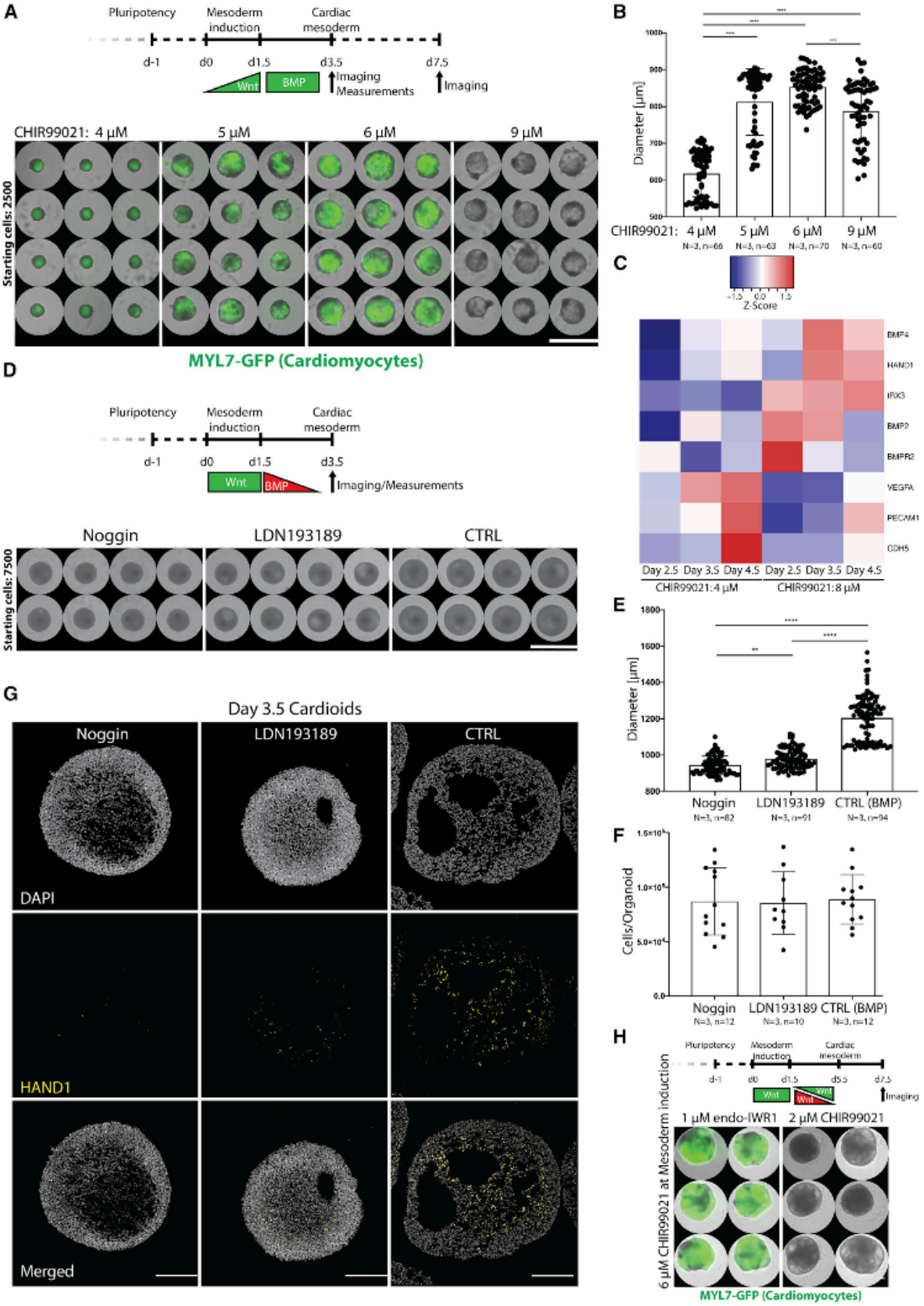

(legend on next page)

WNT and BMP control cardioid self-organization

We next used cardioids to dissect how signaling controls intrinsic morphogenesis and patterning during cardioid specification. To quantify phenotypes with high statistical power, we combined the high-throughput cardioid platform with a custom-made semi-automated imaging/analysis FIJI-pipeline. Using this setup, we examined which signals control cardioid self-organization and at what stage of mesodermal specification they act. We first systematically tested the effects of key mesoderm and cardiac mesoderm signaling dosages (e.g., WNT and BMP) on cardiac cavity self-morphogenesis. Surprisingly, we found that higher dosages of WNT signaling during mesoderm induction drove cavity expansion during the later cardiac mesoderm stage (Figures 3A and 3B), which has not been reported before. An intermediate WNT dosage promoted both cavity morphogenesis and CM specification. The optimal WNT activation range was consistent for each hPSC line but differed across lines, consistent with numerous studies showing line-specific signaling responses (Ortmann and Vallier, 2017; Strano et al., 2020). Importantly, the highest WNT dosage promoted cavity formation without CM specification (Figure 3A), highlighting a striking difference in signaling control of cell-fate specification versus morphogenesis.

To identify downstream mediators of WNT that control cardiac cavity morphogenesis, we performed RNA-seq analysis and compared gene expression profiles of mesoderm induced by higher (large cavity) and lower (small cavity) WNT signaling dosages. Among differentially expressed genes at the later cardiac mesoderm stage, we identified known cardiac mediators of BMP signaling (BMP4, BMP2, and BMPR2) and some of its mesodermal targets (HAND1 and IRX3) (Figure 3C) (Abu-Issa and Kirby, 2007; Lints et al., 1993; Riley et al., 1998). BMP drives cardiac specification at multiple stages, and we asked whether BMPs can instruct patterning and morphogenesis to form a cardiac cavity. To answer this question, we blocked BMP signaling using either the natural inhibitor Noggin or the compound LDN193189 during the initial 2 days of the cardiac mesoderm stage. BMP inhibition resulted in impaired cavity morphogenesis, denser cardiac mesoderm, and decreased cardioid size whereas the cell number per cardioid remained stable (Figures 3D–3G). In contrast, WNT inhibition at the cardiac mesoderm stage was not necessary for cavity formation (Figure 3H) although it is known to be essential for cardiac specification (Marvin et al., 2001; Yang et al., 2008). These findings emphasize that control of specification versus morphogenesis can be fundamentally different processes, and a mesodermal WNT-BMP signaling axis controls self-patterning and self-morphogenesis—both key self-organizing processes.

HAND1 is required for cardioid self-organization

Mutations in signaling and downstream transcription factors affect heart tube and chamber development and cause severe human cardiac malformations (Nees and Chung, 2020). For instance, in hypoplastic left heart syndrome, the most severe congenital defect in humans, disrupted levels of the BMP-regulated genes NKX2-5 and HAND1 are associated with a severely reduced cardiac cavity within the left ventricular chamber (Grossfeld et al., 2019; Kobayashi et al., 2014; Vincentz et al., 2017). The earliest phenotype in mutant Nkx2-5 and Hand1 mice manifests as defects in heart tube and early left ventricular chamber morphogenesis, respectively (Firulli et al., 1998; McFadden et al., 2005; Riley et al., 1998; Risebro et al., 2006; Lyons et al., 1995), however, the disease etiology and the underlying morphogenetic mechanism in humans are less clear. Here, we generated knockout (KO) hPSC lines for either HAND1 or NKX2-5 to assess whether these genes were required to achieve intrinsic self-organization in the absence of non-cardiac tissues. In NKX2-5 KO lines, we did not detect any cavity formation defects at the cardiac mesoderm stage and they eventually formed $TNNT2^{+}$ cardioids (Figures S3A–S3C). HAND1 expression in NKX2-5 KO cardiac mesoderm remained unaffected and this is in line with the delayed onset of NKX2-5 relative to HAND1 expression in cardioids (Figures 1E and S3C) as well as in human and mouse FHF cardiac mesoderm (de Soysa et al., 2019; Tyser et al., 2021). However, HAND1 expression appeared reduced at the CM stage in NKX2-5 KO cardioids (Figure S3C), which is in agreement with findings in mouse and human CMs where NKX2-5 is acting upstream of HAND1 (Anderson et al., 2018; Tanaka et al., 1999).

In HAND1 KOs, on the other hand, we observed reduced NKX2-5 protein levels in cardiac mesoderm but not in CMs (Figures 4A, S3D, and S3E). These results highlight the importance of stage-specific analysis because our data suggest that HAND1 functions upstream of NKX2-5 in cardiac mesoderm whereas NKX2-5 is upstream of HAND1 in CMs. Consistent with this hypothesis, and distinct from NKX2-5 null cardioids, HAND1 KO cardioids showed a clear defect in cardiac cavity self-organization and size at the cardiac mesoderm stage. This phenotype manifested as cardioids of smaller size (N = 9, n = 246) forming smaller cavities (N = 3, n = 130) (Figures 4B–4E and S3G). These defects were not caused by a difference in cell number per cardioid, because both KO and wild-type (WT)

Figure 3. WNT and BMP control cardioid self-organization and specification

(A) Range of CHIR99021 concentrations during mesoderm induction shows dramatic effects on cardioid diameter (day 3.5) and CM specification (day 7.5). Scale bar, 2,500 μm.

(B) Quantification of cardioid diameters at day 3.5.

(C) BMP target genes (HAND1, IRX3, BMP4, BMP2, and BMPR2) are upregulated in cavity-forming conditions (8 μM CHIR99201), whereas EC genes (PECAM1, CDH5, and VEGFA) are upregulated when 4 μM CHIR99021 is used.

(D) BMP-inhibition with either Noggin (100 ng/mL) or LDN193189 (0.2 μM) reduces cardioid diameter. Scale bar, 1,958 μm.

(E) Quantification of cardioid diameters at day 3.5 with or without BMP-inhibition.

(F) Cell counting of cells/organoid reveals that the reduced diameter is not a function of fewer cells.

(G) Noggin and LDN193189 treatments interfere with cavity expansion. Scale bars, 200 μm.

(H) Wnt activation during the cardiac mesoderm stage inhibits CM-differentiation but not cavity expansion. Scale bar, 200 μm. All bar graphs show mean ± SD. Used cell lines in this figure: H9 and WTC. *$p < 0.05$, **$p < 0.01$, *** $p < 0.001$, ****$p < 0.0001$.

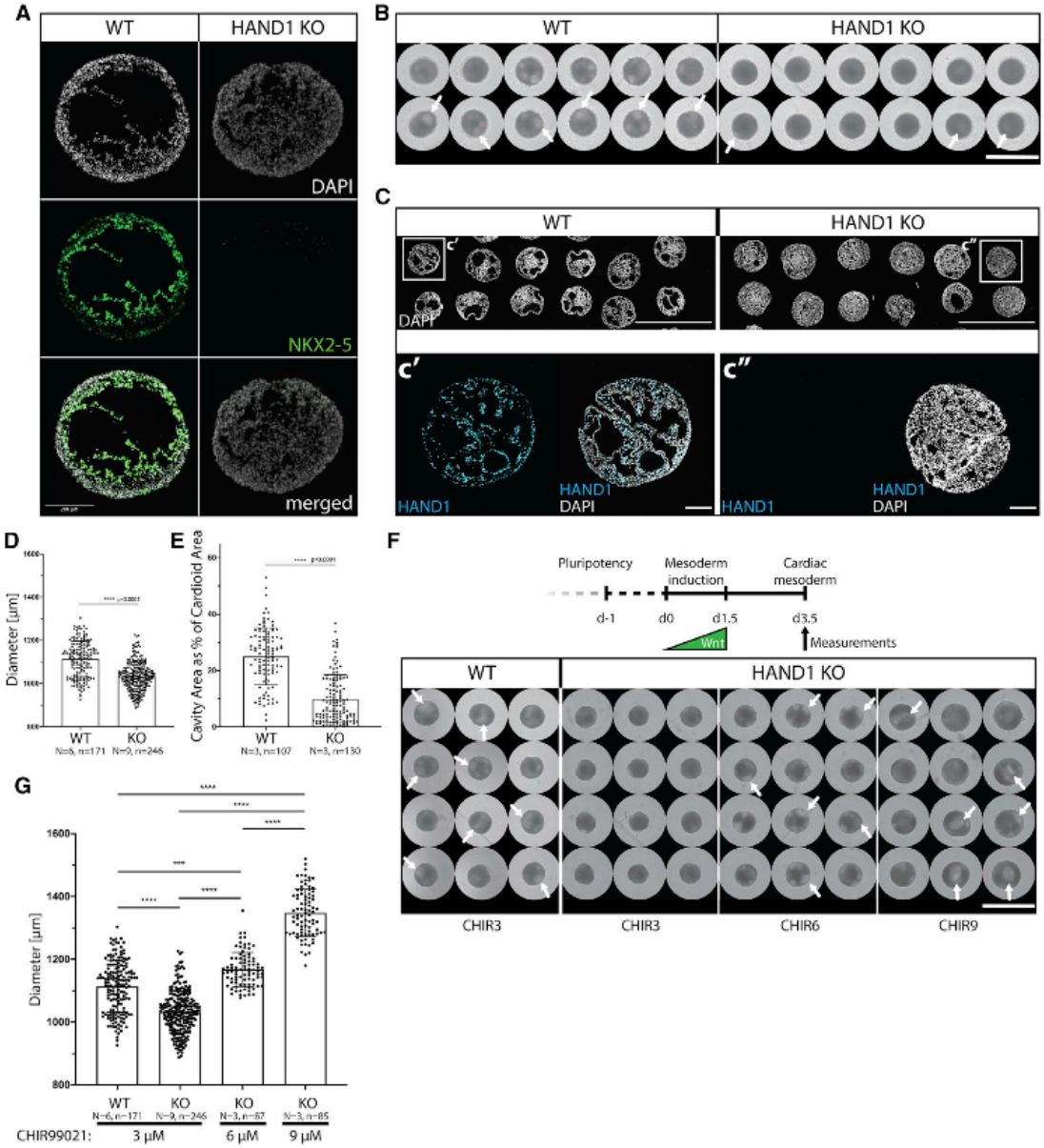

Figure 4. HAND1 is required for cardiac mesoderm (day 3.5) self-organization

(A) HAND1 KO cardioid showing downregulation of NKX2-5. Scale bar, 200 µm.

(B) WT cardioids show increased number of cavities (arrows) compared to HAND1 KO cardioids. Scale bar, 2,000 µm.

(C) HAND1 KO cardioids show smaller and decreased number of cavities. Scale bars, 2000 µm. (c′) and (c″), Detail of (C) and HAND1 KO confirmation. Scale bars, 200 µm.

(D) Quantification of cardioid cavity expansion as a function of diameter in HAND1 KO and WT cardioids.

(E) Percentage of cardioid area covered by cavities in WT and KO cardioids.

(F) Timeline of organoid formation until day 3.5 (cardiac mesoderm stage), the point of analysis. Increased WNT signaling (by CHIR99021) during mesoderm induction rescues cavity defect in HAND1 KO organoids (arrows). Scale bar, 2,500 µm.

(G) Quantification of cardioid diameter shows that increased WNT rescues the cavity defect. All bar graphs show mean ± SD. All data in this figure originated from cardioids at day 3.5. Used cell lines in this figures: WT (H9), HAND1 KO (H9), and NKX2-5 KO (H9). *p < 0.05, **p < 0.01, ***p < 0.001, ****p < 0.0001.

See also Figure S3 and Video S6.

showed similar cell counts (Figure S3F). Importantly, despite these defects in patterning and morphogenesis of cardiac mesoderm, later CM specification (TNNT2^{+}) was still functional in HAND1 KO cardioids (Figure S3E; Video S6). These observations further underscore the crucial distinction between control of cell specification versus tissue patterning and organ

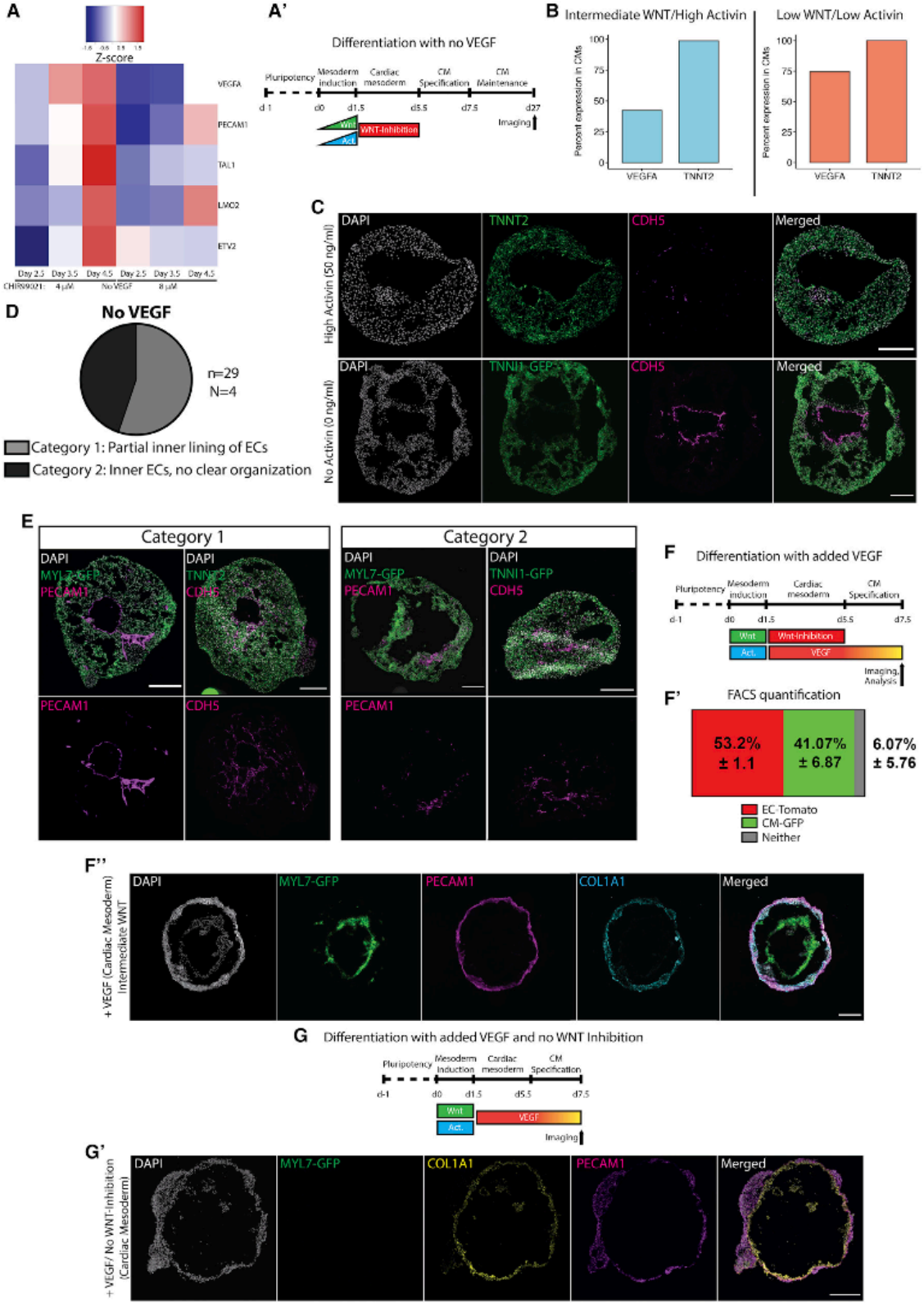

(legend on next page)

morphogenesis that can be dissected in the context of a cardiac malformation in cardioids.

We next asked whether the HAND1 KO phenotype could be rescued by exogenous signaling factors. Increased dosage of WNT signaling during mesoderm induction rescued the HAND1 KO phenotype, confirming the involvement of WNT in cavity morphogenesis (Figures 4F and 4G). Consistently, HAND1, a human-specific FHF and early ventricular chamber marker (Cui et al., 2019), was upregulated in high WNT conditions that also promoted cavity expansion (Figure 3C). Moreover, HAND1 protein levels were diminished on BMP inhibition, confirming that a WNT-BMP-HAND1 axis drives cardioid cavity self-organization (Figure 3G). Taken together, these data show that self-organization and genetic cardiac defects can be quantitatively modeled in our high-throughput cardioid platform.

WNT, ACTIVIN, and VEGF coordinate endothelial and myocardial self-organization

We next explored whether cardioids can be used to dissect signaling pathways directing patterning and separation of the myocardium and endocardium to form an inner lining, a hallmark feature of the heart chamber. To probe these relationships, we compared the RNA-seq time course of cardioids, which were generated using high versus low WNT activation dosage during mesoderm induction. We found that lower WNT activation resulted in upregulation of VEGF-A, and other EC-specifying factors (ETV2, TAL1, LMO2, and PECAM1) during the cardiac mesoderm stage (Figures 5A and 5A′). At the same time, scRNA-seq analysis of ventricular-like cardioids induced with low WNT/low ACTIVIN conditions revealed a higher proportion of CMs expressing VEGF-A in comparison to cardioids induced with intermediate WNT/high ACTIVIN (Figure 5B). We therefore hypothesized that low WNT and ACTIVIN signaling dosages coordinate CM and EC co-specification by inducing VEGF-A in cardiac mesoderm and in CMs to stimulate EC differentiation. Indeed, we discovered that lower levels of WNT signaling in combination with low ACTIVIN signaling dosages during mesoderm induction promoted later ECs self-organization within cardioids (Figures 5C and 5D). Those ECs often (55.2%, N = 4, n = 29) formed a partial inner lining of the cardioid cavity (Figures 5C–5E, S5A, and S5A′) but never on the outside of cardioids, resembling the *in vivo* tissue architecture. In contrast, in higher WNT and ACTIVIN dosage conditions, we never observed EC self-organization in the absence of exogenous VEGF (Figure 5C). In conclusion, optimal WNT and ACTIVIN signaling dosages during mesoderm induction control later EC self-organization resulting in a partial lining of the cardioid cavity.

We next interrogated the effects of exogenous VEGF on CM and EC co-specification in cardioids (Figure 5F). When we included VEGF-A after the CM specification stage, we occasionally observed formation of an EC layer lining the cardioid cavity but also some EC specification on the surface of cardioids (Figures S5B–S5D). To further elucidate whether we can control the early self-organization of CM and EC layers in cardiac mesoderm, we included VEGF-A at this stage. Because CMs and ECs co-differentiated from cardiac mesoderm into cavity-containing structures in the presence of VEGF-A, they separated into CM and EC layers (Figures 5F–5F″). Here, using an optimal (intermediate) WNT activation during mesoderm induction always resulted in an EC layer surrounding the CM layer (Figures 5F″, S4A, and S4C). Moreover, a third layer of COL1A1^{+} cells emerged next to the EC layer (Figure 5F″). In contrast to cardioids, aggregates of ECs and CMs initially differentiated in 2D formed intermingled networks, but they did not pattern into layers (Figure S4B). This suggested that VEGF stimulates the early separation of the two layers, which is an important aspect seen in embryonic cardiac mesoderm and at the heart tube stage. However, exogenous VEGF was not sufficient to control the correct outer versus inner orientation of the EC lining. Thus, the dosage of WNT/ACTIVIN and timing of VEGF signaling coordinate specification, cavity morphogenesis, and *in vivo*-like patterning of CM and EC lineages.

To further dissect the WNT and VEGF signaling control of lineage specification and morphogenesis in cardioids, we asked whether an EC cell layer can be formed without CM co-differentiation. In the absence of WNT inhibition and in the presence of VEGF during the cardiac mesoderm stage, we discovered that cardioid-like structures that contained primarily ECs and COL1A1^{+} cells, without CMs, could be reproducibly formed (Figures 5G, 5G′, and S4F). This observation again underscores how signaling control of morphogenesis could be separated from signaling control of cell specification in cardioids. Collectively, these data show that as cardioids self-organize to give rise to the first two heart lineages, they can be used to dissect

Figure 5. WNT, ACTIVIN, and VEGF coordinate endothelial and myocardial self-organization

(A) Low WNT dosage (CHIR99021, 4 μM) during mesoderm induction results in higher expression of EC-specifying genes (*VEGFA*, *TAL1*, *LMO2*, *ETV2*, and *PECAM1*) compared to high WNT (CHIR99021, 8 μM).

(A′) Timeline of differentiations performed with no VEGF, low or higher WNT, and activin dosages.

(B) Percentage of VEGF expressing CMs (single-cell sequenced) is increased in optimized, ventricular-like CMs (low WNT [CHIR: 4 μM]/low activin [4 ng/mL], N = 2, n = 5,097) compared to the intermediate WNT (CHIR: 6 μM)/high activin [50 ng/mL] condition, N = 2, n = 1,717).

(C) Example images of emergence of partial EC-lining in "no activin" condition. Scale bars, 200 μm.

(D) Quantification of the different EC formation and lining occurrences. N = 4, n = 29.

(E) Example images for categories 1 and 2. Scale bars, 200 μm.

(F) Timeline of differentiations performed with added VEGF and intermediate WNT (CHIR: 6 μM)/high activin (50 ng/mL) dosages as well as WNT inhibition.

(F′) Quantification of FACS data showing a robust ratio of CMs and ECs in cardioids. Mean ± SD.

(F″) Cardioids show separation of CM and EC layers as well as emergence of a layer of fibroblast-like cells (COL1A1^{+}). Scale bars, 200 μm.

(G) Timeline of differentiations performed with added VEGF and intermediate WNT (CHIR: 6 μM)/high activin (50 ng/mL) dosages as well as no WNT inhibition.

(G′) Cryo-section of cardioids containing only ECs and fibroblast-like cells without CMs when WNT is not inhibited during the cardiac mesoderm stage and VEGF is added. Used cell lines in this figure: WTC.

See also Figures S4 and S5.

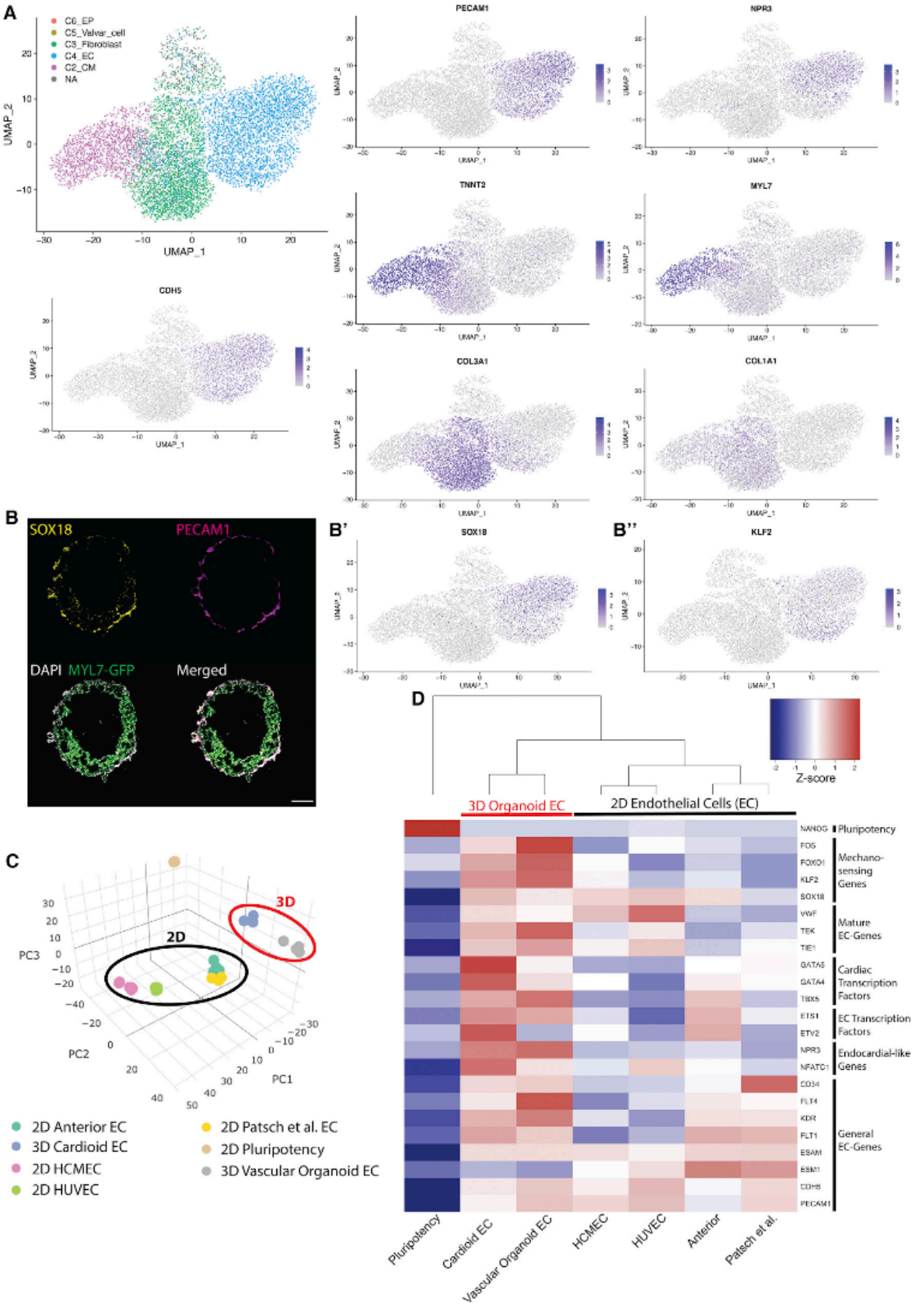

(legend on next page)

aspects and stages of myocardial and endocardial co-development.

Endocardial and fibroblast-like cells in cardioids

All self-organizing organoids share related tissue-like specification, patterning, and morphogenesis processes but are distinguished by their organ-specific cell types. Hence, we next investigated cellular heterogeneity within cardioids. When we used intermediate WNT activation and VEGF, we found that the ratio of CMs to ECs was stable at 41% ($MYL7^+$) to 53% ($CDH5^+$) (Figure 5F′ and S4D), which facilitated quantitative analysis using this model. This observation was further corroborated by the deconvolution of bulk RNA-seq data (Wang et al., 2019) and a cardiac cell-type-specific single-cell expression reference (Cui et al., 2019) for the developing human heart (Figure S6A). Smart-seq2 of sorted cells (Figure S4E) and scRNA-seq analysis used to categorize cells based on the *in vivo* human heart data further confirmed key CM and EC marker profiles and GO-terms (Figures 6A, 6D, S6D, and S6E), while the remaining cells ($MYL7^-$/$CDH5^-$) expressed genes (e.g., SOX9, MSX1/2, COL1A1, and COL3A1) related to putative EC-derived fibroblast-like cells (Huang et al., 2019; Neri et al., 2019) (Figures 6A and S6F). Finally, bulk proteomic analysis of cardioids confirmed their CM and EC proteome expression signatures (Figure S6B).

All vascularized tissues and organs contain specific EC subtypes, and accordingly, the endocardium has an identity-specific EC gene expression signature (Nakano et al., 2016). To determine EC identity in cardioids, we performed a Smart-seq2 analysis on sorted $CDH5^+$ cardioid ECs and compared them to ECs generated using a well-established 2D differentiation protocol (Patsch et al., 2015), our 2D differentiation protocol using similar media conditions as in 3D, ECs from vascular organoids (Wimmer et al., 2019), human umbilical vein endothelial cells (HUVECs), and human cardiac microvascular endothelial cells (HCMECs) (Figures 6C and 6D). We found that cardioid-derived ECs were most similar to ECs from vascular organoids despite their age difference (day 7.5 versus day >18). Importantly, ECs from cardioids showed increased transcript levels for cardiac transcription factors, such as GATA4/5, and genes associated with endocardial-like identity (NFATC1, NPR3) (Tang et al., 2018) (Figure 6D). Importantly, NFATC1 was also found in the proteomics data (Figure S6B) and NPR3 in the scRNA-seq data (Figure 6A). Their anterior HOX gene expression profile matched that of HCMECs from the adult human heart and that of ECs derived from cardiac mesoderm in 2D (anterior ECs), but not that of the other analyzed more posterior EC subtypes (Figure S6C). Thus, the signature of ECs derived from cardioids is consistent with an endocardial-like identity.

The ability of endothelium to sense fluid flow, pressure, and mechanical stretch is an instrumental requirement for its developmental and physiological roles, especially in the heart (Duchemin et al., 2019; Haack and Abdelilah-Seyfried, 2016). As expected for a bona fide model of cardiac development, a Smart-seq2 analysis of sorted ECs from cardioids revealed an upregulation of mechanosensitive genes (SOX18, KLF2, FOXO1, and FOS) compared to ECs in 2D (Figures 6B–6B″ and 6D), similar to the more matured 3D vascular organoid ECs. These observations were confirmed in the scRNA-seq dataset and with staining for SOX18. Markers of EC maturation (VWF, TEK, and TIE1) were also upregulated in cardioid ECs compared to 2D EC differentiations (Figure 6D). Overall, these results indicate that self-organization of CMs and ECs in 3D triggers essential aspects of endocardial identity and endothelial physiology.

Tri-lineage cardioid platform as a developmental injury model

After endocardial lining formation, the epicardium envelopes early myocardial chambers, thereby adding the third major cardiac lineage to the heart (Cao and Poss, 2018; Simões and Riley, 2018). The epicardium originates from a small cellular clump called the pro-epicardial organ and goes on to cover the outer surface of the heart (Andres-Delgado et al., 2018). After engulfment, signals from the CM layer (transforming growth factor β [TGF-β], platelet-derived growth factor β [PDGF-β], and FGFs) drive epicardial cell differentiation into smooth muscle cells (SMCs) and cardiac fibroblasts (CFs)—both crucial for further development, maturation, and regeneration of the heart on injury (Cao and Poss, 2018; Simões and Riley, 2018). To mimic this self-organization process in cardioids, we developed an epicardial differentiation protocol compatible with cardioids and based on the signaling sequence known to specify the pro-epicardial organ in vertebrates and hPSCs (Figures 7A and S7A–S7C) (Guadix et al., 2017; Iyer et al., 2015; Witty et al., 2014). We then co-cultured cardioids with epicardial aggregates in media without exogenous TGF-β, FGF, and PDGF to test whether endogenous expression of these signaling factors by cardioids (Figure S7D) is sufficient to stimulate epicardial/cardioid interactions. Within 2–7 days, we observed spreading of epicardial cells on top of cardioids (Figures S7E–S7G). After 7 days and without additional growth factors, epicardial cells interacted with the CM layer, migrated into it, and underwent differentiation (Figures 7B–7D, S7H, and S7I). The migrating cells downregulated epicardial

Figure 6. Cellular identities of cardioid cells on VEGF treatment

(A) Classification of cells of VEGF-supplemented cardioids based on markers determined by Cui et al. (2019) (human fetal hearts). CM, cardiomyocytes; EC, cardiac endothelial cells; EP, epicardial cells. Selected markers for cardiac ECs (PECAM1, CDH5, and NPR3), CMs (TNNT2 and MYL7), and fibroblast-like cells (COL1A1 and COL3A1) are shown.

(B–B″) Cardiac ECs in cardioids express mechanosensing genes (e.g., KLF2, SOX18). Scale bar, 200 μm.

(C) PCA of 2D-derived ECs (anterior [Patsch et al., 2015] human cardiac microvascular [HCMEC], human umbilical vein [HUVEC]), hPSCs, and 3D-derived ECs from cardioids (day 7.5, intermediate WNT dosage) and vascular organoids (Wimmer et al., 2019) (day >18). Anterior ECs: H9 line (Patsch et al., 2015) vascular organoid ECs as indicated by Wimmer et al. (2019).

(D) Expression of mechanosensing and maturation genes, cardiac transcription factors, EC transcription factors, endocardial-like and general EC genes in FACS-sorted ECs. Used cell lines in this figure (unless otherwise stated): WTC.

See also Figure S6.

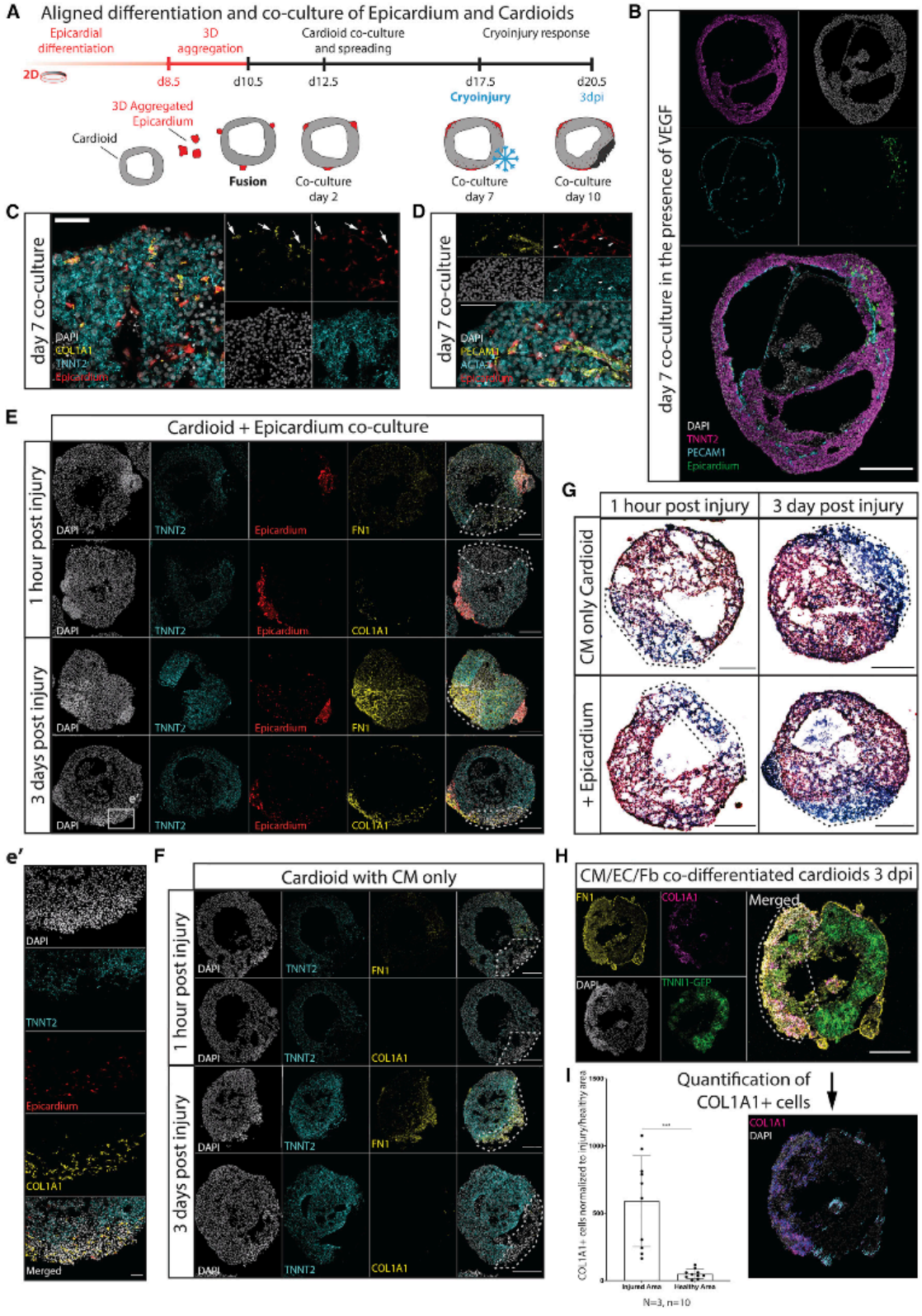

(legend on next page)

WT1 and upregulated the SMC and CF markers ACTA2 (Figures 7D and S7I) and COL1A1 (Figures 7C and S7H), as occurs *in vivo*. Strikingly, some of the migrating epicardium-derived cells started to interact with cardioid ECs (Figures 7B and 7D). We concluded that co-culture in the absence of external signals triggers intrinsic spreading of epicardium on cardioids, its inward migration, differentiation, and interactions with CMs and ECs.

A postulated advantage of self-organizing developmental organoid models are their pathophysiological-like responses (Lancaster and Huch, 2019; Schutgens and Clevers, 2020). However, current cardiac *in vitro* models (Voges et al., 2017) do not recapitulate important aspects of either myocardial regeneration seen in fetal (Drenckhahn et al., 2008; Sturzu et al., 2015), early postnatal (Haubner et al., 2016; Porrello et al., 2011), and adult *in vivo* injury models (Xin et al., 2013) or fibrosis seen in disease models and patients (Tallquist, 2020). For instance, after cryoinjury of bioengineered heart organoids (Voges et al., 2017), there is limited CM proliferation but no initial ECM accumulation typical for the early stages of both regeneration (Hortells et al., 2019; Mercer et al., 2013; Poss et al., 2002) and fibrosis (Tallquist, 2020). Given that cardioids contain all three major cardiac lineages, solely relying on developmental mechanisms and not requiring external ECM scaffolds, we reasoned that cardioids would likely produce a more physiological response upon cryoinjury. To test the potential of the cardioid platform as a developmental injury model, we performed cryoinjuries in mono- (containing CM only) and tri-lineage (containing CMs) (Figures 7G and 7F), either ECs (Figures 7H, 7I, and S7J–S7L), or epicardium (Figures 7E and 7G) and associated fibroblast-like cells (cardioids). The injury sites were characterized by intense, compacted DAPI signals, severe necrosis detected by TUNEL staining (Figure S7J), limited apoptosis, and no clear CM proliferative response (Figure S7K). Cardioids continued to contract after cryoinjury (Video S7). In time course experiments, we observed trichromium staining at the injury site, indicating localized ECM accumulation (Figure 7G). Mono-lineage cardioids showed lower fibronectin accumulation and absence of COL1A1$^+$ expressing fibroblast-like cells at the injury site (Figures 7G and 7F). In contrast, in trilineage cardioids, we observed significant tropism of COL1A1$^+$ fibroblasts toward the injury site and strong fibronectin accumulation (Figures 7E and 7G). This rapid recruitment of either EC or epicardial associated fibroblast-like cells (Figures 7E, 7H, and 7I) is consistent with *in vivo* observations during injury responses (Ali et al., 2014; Moore-Morris et al., 2014). We could therefore dissect cell-type-specific processes on cardiac injury and conclude that cardioids are capable of mimicking an important early aspect of regenerative and fibrotic responses.

In conclusion, we have established a high-throughput human cardioid platform with capacity for intrinsic self-organization into patterned layers and 3D structures reminiscent of the early human left ventricular heart chamber. We also show that this resource can be used to model mechanisms underlying development of the three major cardiac lineages, including cavity formation and injury response.

DISCUSSION

The variability and complexity of self-organizing organoid systems still hinders quantitative modeling of morphogenetic defects (Little and Combes, 2019). In cardioids, we address this challenge by omitting exogenous ECM and using a high-throughput approach to reach optimal signaling conditions. We further increased reproducibility by tightly controlling self-organization via signaling and the stepwise incorporation of the three main cardiac lineages into cardioids. This approach allows dissecting, with high statistical power, when and where the functions of specific factors are required. The simplicity and modularity of the system that can contain either one, two, or three cardiac lineages, without interference of non-cardiac tissues as in more complex embryoid models (Drakhlis et al., 2021; Rossi et al., 2021), makes it possible to reduce self-organization and its underlying molecular and cell biological mechanisms to its bare essentials. Complexity in cardioids can therefore be tailored to the biological question asked. This is an important advantage for an organoid model, because complex biological systems often employ redundant mechanisms that are otherwise challenging to tease apart.

Cardioids, as all other self-organizing organoid systems, recapitulate some aspects of development but also differ from embryogenesis in others. Self-organization encompasses only a subset of intrinsic developmental mechanisms, which are sufficient to recapitulate aspects of the *in vivo*-like architecture (Sasai, 2013). Consequently, using cardioids, we showed that cardiac mesoderm alone, instructed by signaling, is sufficient to form a chamber-like cavity *in vitro*. We propose that this cavity could be analogous to the cavity of the heart tube and early left ventricular

Figure 7. Epicardial- and endocardial-derived fibroblasts react to cryoinjury in cardioids

(A) Schematic of epicardial co-culture and cryoinjury.

(B) Confocal images of fluorescently labeled epicardial derivatives after 7 days of co-culture with cardioids (TNNT2$^+$) encompassing EC (PECAM1$^+$) inner lining in the presence of 100 ng/mL VEGF-A. Scale bar, 200 μm.

(C and D) Confocal images of COL1A1$^+$ (C) and ACTA2$^+$ (D) epicardial derivatives after 7 days of co-culture with cardioids containing ECs (PECAM1$^+$). Scale bars, 50 μm.

(E and F) Confocal images of cryoinjury response (1 h and 3 days after injury) staining fibronectin (FN1) and COL1A1$^+$ cells in cardioids in the presence (E) or absence (F) of epicardium. Scale bar, 200 μm (E and F) and 50 μm (e′, detail of E).

(G) Masson's trichrome staining (blue, connective tissue; red, muscle) of cryoinjured cardioids in the presence or absence of epicardium 1 h and 3 days post injury. Scale bar, 200 μm.

(H) Confocal images of CM+EC+fibroblast co-differentiated cardioids 3 days post injury marking FN1 and COL1A1$^+$ cells. Scale bar, 200 μm.

(I) Quantification of COL1A1$^+$ cells in the injured (purple) versus healthy (blue) area of co-differentiated CM+EC+fibroblast cardioids 3 days post injury. Number of COL1A1$^+$ cells was normalized to injured area/total area. Dashed lines mark the injury area in figures. Used cell lines in epicardial figures: H9, experiments also repeated with WTC lines. Used cell lines for CM/EC/Fibroblast co-differentiations: WTC. All bar graphs show mean +/− SD. *$p < 0.05$, **$p < 0.01$, ***$p < 0.001$, ****$p < 0.0001$. See also Figure S7 and Video S7.

heart chamber. *In vivo*, the first cavity arises from foregut endoderm-assisted migration and fusion of bilateral cardiac mesoderm and endocardial tubes into a single heart tube (Abu-Issa and Kirby, 2007). However, bilateral heart tubes and chambers can form in the absence of either endocardium (Ferdous et al., 2009) or foregut endoderm constriction (DeHaan, 1959; Li et al., 2004), but the mechanism is still unknown. This indicates the inherent capability of cardiac mesoderm to intrinsically form cavities and chambers *in vivo* (Ivanovitch et al., 2017), which is in agreement with the self-organization we observed in cardioids and chick embryo explants *in vitro*. Lateral plate mesoderm, a subtype comprising cardiac mesoderm, has a similar potential to form a cavity—the pericardial body cavity (Schlueter and Mikawa, 2018). Thus, cavitation is likely a more general characteristic of mesoderm that could be called on in embryos with a foregut defect. Finally, the HAND1 KO cavity formation phenotype demonstrates the heart chamber defect modeling potential of cardioids (Grossfeld et al., 2019; McFadden et al., 2005; Risebro et al., 2006).

We used the cardioid platform to demonstrate that WNT and BMP drive chamber-like self-organization. These pathways are known to regulate cardiac specification *in vivo* and *in vitro* (Meilhac and Buckingham, 2018) but whether and at what stage they control cardiac patterning and morphogenesis was unclear. The surprising finding that early mesodermal WNT controls later cardiac self-organization is consistent with early cardiac lineage diversification during mesoderm induction *in vivo* (Garcia-Martinez and Schoenwolf, 1993; Ivanovitch et al., 2021; Lescroart et al., 2018). Patterning and morphogenesis occur in parallel with specification but they are not necessarily linked. In agreement with this notion, cavities can self-organize in the absence of cardiac specification and in HAND1 KO cardioids there is a defect in self-organization but not in CM specification. Conversely, inhibition of WNT signaling at the cardiac mesoderm stage is essential for CM specification but does not regulate cardioid self-organization. Cardioids are therefore a powerful system to intrinsically dissect regulation of specification and morphogenesis. At the same time, cardioids are simple enough to determine sufficiency of a factor for one of these processes and are thus complementary to more complex systems.

We found that WNT, ACTIVIN, and VEGF control CM and EC self-organization in cardioids. *In vivo*, cardiac ECs first form endocardial tubes, later become separated from the outer CM tube by an ECM-filled (cardiac jelly) interspace, and finally form the inner lining of the heart chambers (Abu-Issa and Kirby, 2007; Ivanovitch et al., 2017). How signaling coordinates these patterns and morphogenetic processes with specification was unclear. In cardioids, the patterning and morphogenesis of CM and EC lineages is controlled by the dosage of WNT and ACTIVIN at the earliest stage of mesodermal differentiation and by VEGF that directs both specification and patterning of the EC layer in cardiac mesoderm. Interestingly, the same range of lower WNT and ACTIVIN signaling dosages stimulated ventricular specification and EC lining formation suggesting a potential coordination between these processes. Inner lining of a cardiac chamber-like structure has not been observed before in neither cardiac microtissues (Giacomelli et al., 2017) nor more complex foregut-heart organoids and gastruloids (Drakhlis et al., 2021; Rossi et al., 2021). Generation of a separate EC layer/lining in the context of a chamber cavity is crucial for activation of mechanosensing *in vivo*. Cardiac chamber mechanobiology is required for physiological EC and CM crosstalk, driving the next stages of heart development including trabeculation, myocardial compaction, and interaction with epicardium (Wilsbacher and McNally, 2016). Cardioids are therefore a promising system to study the underlying mechanisms of CM and EC patterning and crosstalk in the context of a beating chamber.

By co-culturing cardioids with epicardium, we observed epicardial spreading, migration, and differentiation reminiscent of these processes *in vivo* (Cao and Poss, 2018; Simões and Riley, 2018). Epicardial and CM co-cultures have been studied before using microtissues (Guadix et al., 2017) but not in the context of a cardiac chamber-like model. This aspect is important because the crosstalk between derivatives of the epicardial, EC, and CM lineages is dependent on the mechanobiology of the heart chamber (Wilsbacher and McNally, 2016). We therefore propose that self-organization of the three cardiac lineages in chamber-like cardioids will be important to reignite the developmental and regenerative crosstalk that drives growth, maturation, and pathophysiological responses of the heart as *in vivo*. The striking difference in response on cryoinjury between bioengineered organoids (Voges et al., 2017) and self-organizing cardioids supports the argument that developmental mechanisms impact later pathophysiology.

Limitations of study

To build the cardioid platform as a resource, we focused primarily on the FHF lineage and the earliest stages of cardiogenesis, in line with the chronology of embryonic development. However, as heart development progresses, additional lineages (second heart field, cardiac neural crest), cell types (pacemakers, immune cells), and structures (atria, right ventricle, outflow/inflow tracts) become integrated into the heart, and most congenital diseases arise during these later stages (Kelly et al., 2014; Meilhac and Buckingham, 2018). Certain aspects of cardiogenesis also depend on interactions with other germ layers, which can be specifically studied with other models (Drakhlis et al., 2021; Rossi et al., 2021; Silva et al., 2020). Cardioids therefore provide a foundation for incorporation of additional cardiac lineages and structures by signaling controlled self-organization but in the present form, are unlikely yet to faithfully recapitulate most cardiac defects. However, we envision that increased complexity using developmental principles will facilitate further *in vitro* maturation and functionalization that could render cardioids transformative for cardiovascular research. In this context, the human cardioid injury model still does not correspond to regenerative fetal and neonatal *in vivo* injury models and will therefore require further development and maturation. More broadly, cardioids are complementary to existing cardiac models as well as embryoids and comprise a significant advance in cardiac-specific organoid technology akin to what has been achieved for other organs.

Overall, the cardioid platform has a wide potential to explore fundamental mechanisms of self-organization and congenital defects as well as to generate future mature and complex human heart models suitable for drug discovery and regenerative medicine.

STAR★METHODS

Detailed methods are provided in the online version of this paper and include the following:

- KEY RESOURCES TABLE
- RESOURCE AVAILABILITY
  - Lead contact
  - Materials availability
  - Data and code availability
- EXPERIMENTAL MODELS AND SUBJECT DETAILS
  - Cell Lines
  - Chicken (Gallus gallus)
- METHOD DETAILS
  - hPSC differentiation into CMs in 2D and 3D aggregates –
  - ECM molecules used –
  - Generation of cardioids –
  - Generation of cardioids containing CMs, ECs and fibroblast-like cells in defined layers –
  - Cryo-injury of cardioids –
  - Cell-line-dependent CHIR99021 concentration –
  - Epicardial co-culture with cardioids –
  - 2D Anterior EC differentiation –
  - Cryosectioning –
  - Immunostaining –
  - Trichrome staining –
  - Electron microscopy –
  - Dextran and Fluo-4 incorporation assays –
  - Contraction characteristics measurements –
  - Optical action potentials –
  - Image acquisition and analysis –
  - Flow cytometry –
  - RNA isolation and RNA-seq/Smart-Seq2/single-cell (sc)RNA-seq preparation –
  - Bioinformatic analysis –
  - Proteomics –
  - Generation of MYL7-GFP/CDH5-Tomato double reporter line –
  - Generation of HAND1 and NKX2-5 Knock Out Cell Lines –
  - Oligos
- QUANTIFICATION AND STATISTICAL ANALYSIS

SUPPLEMENTAL INFORMATION

Supplemental information can be found online at https://doi.org/10.1016/j.cell.2021.04.034.

ACKNOWLEDGMENTS

We thank all laboratory members for help and discussions and Katarzyna Warczok for lab management. We are grateful to the VBC Histology, EM and NGS, IMP/IMBA Core, and IMBA SCCF facilities for their services; the Allen Institute for cell lines; the Knoblich laboratory/Joshua A. Bagley for cell lines, reagents, and discussions; and Penninger laboratory/Reiner Wimmer for sharing data and reagents. We are thankful to Philip Szkokan and Steffen Hering for assisting with the FluoVolt measurements and analysis. We are thankful to the Kicheva laboratory for training on chicken embryo work. We are thankful to the Tanaka and Gerlich laboratories for sharing reagents. We are grateful to Paulina Latos, Alex Stark, Luisa Cochella, Juergen Knoblich, and Elly Tanaka for comments on the manuscript and Life Science Editors for scientific editing. This work was funded by the Austrian Academy of Sciences (OEAW) and Research Promotion Agency (FFG).

AUTHOR CONTRIBUTIONS

P.H., S.M.J., N.P., and S.M. co-designed experiments and co-wrote the paper. P.H. developed CM and EC differentiations in 2D and co-differentiations in 3D aggregates and in cardioids and also set up the high-throughput analysis pipeline and the cardioid injury model. S.M.J. established, optimized, and characterized cardioid generation. N.P. developed and characterized epicardial differentiations in 2D, 3D, and cardioids, characterized cardioids, and set up the cardioid injury model. M.N. helped with the bioinformatic analysis. All other authors performed experiments. S.M. performed experiments and supervised the study.

DECLARATION OF INTERESTS

The Institute for Molecular Biotechnology (IMBA) filed a patent application (EP20164637.9) on different types of cardiac organoids (cardioids) with P.H., S.M.J., N.P., and S.M. named as inventors. P.H. and S.M. are co-founders of HeartBeat.bio AG, an IMBA spin-off company aiming to develop a cardioid drug discovery platform.

INCLUSION AND DIVERSITY

We worked to ensure diversity in experimental samples through the selection of the cell lines. While citing references scientifically relevant for this work, we also actively worked to promote gender balance in our reference list.

Received: July 6, 2020
Revised: February 12, 2021
Accepted: April 19, 2021
Published: May 20, 2021

REFERENCES

Abu-Issa, R., and Kirby, M.L. (2007). Heart field: from mesoderm to heart tube. Annu. Rev. Cell Dev. Biol. *23*, 45–68.

Ali, S.R., Ranjbarvaziri, S., Talkhabi, M., Zhao, P., Subat, A., Hojjat, A., Kamran, P., Müller, A.M.S., Volz, K.S., Tang, Z., et al. (2014). Developmental heterogeneity of cardiac fibroblasts does not predict pathological proliferation and activation. Circ. Res. *115*, 625–635.

Anderson, D.J., Kaplan, D.I., Bell, K.M., Koutsis, K., Haynes, J.M., Mills, R.J., Phelan, D.G., Qian, E.L., Leitoguinho, A.R., Arasaratnam, D., et al. (2018). NKX2-5 regulates human cardiomyogenesis via a HEY2 dependent transcriptional network. Nat. Commun. *9*, 1373.

Andres-Delgado, L., Ernst, A., Galardi-Castilla, M., Bazaga, D., Peralta, M., Münch, J., González-Rosa, J.M., Tessadori, F., Bakkers, J., de la Pompa Mínguez, J.L., et al. (2018). Actomyosin dynamics, Bmp and Notch signaling pathways drive apical extrusion of proepicardial cells. bioRxiv. https://doi.org/10.1101/332593.

Bagley, J.A., Reumann, D., Bian, S., Lévi-Strauss, J., and Knoblich, J.A. (2017). Fused cerebral organoids model interactions between brain regions. Nat. Methods *14*, 743–751.

Birket, M.J., Ribeiro, M.C., Verkerk, A.O., Ward, D., Leitoguinho, A.R., den Hartogh, S.C., Orlova, V.V., Devalla, H.D., Schwach, V., Bellin, M., et al. (2015). Expansion and patterning of cardiovascular progenitors derived from human pluripotent stem cells. Nat. Biotechnol. *33*, 970–979.

Cao, J., and Poss, K.D. (2018). The epicardium as a hub for heart regeneration. Nat. Rev. Cardiol. *15*, 631–647.

Chen, G., Gulbranson, D.R., Hou, Z., Bolin, J.M., Ruotti, V., Probasco, M.D., Smuga-Otto, K., Howden, S.E., Diol, N.R., Propson, N.E., et al. (2011).

Chemically defined conditions for human iPSC derivation and culture. Nat. Methods *8*, 424–429.

Clevers, H. (2016). Modeling Development and Disease with Organoids. Cell *165*, 1586–1597.

Costello, I., Pimeisl, I.-M., Dräger, S., Bikoff, E.K., Robertson, E.J., and Arnold, S.J. (2011). The T-box transcription factor Eomesodermin acts upstream of Mesp1 to specify cardiac mesoderm during mouse gastrulation. Nat. Cell Biol. *13*, 1084–1091.

Cui, Y., Zheng, Y., Liu, X., Yan, L., Fan, X., Yong, J., Hu, Y., Dong, J., Li, Q., Wu, X., et al. (2019). Single-Cell Transcriptome Analysis Maps the Developmental Track of the Human Heart. Cell Rep. *26*, 1934–1950.e5.

de Soysa, T.Y., Ranade, S.S., Okawa, S., Ravichandran, S., Huang, Y., Salunga, H.T., Schricker, A., del Sol, A., Gifford, C.A., and Srivastava, D. (2019). Single-cell analysis of cardiogenesis reveals basis for organ-level developmental defects. Nature *572*, 120–124.

DeHaan, R.L. (1959). Cardia bifida and the development of pacemaker function in the early chick heart. Dev. Biol. *1*, 586–602.

Devalla, H.D., Schwach, V., Ford, J.W., Milnes, J.T., El-Haou, S., Jackson, C., Gkatzis, K., Elliott, D.A., Chuva de Sousa Lopes, S.M., Mummery, C.L., et al. (2015). Atrial-like cardiomyocytes from human pluripotent stem cells are a robust preclinical model for assessing atrial-selective pharmacology. EMBO Mol. Med. *7*, 394–410.

Doblmann, J., Dusberger, F., Imre, R., Hudecz, O., Stanek, F., Mechtler, K., and Dürnberger, G. (2019). apQuant: Accurate Label-Free Quantification by Quality Filtering. J. Proteome Res. *18*, 535–541.

Drakhlis, L., Biswanath, S., Farr, C.-M., Lupanow, V., Teske, J., Ritzenhoff, K., Franke, A., Manstein, F., Bolesani, E., Kempf, H., et al. (2021). Human heart-forming organoids recapitulate early heart and foregut development. Nat. Biotechnol. Published online February 8, 2021. https://doi.org/10.1038/s41587-021-00815-9.

Drenckhahn, J.-D., Schwarz, Q.P., Gray, S., Laskowski, A., Kiriazis, H., Ming, Z., Harvey, R.P., Du, X.-J., Thorburn, D.R., and Cox, T.C. (2008). Compensatory growth of healthy cardiac cells in the presence of diseased cells restores tissue homeostasis during heart development. Dev. Cell *15*, 521–533.

Duchemin, A.-L., Vignes, H., Vermot, J., and Chow, R. (2019). Mechanotransduction in cardiovascular morphogenesis and tissue engineering. Curr. Opin. Genet. Dev. *57*, 106–116.

Eiraku, M., Takata, N., Ishibashi, H., Kawada, M., Sakakura, E., Okuda, S., Sekiguchi, K., Adachi, T., and Sasai, Y. (2011). Self-organizing optic-cup morphogenesis in three-dimensional culture. Nature *472*, 51–56.

Ferdous, A., Caprioli, A., Iacovino, M., Martin, C.M., Morris, J., Richardson, J.A., Latif, S., Hammer, R.E., Harvey, R.P., Olson, E.N., et al. (2009). Nkx2-5 transactivates the Ets-related protein 71 gene and specifies an endothelial/endocardial fate in the developing embryo. Proc. Natl. Acad. Sci. USA *106*, 814–819.

Firulli, A.B., McFadden, D.G., Lin, Q., Srivastava, D., and Olson, E.N. (1998). Heart and extra-embryonic mesodermal defects in mouse embryos lacking the bHLH transcription factor Hand1. Nat. Genet. *18*, 266–270.

Garcia-Martinez, V., and Schoenwolf, G.C. (1993). Primitive-streak origin of the cardiovascular system in avian embryos. Dev. Biol. *159*, 706–719.

Giacomelli, E., Bellin, M., Sala, L., van Meer, B.J., Tertoolen, L.G.J., Orlova, V.V., and Mummery, C.L. (2017). Three-dimensional cardiac microtissues composed of cardiomyocytes and endothelial cells co-differentiated from human pluripotent stem cells. Development *144*, 1008–1017.

Giacomelli, E., Meraviglia, V., Campostrini, G., Cochrane, A., Cao, X., van Helden, R.W.J., Krotenberg Garcia, A., Mircea, M., Kostidis, S., Davis, R.P., et al. (2020). Human-iPSC-Derived Cardiac Stromal Cells Enhance Maturation in 3D Cardiac Microtissues and Reveal Non-cardiomyocyte Contributions to Heart Disease. Cell Stem Cell *26*, 862–879.e11.

Grossfeld, P., Nie, S., Lin, L., Wang, L., and Anderson, R.H. (2019). Hypoplastic Left Heart Syndrome: A New Paradigm for an Old Disease? J. Cardiovasc. Dev. Dis. *6*, 10.

Guadix, J.A., Orlova, V.V., Giacomelli, E., Bellin, M., Ribeiro, M.C., Mummery, C.L., Pérez-Pomares, J.M., and Passier, R. (2017). Human Pluripotent Stem Cell Differentiation into Functional Epicardial Progenitor Cells. Stem Cell Reports *9*, 1754–1764.

Haack, T., and Abdelilah-Seyfried, S. (2016). The force within: endocardial development, mechanotransduction and signalling during cardiac morphogenesis. Development *143*, 373–386.

Haubner, B.J., Schneider, J., Schweigmann, U., Schuetz, T., Dichtl, W., Velik-Salchner, C., Stein, J.-I., and Penninger, J.M. (2016). Functional Recovery of a Human Neonatal Heart After Severe Myocardial Infarction. Circ. Res. *118*, 216–221.

Hockemeyer, D., Wang, H., Kiani, S., Lai, C.S., Gao, Q., Cassady, J.P., Cost, G.J., Zhang, L., Santiago, Y., Miller, J.C., et al. (2011). Genetic engineering of human pluripotent cells using TALE nucleases. Nat. Biotechnol. *29*, 731–734.

Hortells, L., Johansen, A.K.Z., and Yutzey, K.E. (2019). Cardiac Fibroblasts and the Extracellular Matrix in Regenerative and Nonregenerative Hearts. J. Cardiovasc. Dev. Dis. *6*, 29.

Huang, X., Feng, T., Jiang, Z., Meng, J., Kou, S., Lu, Z., Chen, W., Lin, C.-P., Zhou, B., and Zhang, H. (2019). Dual lineage tracing identifies intermediate mesenchymal stage for endocardial contribution to fibroblasts, coronary mural cells, and adipocytes. J. Biol. Chem. *294*, 8894–8906.

Huebsch, N., Loskill, P., Mandegar, M.A., Marks, N.C., Sheehan, A.S., Ma, Z., Mathur, A., Nguyen, T.N., Yoo, J.C., Judge, L.M., et al. (2015). Automated Video-Based Analysis of Contractility and Calcium Flux in Human-Induced Pluripotent Stem Cell-Derived Cardiomyocytes Cultured over Different Spatial Scales. Tissue Eng. Part C Methods *21*, 467–479.

Ivanovitch, K., Esteban, I., and Torres, M. (2017). Growth and Morphogenesis during Early Heart Development in Amniotes. J. Cardiovasc. Dev. Dis. *4*, 20.

Ivanovitch, K., Soro-Barrio, P., Chakravarty, P., Jones, R.A., Bell, D.M., Gharavy, S.N.M., Stamataki, D., Delile, J., Smith, J.C., and Briscoe, J. (2021). Ventricular, atrial and outflow tract heart progenitors arise from spatially and molecularly distinct regions of the primitive streak. bioRxiv. https://doi.org/10.1101/2020.07.12.198994.

Iyer, D., Gambardella, L., Bernard, W.G., Serrano, F., Mascetti, V.L., Pedersen, R.A., Talasila, A., and Sinha, S. (2015). Robust derivation of epicardium and its differentiated smooth muscle cell progeny from human pluripotent stem cells. Development *142*, 1528–1541.

Kelly, R.G., Buckingham, M.E., and Moorman, A.F. (2014). Heart fields and cardiac morphogenesis. Cold Spring Harb. Perspect. Med. *4*, a015750.

Kobayashi, J., Yoshida, M., Tarui, S., Hirata, M., Nagai, Y., Kasahara, S., Naruse, K., Ito, H., Sano, S., and Oh, H. (2014). Directed differentiation of patient-specific induced pluripotent stem cells identifies the transcriptional repression and epigenetic modification of NKX2-5, HAND1, and NOTCH1 in hypoplastic left heart syndrome. PLoS ONE *9*, e102796.

Kuo, C.T., Morrisey, E.E., Anandappa, R., Sigrist, K., Lu, M.M., Parmacek, M.S., Soudais, C., and Leiden, J.M. (1997). GATA4 transcription factor is required for ventral morphogenesis and heart tube formation. Genes Dev. *11*, 1048–1060.

Lancaster, M.A., and Huch, M. (2019). Disease modelling in human organoids. Dis. Models Mech. *12*, dmm039347.

Lancaster, M.A., and Knoblich, J.A. (2014). Organogenesis in a dish: modeling development and disease using organoid technologies. Science *345*, 1247125.

Lancaster, M.A., Renner, M., Martin, C.-A., Wenzel, D., Bicknell, L.S., Hurles, M.E., Homfray, T., Penninger, J.M., Jackson, A.P., and Knoblich, J.A. (2013). Cerebral organoids model human brain development and microcephaly. Nature *501*, 373–379.

Marvin, M.J., Di Rocco, G., Gardiner, A., Bush, S.M., and Lassar, A.B. (2001). Inhibition of Wnt activity induces heart formation from posterior mesoderm. Genes Dev. *15*, 316–327.

Lee, J.H., Protze, S.I., Laksman, Z., Backx, P.H., and Keller, G.M. (2017). Human Pluripotent Stem Cell-Derived Atrial and Ventricular Cardiomyocytes Develop from Distinct Mesoderm Populations. Cell Stem Cell *21*, 179–194.e4.

Lescroart, F., Wang, X., Lin, X., Swedlund, B., Gargouri, S., Sànchez-Dànes, A., Moignard, V., Dubois, C., Paulissen, C., Kinston, S., et al. (2018). Defining the earliest step of cardiovascular lineage segregation by single-cell RNA-seq. Science *359*, 1177–1181.

Li, S., Zhou, D., Lu, M.M., and Morrisey, E.E. (2004). Advanced cardiac morphogenesis does not require heart tube fusion. Science *305*, 1619–1622.

Lian, X., Hsiao, C., Wilson, G., Zhu, K., Hazeltine, L.B., Azarin, S.M., Raval, K.K., Zhang, J., Kamp, T.J., and Palecek, S.P. (2012). Robust cardiomyocyte differentiation from human pluripotent stem cells via temporal modulation of canonical Wnt signaling. Proc. Natl. Acad. Sci. USA *109*, E1848–E1857.

Linask, K.K. (2003). Regulation of heart morphology: current molecular and cellular perspectives on the coordinated emergence of cardiac form and function. Birth Defects Res. C Embryo Today *69*, 14–24.

Lints, T.J., Parsons, L.M., Hartley, L., Lyons, I., and Harvey, R.P. (1993). Nkx-2.5: a novel murine homeobox gene expressed in early heart progenitor cells and their myogenic descendants. Development *119*, 419–431.

Little, M.H., and Combes, A.N. (2019). Kidney organoids: accurate models or fortunate accidents. Genes Dev. *33*, 1319–1345.

Lyons, I., Parsons, L.M., Hartley, L., Li, R., Andrews, J.E., Robb, L., and Harvey, R.P. (1995). Myogenic and morphogenetic defects in the heart tubes of murine embryos lacking the homeo box gene Nkx2-5. Genes Dev. *9*, 1654–1666.

Ma, Z., Wang, J., Loskill, P., Huebsch, N., Koo, S., Svedlund, F.L., Marks, N.C., Hua, E.W., Grigoropoulos, C.P., Conklin, B.R., and Healy, K.E. (2015). Self-organizing human cardiac microchambers mediated by geometric confinement. Nat. Commun. *6*, 7413.

Majumdar, U., Yasuhara, J., and Garg, V. (2021). In Vivo and In Vitro Genetic Models of Congenital Heart Disease. Cold Spring Harb. Perspect. Biol. *13*, a036764.

McFadden, D.G., Barbosa, A.C., Richardson, J.A., Schneider, M.D., Srivastava, D., and Olson, E.N. (2005). The Hand1 and Hand2 transcription factors regulate expansion of the embryonic cardiac ventricles in a gene dosage-dependent manner. Development *132*, 189–201.

Meilhac, S.M., and Buckingham, M.E. (2018). The deployment of cell lineages that form the mammalian heart. Nat. Rev. Cardiol. *15*, 705–724.

Mendjan, S., Mascetti, V.L., Ortmann, D., Ortiz, M., Karjosukarso, D.W., Ng, Y., Moreau, T., and Pedersen, R.A. (2014). NANOG and CDX2 pattern distinct subtypes of human mesoderm during exit from pluripotency. Cell Stem Cell *15*, 310–325.

Mercer, S.E., Odelberg, S.J., and Simon, H.-G. (2013). A dynamic spatiotemporal extracellular matrix facilitates epicardial-mediated vertebrate heart regeneration. Dev. Biol. *382*, 457–469.

Mills, R.J., Titmarsh, D.M., Koenig, X., Parker, B.L., Ryall, J.G., Quaife-Ryan, G.A., Voges, H.K., Hodson, M.P., Ferguson, C., Drowley, L., et al. (2017). Functional screening in human cardiac organoids reveals a metabolic mechanism for cardiomyocyte cell cycle arrest. Proc. Natl. Acad. Sci. USA *114*, E8372–E8381.

Moore-Morris, T., Guimarães-Camboa, N., Banerjee, I., Zambon, A.C., Kisseleva, T., Velayoudon, A., Stallcup, W.B., Gu, Y., Dalton, N.D., Cedenilla, M., et al. (2014). Resident fibroblast lineages mediate pressure overload-induced cardiac fibrosis. J. Clin. Invest. *124*, 2921–2934.

Nakano, T., Ando, S., Takata, N., Kawada, M., Muguruma, K., Sekiguchi, K., Saito, K., Yonemura, S., Eiraku, M., and Sasai, Y. (2012). Self-formation of optic cups and storable stratified neural retina from human ESCs. Cell Stem Cell *10*, 771–785.

Nakano, A., Nakano, H., Smith, K.A., and Palpant, N.J. (2016). The developmental origins and lineage contributions of endocardial endothelium. Biochim. Biophys. Acta *1863* (7 Pt B), 1937–1947.

Nees, S.N., and Chung, W.K. (2020). Genetic Basis of Human Congenital Heart Disease. Cold Spring Harb. Perspect. Biol. *12*, 036749.

Neri, T., Hiriart, E., van Vliet, P.P., Faure, E., Norris, R.A., Farhat, B., Jagla, B., Lefrancois, J., Sugi, Y., Moore-Morris, T., et al. (2019). Human pre-valvular endocardial cells derived from pluripotent stem cells recapitulate cardiac pathophysiological valvulogenesis. Nat. Commun. *10*, 1929.

Orlova, V.V., van den Hil, F.E., Petrus-Reurer, S., Drabsch, Y., Ten Dijke, P., and Mummery, C.L. (2014). Generation, expansion and functional analysis of endothelial cells and pericytes derived from human pluripotent stem cells. Nat. Protoc. *9*, 1514–1531.

Ortmann, D., and Vallier, L. (2017). Variability of human pluripotent stem cell lines. Curr. Opin. Genet. Dev. *46*, 179–185.

Palpant, N.J., Pabon, L., Friedman, C.E., Roberts, M., Hadland, B., Zaunbrecher, R.J., Bernstein, I., Zheng, Y., and Murry, C.E. (2017). Generating high-purity cardiac and endothelial derivatives from patterned mesoderm using human pluripotent stem cells. Nat. Protoc. *12*, 15–31.

Patsch, C., Challet-Meylan, L., Thoma, E.C., Urich, E., Heckel, T., O'Sullivan, J.F., Grainger, S.J., Kapp, F.G., Sun, L., Christensen, K., et al. (2015). Generation of vascular endothelial and smooth muscle cells from human pluripotent stem cells. Nat. Cell Biol. *17*, 994–1003.

Porrello, E.R., Mahmoud, A.I., Simpson, E., Hill, J.A., Richardson, J.A., Olson, E.N., and Sadek, H.A. (2011). Transient regenerative potential of the neonatal mouse heart. Science *331*, 1078–1080.

Poss, K.D., Wilson, L.G., and Keating, M.T. (2002). Heart regeneration in zebrafish. Science *298*, 2188–2190.

Prandini, et al. (2005). The human VE-cadherin promoter is subjected to organ-specific regulation and is activated in tumour angiogenesis. Oncogene *24* (18), 2992–3001.

Ran, F.A., Hsu, P.D., Wright, J., Agarwala, V., Scott, D.A., and Zhang, F. (2013). Genome engineering using the CRISPR-Cas9 system. Nat. Protoc. *8*, 2281–2308.

Richards, D.J., Li, Y., Kerr, C.M., Yao, J., Beeson, G.C., Coyle, R.C., Chen, X., Jia, J., Damon, B., Wilson, R., et al. (2020). Human cardiac organoids for the modelling of myocardial infarction and drug cardiotoxicity. Nat. Biomed. Eng. *4*, 446–462.

Riley, P., Anson-Cartwright, L., and Cross, J.C. (1998). The Hand1 bHLH transcription factor is essential for placentation and cardiac morphogenesis. Nat. Genet. *18*, 271–275.

Risebro, C.A., Smart, N., Dupays, L., Breckenridge, R., Mohun, T.J., and Riley, P.R. (2006). Hand1 regulates cardiomyocyte proliferation versus differentiation in the developing heart. Development *133*, 4595–4606.

Roberts, B., Hendershott, M.C., Arakaki, J., Gerbin, K.A., Malik, H., Nelson, A., Gehring, J., Hookway, C., Ludmann, S.A., Yang, R., et al. (2019). Fluorescent Gene Tagging of Transcriptionally Silent Genes in hiPSCs. Stem Cell Reports *12*, 1145–1158.

Ronaldson-Bouchard, K., Ma, S.P., Yeager, K., Chen, T., Song, L., Sirabella, D., Morikawa, K., Teles, D., Yazawa, M., and Vunjak-Novakovic, G. (2018). Advanced maturation of human cardiac tissue grown from pluripotent stem cells. Nature *556*, 239–243.

Rossi, G., Broguiere, N., Miyamoto, M., Boni, A., Guiet, R., Girgin, M., Kelly, R.G., Kwon, C., and Lutolf, M.P. (2021). Capturing Cardiogenesis in Gastruloids. Cell Stem Cell *28*, 230–240.e6.

Sasai, Y. (2013). Cytosystems dynamics in self-organization of tissue architecture. Nature *493*, 318–326.

Schindelin, J., Arganda-Carreras, I., Frise, E., Kaynig, V., Longair, M., Pietzsch, T., Preibisch, S., Rueden, C., Saalfeld, S., Schmid, B., et al. (2012). Fiji: an open-source platform for biological-image analysis. Nat. Methods *9*, 676–682.

Schlueter, J., and Mikawa, T. (2018). Body Cavity Development Is Guided by Morphogen Transfer between Germ Layers. Cell Rep. *24*, 1456–1463.

Schutgens, F., and Clevers, H. (2020). Human Organoids: Tools for Understanding Biology and Treating Diseases. Annu. Rev. Pathol. *15*, 211–234.

Serra, D., Mayr, U., Boni, A., Lukonin, I., Rempfler, M., Challet-Meylan, L., Stadler, M.B., Strnad, P., Papasaikas, P., Vischi, D., et al. (2019). Self-organization and symmetry breaking in intestinal organoid development. Nature *569*, 66–72.

Silva, A.C., Matthys, O.B., Joy, D.A., Kauss, M.A., Natarajan, V., Lai, M.H., Turaga, D., Alexanian, M., Bruneau, B.G., and McDevitt, T.C. (2020). Developmental co-emergence of cardiac and gut tissues modeled by human iPSC-derived organoids. bioRxiv. https://doi.org/10.1101/2020.04.30.071472.

Simões, F.C., and Riley, P.R. (2018). The ontogeny, activation and function of the epicardium during heart development and regeneration. Development *145*, dev155994.

Strano, A., Tuck, E., Stubbs, V.E., and Livesey, F.J. (2020). Variable Outcomes in Neural Differentiation of Human PSCs Arise from Intrinsic Differences in Developmental Signaling Pathways. Cell Rep. *31*, 107732.

Sturzu, A.C., Rajarajan, K., Passer, D., Plonowska, K., Riley, A., Tan, T.C., Sharma, A., Xu, A.F., Engels, M.C., Feistritzer, R., et al. (2015). Fetal Mammalian Heart Generates a Robust Compensatory Response to Cell Loss. Circulation *132*, 109–121.

Tallquist, M.D. (2020). Cardiac Fibroblast Diversity. Annu. Rev. Physiol. *82*, 63–78.

Tanaka, M., Chen, Z., Bartunkova, S., Yamasaki, N., and Izumo, S. (1999). The cardiac homeobox gene Csx/Nkx2.5 lies genetically upstream of multiple genes essential for heart development. Development *126*, 1269–1280.

Tang, J., Zhang, H., He, L., Huang, X., Li, Y., Pu, W., Yu, W., Zhang, L., Cai, D., Lui, K.O., and Zhou, B. (2018). Genetic Fate Mapping Defines the Vascular Potential of Endocardial Cells in the Adult Heart. Circ. Res. *122*, 984–993.

Tiburcy, M., Hudson, J.E., Balfanz, P., Schlick, S., Meyer, T., Chang Liao, M.-L., Levent, E., Raad, F., Zeidler, S., Wingender, E., et al. (2017). Defined Engineered Human Myocardium With Advanced Maturation for Applications in Heart Failure Modeling and Repair. Circulation *135*, 1832–1847.

Tuveson, D., and Clevers, H. (2019). Cancer modeling meets human organoid technology. Science *364*, 952–955.

Tyser, R.C.V., Ibarra-Soria, X., McDole, K., Arcot Jayaram, S., Godwin, J., van den Brand, T.A.H., Miranda, A.M.A., Scialdone, A., Keller, P.J., Marioni, J.C., and Srinivas, S. (2021). Characterization of a common progenitor pool of the epicardium and myocardium. Science *371*, eabb2986.

Vincentz, J.W., Toolan, K.P., Zhang, W., and Firulli, A.B. (2017). Hand factor ablation causes defective left ventricular chamber development and compromised adult cardiac function. PLoS Genet. *13*, e1006922.

Voges, H.K., Mills, R.J., Elliott, D.A., Parton, R.G., Porrello, E.R., and Hudson, J.E. (2017). Development of a human cardiac organoid injury model reveals innate regenerative potential. Development *144*, 1118–1127.

Wang, X., Park, J., Susztak, K., Zhang, N.R., and Li, M. (2019). Bulk tissue cell type deconvolution with multi-subject single-cell expression reference. Nat. Commun. *10*, 380.

Wilsbacher, L., and McNally, E.M. (2016). Genetics of Cardiac Developmental Disorders: Cardiomyocyte Proliferation and Growth and Relevance to Heart Failure. Annu. Rev. Pathol. *11*, 395–419.

Wimmer, R.A., Leopoldi, A., Aichinger, M., Wick, N., Hantusch, B., Novatchkova, M., Taubenschmid, J., Hämmerle, M., Esk, C., Bagley, J.A., et al. (2019). Human blood vessel organoids as a model of diabetic vasculopathy. Nature *565*, 505–510.

Witty, A.D., Mihic, A., Tam, R.Y., Fisher, S.A., Mikryukov, A., Shoichet, M.S., Li, R.-K., Kattman, S.J., and Keller, G. (2014). Generation of the epicardial lineage from human pluripotent stem cells. Nat. Biotechnol. *32*, 1026–1035.

Xin, M., Olson, E.N., and Bassel-Duby, R. (2013). Mending broken hearts: cardiac development as a basis for adult heart regeneration and repair. Nat. Rev. Mol. Cell Biol. *14*, 529–541.

Yang, L., Soonpaa, M.H., Adler, E.D., Roepke, T.K., Kattman, S.J., Kennedy, M., Henckaerts, E., Bonham, K., Abbott, G.W., Linden, R.M., et al. (2008). Human cardiovascular progenitor cells develop from a KDR+ embryonic-stem-cell-derived population. Nature *453*, 524–528.

Yap, L., Tay, H.G., Nguyen, M.T.X., Tjin, M.S., and Tryggvason, K. (2019). Laminins in Cellular Differentiation. Trends Cell Biol. *29*, 987–1000.

Zaidi, S., and Brueckner, M. (2017). Genetics and Genomics of Congenital Heart Disease. Circ. Res. *120*, 923–940.

Zhao, Y., Rafatian, N., Feric, N.T., Cox, B.J., Aschar-Sobbi, R., Wang, E.Y., Aggarwal, P., Zhang, B., Conant, G., Ronaldson-Bouchard, K., et al. (2019). A Platform for Generation of Chamber-Specific Cardiac Tissues and Disease Modeling. Cell *176*, 913–927.e18.

7. Discussion

In the last few years, many breakthroughs have been achieved in developing cardiac *in vitro* systems. Most of these self-organizing models focus on mimicking the development of the left ventricle and atria derived from the FHF progenitor population, while only a few studies also started to include the SHF progenitor populations. However, most of these SHF protocols have several limitations, including heterogeneity, the unclear identity of CMs, and they miss the genetic and functional validation of compartment specificity. In addition, present cardiac organoid systems exhibit significant variability during generation, including the ratio of FHF versus SHF cells within one organoid, thereby hindering the quantitative analysis of developmental processes or morphogenetic disorders.

We developed a cardiac *in vitro* system that is signaling controlled, aligned with development, and encompasses all major compartments of the developing embryonic human heart. We generated differentiation protocols for the three cardiac progenitor populations (FHF, aSHF, and pSHF) and differentiated them further into different regions of the heart, including LV, RV, OFT, Atria, and AVC. The 2D to 3D differentiation approach, where we aggregate cells in 3D only after they undergo mesoderm induction, ensures that we generate homogenous progenitors and that no sorting step is required. We discovered that different levels of Activin/Nodal and WNT signaling during mesoderm induction, followed by TGF-beta/Nodal signaling inhibition during the patterning stage, determine the specificity of the SHF lineage vs. the FHF. This contrasts with most other SHF protocols, which mainly change mesoderm induction conditions to specify the SHF. However, TGF-beta/Nodal inhibition has been previously shown to instruct cells towards the head mesoderm region of the embryo, which springs from a shared cardio-pharyngeal progenitor pool as the aSHF (Nandkishore et al. 2018; Arkell and Tam 2012).

Additionally, the role of RA signaling in our system is particularly noteworthy. We showed that the timing and dosage of RA signaling play a crucial role in the specification ((Niederreither and Dollé 2008; Zaffran, El Robrini, and Bertrand 2014; Nakajima 2019). We found that aSHF patterning and further OFT differentiation do not require any RA addition, while for RV specification, high levels of RA at a later stage are necessary. Additionally, high levels of RA during the patterning stage are needed for pSHF and subsequent atrial and AVC specification. In contrast to many other SHF protocols, we performed an extensive analysis of the identity of the CMs, where we were able to confirm region-specific gene expression, morphogenesis, and functionality.

We validated our cardioid platform using compartment-specific teratogens and knockout lines. Drug experiments were performed using acitretin, which led to specific effects and highlighted again the importance of RA signaling in our system. Retinols have a strong effect on differentiation speed, morphogenesis, differentiation efficiency, and, most importantly, cardioid identity. We were able to demonstrate that the addition of acitretin leads to an identity switch of the OFT cardioids more towards an atrial fate. Furthermore, we used well-studied KO lines (TBX5 and ISL1) (Bruneau et al. 2001; Cai et al. 2003) that are known to lead to region-specific effects, as well as less characterized transcription factors in the cardiac context, like FOXF1. Since the cardioid system is very robust and quantifiable, it enables us to study so far unknown factors that could cause cardiac defects and allows for cardiac drug discovery and drug toxicity testing. Additionally, our HTP platform will enable the study of patient-specific mutation lines, which could be vital to modeling diseases and developing therapies.

Multi-chambered cardioids provide a unique opportunity to investigate a time window of development inaccessible in the human embryo. In particular, the initiation of the beat in the human heart is very difficult to explore (Watanabe et al. 2016). Data from mice and chickens suggest directional electrochemical signal propagation occurs early in heart development. The differentiating LV derived from FHF progenitors is the region where the electrochemical signal first appears (R. C. Tyser et al. 2016). In our

multi-chambered cardioids, we were able to recapitulate this process and have shown that the LV starts to beat and that the electrochemical signal can propagate through the other compartments of the multi-chambered cardioid. This allows a unidirectional flow within the cardioid. Taken together, using multi-chambered cardioids, we were able to study so far hidden aspects of early human heart development, like the crosstalk of different compartments and the unidirectional electrochemical signal propagation.

Regardless of the utility, there are still several limitations to the current cardioid system that need to be addressed in the future. One major limitation is the morphology of the cardioids. Migration of SHF progenitors into the heart tube, looping, septation, and the inclusion of pacemaker cells are important factors that need to be considered to fully mimic the development of the human heart. Another limitation is the maturation of the CMs within the cardioids. We observed that when the cardioids are kept in our standard media composition (CDM-I), they slowly lose their identity. To be able to mature the CMs and to ensure that they keep their identity, we cultured our cardioids in published maturation conditions (M. Feyen et al. 2020; Garay et al. 2022). We tested these protocols successfully on the LV and RV and observed the upregulation of maturation markers and the development of organized sarcomeres. However, these protocols only focus on the maturation of ventricular CMs and do not promote the maturation of atrial cardioids. This treatment led to the upregulation of MYL2, a ventricular maturation marker independent on the identity of the CMs. This suggests that all cardioid subtypes need separate maturation conditions, and further optimization is still needed for atria, AVC, and OFT cardioids.

Aspects missing in Schmidt, Deyett et al., 2023			
Progenitor identities	**CM identities**	**morphogenesis**	**disease aspect**
Juxta-cardiac field progenitors	SAN and AVN	Migration of SHF progenitors and looping	Patient specific defects
	Atria derived from FHF	Interaction with endoderm	Adult-onset cardiomyopathies
		Later processes including valve initiation, septation, pacemakers, chamber trabeculation and ballooning, coronary vasculature and circulation	Validation of the platform at a more mature stage
		Growth of cardioids and maturation of CMs	

Table 3: Limitations of this study.

In vivo, after the looping of the heart, cardiac valve development gets initiated in the AVC and OFT region (human embryonic day 31 to 35) to ensure unidirectional flow. This process requires the interaction of two cardiac layers, CMs and ECs, as well as the cardiac jelly in between, an ECM layer filled with hyaluronan (Haack and Abdelilah-Seyfried 2016). In Hofbauer et al., 2021, we demonstrated that by modulating the Activin and WNT signaling during the mesoderm induction, we observe an inner lining of EC, an outer lining of CMs, and in-between a fibroblast population. Since the epicardium was absent in these cardioids, we assume that the ECs underwent EMT and differentiated into fibroblasts, thereby mimicking the early steps of valve initiation (cushion formation). However, in Hofbauer et al. 2021, the CMs had an LV-like identity and not OFT or AVC-like. Therefore, we optimized the valve initiation approach in our current cardioid system and used OFT and AVC cardioids containing a CM and an EC layer. Based on developmental literature (O'Donnell and Yutzey 2020) and protocols to generate 2D valve cells from hiPSC (Neri et al. 2019; Cheng et al. 2021), we added TGF beta, BMP, and FGF to induce valve initiation. This led to an additional cell layer between ECs and CMs that was SOX9 positive, which is a marker for interstitial valve

cells. This suggests that cardioids are a promising system for future studies to understand developmental mechanisms driving early human vasculogenesis in development and disease. This would be particularly important since most of the described human cardiac mutations are causing developmental valve defects (Houyel and Meilhac 2021).

One challenge in the cardiac organoid field is the generation of endothelial cells with distinct gene expression profiles and functional properties within the heart, which are called endocardial cells. The ECs appearing in our cardioids mainly lack the expression of these key endocardial markers (NKX2-5 and NPR3). Our hypothesis is that adding VEGF inhibits endocardium identity; however, most of our protocols to co-differentiate CMs and ECs include VEGF. We envision that an alternative approach could be to adapt a published endocardial protocol based on FGF2- and BMP10-mediated specification and generate separate cardioids with either CM or endocardial cells. After the specification of these cell types, these cardioids can be combined again, allowing the use of cardioids containing CMs representing all regions, as well as region-specific endocardial cells in a more precise media composition independent of signaling important for CMs development. This approach would more closely mimic *in vivo* development since ECs and CMs progenitors split up very early in development.

Another related aspect that is still missing in our cardioid system is coronary vascularization. Organs must be supplied with nutrients, remove waste, and maintain gas exchange via a vascular network filled with blood. Since in all organoids, proper circulatory vascularization is missing, many systems, for example, cerebral organoids, show a necrotic core. Recently, there have been attempts to generate vascular networks in cardiac organoids (Lewis-Israeli, Wasserman, and Aguirre 2021), but real circulation has not yet been achieved.

In summary, cardioids provide an advanced platform to study human compartment-specific cardiac defects and the underlying mechanisms. In addition, they allow us to investigate the interaction of different compartments and study signal propagation at a time window of human development that is inaccessible. Lastly, because of the HTP

aspect, cardioids have a great potential to develop novel drug discovery and toxicity testing pipelines. Nevertheless, cardioids are unlikely to fully replace animal models in preclinical investigations, but they are highly complementary and will allow us to bridge fundamental and translational research as the system develops further.

8. References

Abu-Issa, Radwan, and Margaret L. Kirby. 2007. 'Heart Field: From Mesoderm to Heart Tube'. *Annual Review of Cell and Developmental Biology* 23 (1): 45–68. https://doi.org/10.1146/annurev.cellbio.23.090506.123331.

Andersen, Peter, Emmanouil Tampakakis, Dennisse V. Jimenez, Suraj Kannan, Matthew Miyamoto, Hye Kyung Shin, Amir Saberi, et al. 2018. 'Precardiac Organoids Form Two Heart Fields via Bmp/Wnt Signaling'. *Nature Communications* 9 (1): 3140. https://doi.org/10.1038/s41467-018-05604-8.

Arkell, Ruth M., and Patrick P. L. Tam. 2012. 'Initiating Head Development in Mouse Embryos: Integrating Signalling and Transcriptional Activity'. *Open Biology* 2 (3): 120030. https://doi.org/10.1098/rsob.120030.

Bruneau, B. G., G. Nemer, J. P. Schmitt, F. Charron, L. Robitaille, S. Caron, D. A. Conner, et al. 2001. 'A Murine Model of Holt-Oram Syndrome Defines Roles of the T-Box Transcription Factor Tbx5 in Cardiogenesis and Disease'. *Cell* 106 (6): 709–21. https://doi.org/10.1016/s0092-8674(01)00493-7.

Cai, Chen-Leng, Xingqun Liang, Yunqing Shi, Po-Hsien Chu, Samuel L. Pfaff, Ju Chen, and Sylvia Evans. 2003. 'Isl1 Identifies a Cardiac Progenitor Population That Proliferates Prior to Differentiation and Contributes a Majority of Cells to the Heart'. *Developmental Cell* 5 (6): 877–89.

Cheng, LinXi, MingHui Xie, WeiHua Qiao, Yu Song, YanYong Zhang, YingChao Geng, WeiLin Xu, et al. 2021. 'Generation and Characterization of Cardiac Valve Endothelial-like Cells from Human Pluripotent Stem Cells'. *Communications Biology* 4 (1): 1–15. https://doi.org/10.1038/s42003-021-02571-7.

Cui, Yueli, Yuxuan Zheng, Xixi Liu, Liying Yan, Xiaoying Fan, Jun Yong, Yuqiong Hu, et al. 2019. 'Single-Cell Transcriptome Analysis Maps the Developmental Track of the Human Heart'. *Cell Reports* 26 (7): 1934-1950.e5. https://doi.org/10.1016/j.celrep.2019.01.079.

De Bono, Christopher, Charlotte Thellier, Nicolas Bertrand, Rachel Sturny, Estelle Jullian, Claudio Cortes, Sonia Stefanovic, Stéphane Zaffran, Magali Théveniau-Ruissy, and Robert G. Kelly. 2018. 'T-Box Genes and Retinoic Acid Signaling Regulate the Segregation of Arterial and Venous Pole Progenitor Cells in the Murine Second Heart Field'. *Human Molecular Genetics* 27 (21): 3747–60. https://doi.org/10.1093/hmg/ddy266.

Devine, W Patrick, Joshua D Wythe, Matthew George, Kazuko Koshiba-Takeuchi, and Benoit G Bruneau. 2014. 'Early Patterning and Specification of Cardiac Progenitors in Gastrulating Mesoderm'. Edited by Marianne E Bronner. *eLife* 3 (October): e03848. https://doi.org/10.7554/eLife.03848.

Drakhlis, Lika, Santoshi Biswanath, Clara-Milena Farr, Victoria Lupanow, Jana Teske, Katharina Ritzenhoff, Annika Franke, et al. 2021. 'Human Heart-Forming Organoids Recapitulate Early Heart and Foregut Development'. *Nature Biotechnology*, February, 1–10. https://doi.org/10.1038/s41587-021-00815-9.

Fahed, Akl C., Bruce D. Gelb, J. G. Seidman, and Christine E. Seidman. 2013. 'Genetics of Congenital Heart Disease: The Glass Half Empty'. *Circulation*

Research 112 (4): 707–20. https://doi.org/10.1161/CIRCRESAHA.112.300853.
Fc, Simões, and Riley Pr. 2018. 'The Ontogeny, Activation and Function of the Epicardium during Heart Development and Regeneration'. *Development (Cambridge, England)* 145 (7). https://doi.org/10.1242/dev.155994.
G, Rossi, Broguiere N, Miyamoto M, Boni A, Guiet R, Girgin M, Kelly Rg, Kwon C, and Lutolf Mp. 2021. 'Capturing Cardiogenesis in Gastruloids'. *Cell Stem Cell* 28 (2). https://doi.org/10.1016/j.stem.2020.10.013.
Garay, Bayardo I., Sophie Givens, Phablo Abreu, Man Liu, Doğacan Yücel, June Baik, Noah Stanis, et al. 2022. 'Dual Inhibition of MAPK and PI3K/AKT Pathways Enhances Maturation of Human iPSC-Derived Cardiomyocytes'. *Stem Cell Reports* 17 (9): 2005–22. https://doi.org/10.1016/j.stemcr.2022.07.003.
Greulich, Franziska, Carsten Rudat, and Andreas Kispert. 2011. 'Mechanisms of T-Box Gene Function in the Developing Heart'. *Cardiovascular Research* 91 (2): 212–22. https://doi.org/10.1093/cvr/cvr112.
Haack, Timm, and Salim Abdelilah-Seyfried. 2016. 'The Force within: Endocardial Development, Mechanotransduction and Signalling during Cardiac Morphogenesis'. *Development* 143 (3): 373–86. https://doi.org/10.1242/dev.131425.
Hofbauer, Pablo, Stefan M. Jahnel, Nora Papai, Magdalena Giesshammer, Alison Deyett, Clara Schmidt, Mirjam Penc, et al. 2021. 'Cardioids Reveal Self-Organizing Principles of Human Cardiogenesis'. *Cell*, May. https://doi.org/10.1016/j.cell.2021.04.034.
Houyel, Lucile, and Sigolène M. Meilhac. 2021. 'Heart Development and Congenital Structural Heart Defects'. *Annual Review of Genomics and Human Genetics* 22 (1): annurev-genom-083118-015012. https://doi.org/10.1146/annurev-genom-083118-015012.
Ivanovitch, Kenzo, Pablo Soro-Barrio, Probir Chakravarty, Rebecca A. Jones, Donald M. Bell, S. Neda Mousavy Gharavy, Despina Stamataki, Julien Delile, James C. Smith, and James Briscoe. 2021. 'Ventricular, Atrial, and Outflow Tract Heart Progenitors Arise from Spatially and Molecularly Distinct Regions of the Primitive Streak'. *PLOS Biology* 19 (5): e3001200. https://doi.org/10.1371/journal.pbio.3001200.
Jin, Sheng Chih, Jason Homsy, Samir Zaidi, Qiongshi Lu, Sarah Morton, Steven R. DePalma, Xue Zeng, et al. 2017. 'Contribution of Rare Inherited and de Novo Variants in 2,871 Congenital Heart Disease Probands'. *Nature Genetics* 49 (11): 1593–1601. https://doi.org/10.1038/ng.3970.
Kelly, Robert G. 2023. 'The Heart Field Transcriptional Landscape at Single-Cell Resolution'. *Developmental Cell* 58 (4): 257–66. https://doi.org/10.1016/j.devcel.2023.01.010.
Kelly, Robert G., Margaret E. Buckingham, and Antoon F. Moorman. 2014. 'Heart Fields and Cardiac Morphogenesis'. *Cold Spring Harbor Perspectives in Medicine* 4 (10). https://doi.org/10.1101/cshperspect.a015750.
Korte, Tessa de, Puspita A. Katili, Nurul A. N. Mohd Yusof, Berend J. van Meer, Umber Saleem, Francis L. Burton, Godfrey L. Smith, et al. 2020. 'Unlocking Personalized Biomedicine and Drug Discovery with Human Induced

Pluripotent Stem Cell-Derived Cardiomyocytes: Fit for Purpose or Forever Elusive?' *Annual Review of Pharmacology and Toxicology* 60 (January): 529–51. https://doi.org/10.1146/annurev-pharmtox-010919-023309.
Lescroart, Fabienne, Samira Chabab, Xionghui Lin, Steffen Rulands, Catherine Paulissen, Annie Rodolosse, Herbert Auer, et al. 2014. 'Early Lineage Restriction and Regional Segregation during Mammalian Heart Development'. *Nature Cell Biology* 16 (9): 829–40. https://doi.org/10.1038/ncb3024.
Lescroart, Fabienne, Xiaonan Wang, Xionghui Lin, Benjamin Swedlund, Souhir Gargouri, Adriana Sànchez-Dànes, Victoria Moignard, et al. 2018. 'Defining the Earliest Step of Cardiovascular Lineage Segregation by Single-Cell RNA-Seq'. *Science* 359 (6380): 1177–81. https://doi.org/10.1126/science.aao4174.
Lewis-Israeli, Yonatan R, Aaron H Wasserman, and Aitor Aguirre. 2021. 'Heart Organoids and Engineered Heart Tissues: Novel Tools for Modeling Human Cardiac Biology and Disease', 14.
Lewis-Israeli, Yonatan R., Aaron H. Wasserman, Mitchell A. Gabalski, Brett D. Volmert, Yixuan Ming, Kristen A. Ball, Weiyang Yang, et al. 2021. 'Self-Assembling Human Heart Organoids for the Modeling of Cardiac Development and Congenital Heart Disease'. *Nature Communications* 12 (1): 5142. https://doi.org/10.1038/s41467-021-25329-5.
M. Feyen, Dries A., Wesley L. McKeithan, Arne A. N. Bruyneel, Sean Spiering, Larissa Hörmann, Bärbel Ulmer, Hui Zhang, et al. 2020. 'Metabolic Maturation Media Improve Physiological Function of Human iPSC-Derived Cardiomyocytes'. *Cell Reports* 32 (3): 107925. https://doi.org/10.1016/j.celrep.2020.107925.
Meilhac, Sigolène M., and Margaret E. Buckingham. 2018. 'The Deployment of Cell Lineages That Form the Mammalian Heart'. *Nature Reviews Cardiology* 15 (11): 705–24. https://doi.org/10.1038/s41569-018-0086-9.
Nakajima, Yuji. 2019. 'Retinoic Acid Signaling in Heart Development'. *Genesis*, April, e23300. https://doi.org/10.1002/dvg.23300.
Nandkishore, Nitya, Bhakti Vyas, Alok Javali, Subho Ghosh, and Ramkumar Sambasivan. 2018. 'Divergent Early Mesoderm Specification Underlies Distinct Head and Trunk Muscle Programmes in Vertebrates'. *Development* 145 (18). https://doi.org/10.1242/dev.160945.
Neri, Tui, Emilye Hiriart, Patrick P. van Vliet, Emilie Faure, Russell A. Norris, Batoul Farhat, Bernd Jagla, et al. 2019. 'Human Pre-Valvular Endocardial Cells Derived from Pluripotent Stem Cells Recapitulate Cardiac Pathophysiological Valvulogenesis'. *Nature Communications* 10 (1): 1929. https://doi.org/10.1038/s41467-019-09459-5.
Niederreither, Karen, and Pascal Dollé. 2008. 'Retinoic Acid in Development: Towards an Integrated View'. *Nature Reviews Genetics* 9 (7): 541–53. https://doi.org/10.1038/nrg2340.
O'Donnell, Anna, and Katherine E. Yutzey. 2020. 'Mechanisms of Heart Valve Development and Disease'. *Development (Cambridge, England)* 147 (13): dev183020. https://doi.org/10.1242/dev.183020.
Pezhouman, Arash, James L Engel, Ngoc B Nguyen, Rhys J P Skelton, William Blake Gilmore, Rong Qiao, Debashis Sahoo, Peng Zhao, David A Elliott, and Reza Ardehali. 2022. 'Isolation and Characterization of Human Embryonic

Stem Cell-Derived Heart Field-Specific Cardiomyocytes Unravels New Insights into Their Transcriptional and Electrophysiological Profiles'. *Cardiovascular Research* 118 (3): 828–43. https://doi.org/10.1093/cvr/cvab102.

Rao, Kavitha S., Vasumathi Kameswaran, and Benoit G. Bruneau. 2022. 'Modeling Congenital Heart Disease: Lessons from Mice, hPSC-Based Models, and Organoids'. *Genes & Development* 36 (11–12): 652–63. https://doi.org/10.1101/gad.349678.122.

Ryckebusch, Lucile, Zengxin Wang, Nicolas Bertrand, Song-Chang Lin, Xuan Chi, Robert Schwartz, Stéphane Zaffran, and Karen Niederreither. 2008. 'Retinoic Acid Deficiency Alters Second Heart Field Formation'. *Proceedings of the National Academy of Sciences of the United States of America* 105 (8): 2913–18. https://doi.org/10.1073/pnas.0712344105.

Sirbu, Ioan Ovidiu, Lionel Gresh, Jacqueline Barra, and Gregg Duester. 2005. 'Shifting Boundaries of Retinoic Acid Activity Control Hindbrain Segmental Gene Expression'. *Development* 132 (11): 2611–22. https://doi.org/10.1242/dev.01845.

Srivastava, Deepak. 2021. 'Modeling Human Cardiac Chambers with Organoids'. *The New England Journal of Medicine* 385 (9): 847–49. https://doi.org/10.1056/NEJMcibr2108627.

Swedlund, Benjamin, and Fabienne Lescroart. 2020. 'Cardiopharyngeal Progenitor Specification: Multiple Roads to the Heart and Head Muscles'. *Cold Spring Harbor Perspectives in Biology* 12 (8): a036731. https://doi.org/10.1101/cshperspect.a036731.

Tyser, Richard CV, Antonio MA Miranda, Chiann-mun Chen, Sean M Davidson, Shankar Srinivas, and Paul R Riley. 2016. 'Calcium Handling Precedes Cardiac Differentiation to Initiate the First Heartbeat'. Edited by Margaret Buckingham. *eLife* 5 (October): e17113. https://doi.org/10.7554/eLife.17113.

Tyser, Richard C.V., and Shankar Srinivas. 2020. 'The First Heartbeat—Origin of Cardiac Contractile Activity'. *Cold Spring Harbor Perspectives in Biology* 12 (7): a037135. https://doi.org/10.1101/cshperspect.a037135.

Wang, Jun, Stephanie B. Greene, and James F. Martin. 2011. 'Bmp Signaling in Congenital Heart Disease: New Developments and Future Directions'. *Birth Defects Research. Part A, Clinical and Molecular Teratology* 91 (6): 441–48. https://doi.org/10.1002/bdra.20785.

Watanabe, Michiko, Andrew M. Rollins, Luis Polo-Parada, Pei Ma, Shi Gu, and Michael W. Jenkins. 2016. 'Probing the Electrophysiology of the Developing Heart'. *Journal of Cardiovascular Development and Disease* 3 (1). https://doi.org/10.3390/jcdd3010010.

Yang, Donghe, Juliana Gomez-Garcia, Shunsuke Funakoshi, Thinh Tran, Ian Fernandes, Gary D. Bader, Michael A. Laflamme, and Gordon M. Keller. 2022. 'Modeling Human Multi-Lineage Heart Field Development with Pluripotent Stem Cells'. *Cell Stem Cell* 29 (9): 1382-1401.e8. https://doi.org/10.1016/j.stem.2022.08.007.

Zaffran, Stéphane, Nicolas El Robrini, and Nicolas Bertrand. 2014. 'Retinoids and Cardiac Development'. In *Journal of Developmental Biology*. Vol. 2. https://doi.org/10.3390/jdb2010050.

Zaidi, Samir, and Martina Brueckner. 2017. ‘Genetics and Genomics of Congenital Heart Disease’. *Circulation Research* 120 (6): 923–40. https://doi.org/10.1161/CIRCRESAHA.116.309140.

Zawada, Dorota, Jessica Kornherr, Anna B. Meier, Gianluca Santamaria, Tatjana Dorn, Monika Nowak-Imialek, Daniel Ortmann, et al. 2023. ‘Retinoic Acid Signaling Modulation Guides in Vitro Specification of Human Heart Field-Specific Progenitor Pools’. *Nature Communications* 14 (1): 1722. https://doi.org/10.1038/s41467-023-36764-x.